**University of Plymouth**

**PEARL** **https://pearl.plymouth.ac.uk**

04 University of Plymouth Research Theses 01 Research Theses Main Collection

2013

# Understanding Sediment Mobilisation Under Plunging Waves Within a Gravel Beach

Ball, Ian Phillip

http://hdl.handle.net/10026.1/1471

http://dx.doi.org/10.24382/3681
University of Plymouth

*All content in PEARL is protected by copyright law. Author manuscripts are made available in accordance with publisher policies. Please cite only the published version using the details provided on the item record or document. In the absence of an open licence (e.g. Creative Commons), permissions for further reuse of content should be sought from the publisher or author.*

This copy of the thesis has been supplied on condition that anyone who consults it is understood to recognise that its copyright rests with its author and that no quotation from the thesis and no information derived from it may be published without the author's prior consent.

# Understanding Sediment Mobilisation Under Plunging Waves Within a Gravel Beach.

Ian Phillip Ball

School of Marine Science and Technology
Faculty of Science and Technology

Plymouth University

A thesis submitted to Plymouth University in partial fulfillment of the requirements for the degree of:

*Doctor of Philosophy*

September 2012.

# Abstract

## Understanding Sediment Mobilisation Under Plunging Waves Within a Gravel Beach.

Ian Phillip Ball

Numerical modelling currently cannot accurately reproduce the onshore-offshore transport asymmetry observed on gravel beaches. The role of the impulsive pressure response generated by plunging waves has been hypothesised to aid mobilisation of sediment, and thus may contribute to transport asymmetry. This process is not currently included in models.

Laboratory tests were conducted across a range of wave conditions to investigate the role of plunging wave-breaker impacts on the mobilisation of sediment of gravel beaches.

Pressure records were obtained at positions close to the plunging impact locations, to monitor the localised pressures that lead to sediment mobilisation. The correction of the recorded pressure to the bed surface, for further analysis, was achieved through a two stage approach. Adoption of a new technique for separating the pressure records into two components, each determined by different processes is presented. Each component is then corrected to the bed surface with the application of a pragmatic prediction of the experienced attenuation.

Data covering a wide range of Iribarren values was assessed, and the impact pressure was parameterised against the wave-breaker type. This procedure identified a potential peak in the impact pressure-Iribarren space in the plunging breaker region, consistent with the previous hypothesis.

Comparison of cross-shore profile records provides further limited evidence that morphological prediction fails to reproduce specific characteristics associated with profiles generated under plunging breaker action.

Finally, a brief discussion is provided on how the role of the additional pressure generated under plunging impacts can be incorporated into future numerical models.

# Contents

**Abstract** **v**

**List of Tables** **xi**

**List of Figures** **xiii**

**Nomenclature** **xvii**

**Acknowledgements** **xix**

**Author's declaration** **xxi**

**1 Introduction** **1**

**2 Processes that Shape Gravel Beaches** **9**

2.1 Nature of swash . . . . . 12

2.1.1 Sediment transport . . . . . 13

2.1.1.1 Suspended sediment transport . . . . . 14

2.1.1.2 Bed load transport . . . . . 15

2.1.2 Interactions with porous beds . . . . . 18

2.1.2.1 Turbulence and Wave Breaking . . . . . 22

2.1.2.2 Groundwater dynamics . . . . . 25

2.1.2.3 Infiltration and exfiltration . . . . . 29

2.1.2.4 Flow acceleration . . . . . 33

2.1.2.5 Bottom friction . . . . . 35

2.1.3 Plunging wave impact pressure response . . . . . 37

2.2 Cross-shore profile evolution modelling . . . . . 38

2.3 Summary . . . . . 42

2.4 Project Aims . . . . . 44

**3 Experimental procedure** **45**

3.1 Facilities . . . . . 45

3.2 Sediment characteristics . . . 47
3.3 Instrumentation . . . 49
3.4 Calibration . . . 55
3.5 Hydrodynamics . . . 56

**4 Data handling for analysis** **59**
4.1 Wave height determination . . . 59
4.1.1 Incident wave separation . . . 59
4.1.2 Incident wave calculation . . . 61
4.1.3 Comparison of wave separation techniques . . . 62
4.1.4 Wave shoaling . . . 65
4.1.4.1 De-shoaling recorded wave data . . . 67
4.1.4.2 Sensitivity to beach slope . . . 68
4.1.4.3 Wave shoaling sensitivity analysis . . . 68
4.2 Surface pressure correction . . . 69
4.2.1 Attenuation in poro-elastic material . . . 70
4.2.2 Wave attenuation . . . 71
4.2.3 Attenuation of impacting event . . . 73
4.2.4 Pressure signal separation . . . 76
4.2.4.1 Wavelet analysis . . . 79
4.2.4.2 Impulsive attenuation review . . . 88
4.2.5 Impulse attenuation summary . . . 91
4.2.6 Attenuation correction of separated signal components . . . 92
4.2.7 Attenuation correction methodology . . . 96
4.2.8 Validation of attenuation correction . . . 100
4.3 Beach profile calibration . . . 103
4.4 Summary . . . 105

**5 Observations of coarse beach dynamics** **107**
5.1 Introduction . . . 107
5.2 Morphological change results . . . 110
5.3 Sediment transport analysis . . . 120

**6 Impact pressure investigation** **127**

6.1 Impact event identification . . . 127
6.2 Previous parametrisations . . . 130
6.2.1 Impact pressure vs. wave height relationship . . . 130
6.2.2 Impact pressure vs. Iribarren number . . . 132
6.2.3 Impact pressure vs. wave steepness . . . 133
6.2.4 Description of new peak pressure normalisation . . . 134
6.3 Impact pressure to wave height for UNAM data . . . 135
6.4 Impact pressure to breaker type for UNAM data . . . 136
6.5 Impact pressure to wave steepness for UNAM data . . . 139

**7 Discussions and conclusions** **141**
7.1 Discussion of analysis conducted . . . 144
7.1.1 Discussion and conclusion of morphological analysis . . . 144
7.1.2 Discussion and conclusion of pressure response analysis . . . 146
7.1.2.1 Speculation for untested data region . . . 152
7.1.2.2 Discussion within tested data region . . . 154
7.2 Discussion of error . . . 155
7.3 Consequences of speculative relationship for numerical modelling . . . 157
7.4 Additional process consideration . . . 160
7.5 Review of research programme objectives . . . 161

**8 Future Work** **163**

**A Sediment characteristics** **165**

**B Results in full** **167**
B.1 Wave records . . . 169
B.2 Beach profile results . . . 170
B.3 Berm morphological change details . . . 177
B.4 Integral-corrected net sediment transport results . . . 179

**References** **185**

# List of Tables


3.1 Chainages of measurement devices. . . . . 53

3.2 Intended wave conditions and associated Iribarren values. . . . . 57

3.3 Test data recording details. . . . . 58

4.1 Calculated initial and final reflection coefficients (Meneses Fernández 2009) 62

4.2 Calculated initial and final reflection coefficients using SIRW method. . 63

4.3 Sensitivity analysis results for wave shoaling at various beach slopes for 20080624T164058 (Test 8 - part 2). . . . . 69

5.1 Test conditions estimated after separation of incident and reflected waves. 108

5.2 Berm morphological change for test 9. . . . . 117

5.3 Peak integral-corrected net sediment transport rates . . . . . 123

A.1 Sediment sieve analysis details. . . . . 165

A.2 Porosity test details. . . . . 165

A.3 Permeability tests, with associated hydraulic gradient and hydraulic conductivity values . . . . . 166

B.1 2-second wave test details. . . . . 167

B.2 3-second wave test details. . . . . 168

B.3 4-second wave test details. . . . . 168

B.4 Calculated reflection coefficients for each experiment, using SIRW method. 169

B.5 Berm morphological change for tests 6 to 11. . . . . 177

B.6 Berm morphological change for tests 12 to 17. . . . . 178

# List of Figures


1.1 An example pure gravel beach (Jennings and Shulmeister 2002). . . . . 2

1.2 Typical beach profile (US Army Corps of Engineers 2012). . . . . 5

2.1 Swash and surf zone definition. . . . . 10

2.2 Swash water infiltration through pathways 1 and 2 (Austin and Masselink 2006*b*). . . . . 27

2.3 Schematic representation of a plunging impact after (Bullock et al. 2007). 37

2.4 Gravel beach profile evolution during GWK testing (Pedrozo-Acuña et al. 2006). . . . . 39

3.1 Wave flume at the UNAM facility. . . . . 47

3.2 UNAM experimental equipment arrangement. . . . . 49

3.3 Sediment grain size distribution of the gravel beach. . . . . 50

3.4 Schematic representation of the pressure transducer localisation during the testing at UNAM. . . . . 52

3.5 Pressure record for preliminary test. . . . . 54

3.6 Single-sided amplitude spectrum of P(t) for preliminary test. . . . . 55

4.1 Pressure response from four co-located pressure transducers (Pedrozo-Acuña et al. 2008). . . . . 76

4.2 Idealised pressure response of plunging impact event. . . . . 77

4.3 Single-sided amplitude spectrum of idealised pressure response. . . . . 78

4.5 Pressure response and associated Continuous Wavelet Transform . . . . 82

4.6 Pressure response and associated Continuous Wavelet Transform . . . . 84

4.7 Pressure response before and after CWTFT/ICWTFT . . . . . 86

4.8 Separated impulsive and pseudo-sinusoidal pressure responses, and re-combined signal . . . . . 87

4.9 Wave attenuation of fast and slow waves as a function of frequency (Chotiros 1995). . . . . 89

4.10 Application of pressure correction approach to GWK data . . . . . 94

4.11 Application of pseudo-sinusoidal pressure correction approach to GWK data . . . . . 95

4.12 Application of peak pressure correction approach to GWK data . . . . . 95
4.13 Example RMS of CWT coefficients for buried pressure transducer array across all scales considered . . . . . 99
4.14 Frequency vs. attenuation-correction . . . . . 100
4.15 Co-ordinate adjustment for profile measurements . . . . . 104

5.1 Sequence of six video frame captures describing a single swash event of a plunging breaker-type for test 20080617T110846. . . . . 109
5.2 Sequence of six video frame captures describing a single swash event of a collapsing/surging breaker-type for test 20080703T135742. . . . . 110
5.3 Cross-shore profile evolution for test 9. . . . . 111
5.4 Cross-shore profile comparison and morphological change between Test 9 Initial conditions and part 1. . . . . 112
5.5 Cross-shore profile comparison and morphological change between Test 9 part 1 and part 2. . . . . 113
5.6 Cross-shore profile comparison and morphological change between Test 9 part 2 and part 3. . . . . 114
5.7 Cross-shore profile comparison and morphological change between Test 9 part 3 and part 4. . . . . 115
5.8 Cross-shore profile comparison and morphological change between Test 9 part 4 and part 5. . . . . 116
5.9 Final berm crest chainage from baseline vs average wave height at breaking. 118
5.10 Final berm crest elevation above datum vs average wave height at breaking. 119
5.11 Final berm volume vs average wave height at breaking. . . . . 120
5.12 Integral-corrected sediment transport rates for Test 9. . . . . 122
5.13 Peak sediment transport rate for part 1 of each test vs average wave height at breaking. . . . . 124
5.14 Beach profile evolution for Test 7 (Plunging). . . . . 124
5.15 Beach profile evolution for Test 13 (Collapsing). . . . . 125
5.16 Experimentally observed and numerically predicted profile evolution for tests conducted at GWK (López de San Román Blanco 2003). . . . . 126

6.1 Example pressure response ratings, rated five (top left panel); rated four (top right panel); rated three (bottom left left panel); rated two (bottom right panel). Response rated as one are not shown. . . . . 128
6.2 Non-dimensional impact pressures vs the non-dimensional local wave height (Pedrozo-Acuña et al. 2008) . . . . . 131

6.3 Non-dimensional impact pressures vs. Iribarren (For three alternative wave cases). Pedrozo-Acuña et al. (2008). . . . . 133

6.4 Non-dimensional impact pressures vs. individual wave steepness (For three alternative wave cases). Pedrozo-Acuña et al. (2008) . . . . . 134

6.5 Non-dimensional impact pressures vs. breaking wave height. . . . . 135

6.6 Non-dimensional impact pressures vs. Iribarren number. . . . . 137

6.7 Non-dimensional impact pressures vs. wave steepness. . . . . 139

7.1 Indicative and hypothesised trends between non-dimensional impact pressure and Iribarren number . . . . . 153

B.1 Beach profile evolution for Test 7. . . . . 170

B.2 Beach profile evolution for Test 6. . . . . 171

B.3 Beach profile evolution for Test 8. . . . . 171

B.4 Beach profile evolution for Test 9. . . . . 172

B.5 Beach profile evolution for Test 10. . . . . 172

B.6 Beach profile evolution for Test 11. . . . . 173

B.7 Beach profile evolution for Test 12. . . . . 173

B.8 Beach profile evolution for Test 13. . . . . 174

B.9 Beach profile evolution for Test 14. . . . . 174

B.10 Beach profile evolution for Test 15. . . . . 175

B.11 Beach profile evolution for Test 16. . . . . 175

B.12 Beach profile evolution for Test 17. . . . . 176

B.13 Integral-corrected sediment transport rates for Test 7. . . . . 179

B.14 Integral-corrected sediment transport rates for Test 6. . . . . 180

B.15 Integral-corrected sediment transport rates for Test 8. . . . . 180

B.16 Integral-corrected sediment transport rates for Test 9. . . . . 181

B.17 Integral-corrected sediment transport rates for Test 10. . . . . 181

B.18 Integral-corrected sediment transport rates for Test 11. . . . . 182

B.19 Integral-corrected sediment transport rates for Test 12. . . . . 182

B.20 Integral-corrected sediment transport rates for Test 13. . . . . 183

B.21 Integral-corrected sediment transport rates for Test 14. . . . . 183

B.22 Integral-corrected sediment transport rates for Test 15. . . . . 184

B.23 Integral-corrected sediment transport rates for Test 16. . . . . 184

# Nomenclature

| | |
|---|---|
| $D$ | Thickness of sediment layer |
| $d_{50}$ | Median grain diameter of sediment sample |
| $E'_w$ | Bulk modulus of porous media |
| $f$ | Wave frequency |
| $G$ | Shear modulus |
| $g$ | Acceleration due to gravity |
| $H_0$ | Offshore wave height |
| $H_b$ | Breaking wave height |
| $H_i$ | Incident wave height |
| $H_s$ | Significant wave height |
| $h$ | Water depth |
| $h_b$ | Breaking water depth |
| $K$ | Sediment permeability |
| $k$ | Wavenumber |
| $L$ | Wavelength |
| $L_0$ | Offshore wavelength |
| $n$ | Porosity |
| $T$ | Wave period |
| $T_p$ | Peak wave period |
| $z$ | Depth below bed surface |
| $\alpha$ | Angle between current flow and incident waves |
| $\beta$ | Beach slope angle |
| $\eta$ | Vetical displacement of water surface |
| $\theta$ | Argument of the complex quantity $\lambda$ |
| $\theta$ | Shields parameter |
| $\theta_{cr}$ | Critical Shields parameter |
| $\theta_{\beta cr}$ | Slope-corrected critical Shields parameter |
| $\lambda$ | Wavenumber within the porous media |
| $\nu$ | Poisson's ratio |
| $\upsilon$ | Kinematic viscosity |
| $\tau$ | Instantaneous bed shear stress |
| $\tau_{cr}$ | Critical bed shear stress |
| $\tau_{\beta cr}$ | Slope-corrected critical bed shear stress |
| $\xi_0$ | Iribarren number |
| $\rho$ | Density of water |
| $\omega$ | Angular frequency |
| $\phi_i$ | Angle of repose of sediment |

# Acknowledgements

I would like to begin by relating my humble appreciation for all of those who have been invaluable in helping to bring this work to completion. Firstly I would like to thank my supervisors David Simmonds and Vanesa Magar for their patience and guidance throughout this work, and particularly in providing direction in times of adversity. I would also like to convey my appreciation for the assistance and advice offered by Dr. Adrián Pedrozo-Acuña throughout the work contained herein.

I gratefully acknowledge the support received through an Engineering and Physical Research Council scholarship, without which pursuance of this research would not have been possible.

I am indebted to Dr. Rodolfo Silva Casarin and Dr. Edgar Gerardo Mendoza Baldwin at the Universidad Nacional Autónoma de México for graciously allowing access to the laboratory facilities at the university, and for allowing me to spend time working with their research group. I would especially like to thank Ana Laura Meneses Fernández and Miguel Angel Delgadillo Calzadilla for their invaluable help in conducting the experimental work at UNAM.

The assistance by Dr. Belén López de San Román-Blanco in provided experimental data is thankfully recognised. The large scale tests in the Large Wave Channel (GWK) of the Coastal Research Centre (FZK) in Germany were supported by the European Community under the Access to Research Infrastructures action of the Human Potential Programme (contract HPRI-CT-1999-00101).

Thanks are due to my friends who offered support and advice in times of difficulty, and made my time studying an enjoyable experience, especially Peter, Daniel, Alexis, Corin and James.

Finally, particular gratitude is offered to my family. The support and constant love of my parents Anthony and Elizabeth provided stability throughout my studies, allowing me to follow my own path. I greatly thank my brother Simon and sister-in-law Mary, for proving to be a constant inspiration, and always offering humour when the opportunity arose.

In ever loving memory of Jimmy P.

# Authors declaration

At no time during the registration for the degree of Doctor of Philosophy has the author been registered for any other University award.

This study was financed with the aid of a studentship from the Engineering and Physical Sciences Research Council.

Relevant scientific seminars and conferences were attended, and work from this thesis was presented at one international conference, detailed below.

**Signed:** _____

**Date:** _____

**Publications** :

**Posters and conference presentations** :

**2010:**

32nd International Conference on Coastal Engineering, *Shanghai.* Oral presentation: **Laboratory Observations of Impacts on Coarse Grained Beaches.**

**Word count for the main body of this thesis:** 38400

# Chapter 1

# Introduction

Coarse-grained beaches are created through glacial and mountain weathering and as such are found in mid- to high-latitude regions, such as the United Kingdom, Ireland, Canada and the United States of America. The coarse-grained material forms a natural defence by creating a barrier beach protecting low lying land from inundation, or forming a beach in front of an eroding cliff.

Despite the abundant presence of coarse-grained and mixed sand and gravel beaches, and the high social, economic, and environmental importance of these locations, research into their behaviour remains limited when compared to the sandy environment. This is predominantly due to the difficulties associated with conducting monitoring programs on coarse-grained beaches caused by the high energy levels in the swash and surf zones, though recent studies continue to inform the research community (e.g. Butt and Russell (2000), Austin and Masselink (2006*a*), and *BARDEX - editorial* (2012)).

Management of the coastline in the United Kingdom has evolved in recent times, complicated by the shift away from coastal protection through hard defences, such as concrete seawalls and rock revetments, which had lead to an unnatural coastline orientation with expensive maintenance requirements, towards application of less artificial approaches. Adoption of 'soft' defence techniques, including beach renourishment and beach recycling, allows for a more natural form of defence that utilises the efficient and hydraulically-rough form characteristic of coarse-grained material.

With the increase in prevalence of coarse grain sediment as a defence (Moses and Williams 2008; Hoagland et al. 2012), it is important to understand how this sediment is mobilised and transported. This is necessary to assess whether a proposal is viable, and will provide a sufficient standard of protection to the assets behind the shoreline. The relevance of a more thorough understanding of beach dynamics for coastal management has been highlighted in recent research (López de San Román-Blanco et al. 2003; Mason and Coates 2001).

Gravel is sediment material that typically varies in size between 2mm-64mm, and tends to form beaches with a slope between 1:8 and 1:2 (Figure 1.1). This characteristic steep slope produces much narrower surf zones than those occurring on finer sand beaches, with a consistent breaker location very close to the shoreline.

*Figure 1.1:* An example pure gravel beach (Jennings and Shulmeister 2002).

Under wave action, sediment moves in both the long-shore and cross-shore directions. Long-shore motion is well documented; however the cross-shore movement of material

has received less attention, yet plays an equally important role in determining whether assets are at risk of flooding.

When exposed to wave action, gravel beaches experience morphological change, with the cross-shore steepening or flattening depending on the specific wave conditions the shoreline experiences. The steep slope formed by gravel beaches contributes to a very complex environment, distinguished by a high level of turbulence and sediment transport, and further complicated by a significant interaction between the swash zone and the water level within the beach. Understanding the processes acting here, and effectively modelling them is of high importance to coastal scientists and engineers. Such understanding has improved thanks to some significant recent developments (Buscombe and Masselink (2006), Hughes et al. (1997)).

The type of wave breaking that occurs on a beach is dependent upon the wave conditions and the beach slope. Battjes (1974) provided a classification system for wave breaking that has been widely adopted across the scientific community, with wave breaker type identified by the Iribarren number. The specific formulation of the Iribarren number, and associated limits indicating breaker type, are determined by the wave conditions adopted during calculation. The formulation by Battjes adopts the wave height at the beach toe for formulation, $\xi$, while the breaking wave conditions offer an alternative, $\xi_b$, where the Iribarren number is defined as:

$$\xi = \frac{\tan\beta}{\sqrt{\frac{H}{L_0}}} \quad or \quad \xi_b = \frac{\tan\beta}{\sqrt{\frac{H_b}{L_0}}}, \tag{1.1}$$

where $H$ is the wave height at the toe of the beach, $H_b$ is the wave height at breaking,

$L_0$ is the offshore wavelength, and $\tan\beta$ is the slope of the beach. On a beach of uniform slope the breaker type is estimated as follows:

- Spilling: $\xi < 0.5$ or $\xi_b < 0.4$
- Plunging: $0.5 < \xi_0 < 2.3$ or $0.4 < \xi_b < 2.0$
- Collapsing: $2.3 < \xi_0 < 3.2$
- Surging: $3.2 < \xi_0$

Fredsøe and Deigaard (1992) did not offer specific details for the transition of wave breakers between collapsing and surging breakers, but instead offers only an interface between plunging and surging breakers at $\xi_b$=2.0. To avoid confusion in this work, a single definition of Iribarren number is taken henceforth as $\xi_b$.

The steeper slope formed by gravel beaches discussed above tends to lead to lower values of $\xi_b$ and wave breaking through plunging breaker types. More details of wave breaking and its consequences are detailed in the next chapter.

The morphological response of gravel beaches to changing wave hydrodynamics is driven by many factors. Perhaps the most easily comprehended contributor to this morphological change is the asymmetry in the flow velocity between the uprush and backwash that occurs during swell conditions. Larger flow velocities are capable of entraining larger sediment particles, or a greater volumes of sediment, producing a variation between onshore and offshore transport. This results in a steepening of the beach face, and an increase in the crest level of the berm (Austin 2005). Figure 1.2 indicates a typical profile highlighting the key features found on gravel beaches.

The saturation of the swash zone also plays a significant role in the morphological response of beaches. The surf-zone of a beach can be classified as saturated or unsatu-

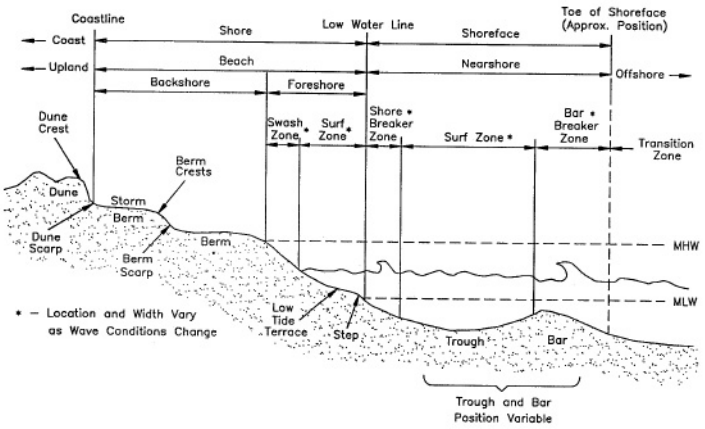


*Figure 1.2:* Typical beach profile (US Army Corps of Engineers 2012).

rated, determined by the dissipation of incident wave energy in the surf-zone. Saturated beaches possess an inner surf-zone with wave height and energy independent of the incident wave height and energy (Miche (1951), Battjes and Janssen (1978), and Thornton and Guza (1983)). This will typically occur on shallower slopes where incident waves are dissipated over a long distance, providing stable conditions at an inner surf-zone location. Conversely on a steeper slope, the surf-zone can be very narrow, offering little opportunity for wave energy dissipation, and permitting the transmission of short wave bores to the shoreline (Hibberd and Peregrine (1979) and Hughes (1992)). These short wave frequency hydrodynamics are significantly different from the hydrodynamics found on beaches with saturated surf-zones, where swash motions are dominated by long waves (Aagaard and Hughes 2006; Karunarathna and Chadwick 2007), resulting in different sediment transport regimes and profile development.

The specific sediment properties of the beach material play a critical role in the response of a beach to hydrodynamic conditions. Clearly the size and mass of the individual sediment particles is a key determinant in whether they become mobilised, but the porosity also plays a very significant role in the rate of infiltration/exfiltration, which determines the volume and velocity of water in the uprush and backwash phases.

Higher groundwater levels within the beach can occur during longer storm events, or periods of higher rainfall (or high lagoon water levels behind the beach for barrier beaches). This higher groundwater level offers a reduced volume into which infiltration can occur, resulting in a larger volume of the uprush returning seawards in the subsequent backwash event. This lessens the flow velocity asymmetry in the swash zone and can result in a reversal of the net transport direction (Jamal 2011).

The steepening of the cross-shore profile of a gravel beach under wave action is caused by the larger comparative onshore transport than offshore transport. The asymmetry of this transport produces a distinctive step below the still water level, responsible for inducing wave breaking, and a berm above the water level with a crest elevation determined by the run-up limit (Figure 1.2).

The modelling of this evolution has been limited, as research into the cross-shore movement of sediment has predominantly concentrated on fine-grained material. This has proved useful as a starting point for coarse-grained beaches, but there are several deficiencies in the direct application of such theories to the environment posed by coarse material, such as the more complicated flow regime and beach interactions on the steeper, porous beach. The development of these theories conducted in recent years has increased understanding of sediment movement on coarse-grained beaches (Pedrozo-Acuña et al. (2008) and Jamal et al. (2010)). However the models adapted and large-scale experiments performed still show discrepancies between predictions and observations of cross-shore profile evolution.

One of the potential contributors to the discrepancy in the observed and modelled cross-shore profiles is the large pressure generated by plunging breaker impacts in mobilising additional sediment for transportation. The role of these plunging impact pressures

on the cross-shore profile evolution of gravel beaches will be investigated to establish whether this may be responsible in part for the observed differences in profiles.

This thesis is organised as follows. Chapter 2 presents a description of the physical processes involved in cross-shore profile evolution, reviews the existing numerical modelling approaches for morphological response, outlines the limitations of these previous approaches, and offers the intentions of the research. Chapter 3 outlines the physical experiments conducted, and provides details of the sediment characteristics utilised in the tests. Chapter 4 describes the analytical techniques used in the transformation of data for analysis, and presents an approach for the handling of signal attenuation experienced by the buried pressure transducers. Chapter 5 presents the beach profile results (with fuller details available in Appendix B) and an investigation of the morphological response and estimated sediment transport rates. Chapter 6 presents pressure responses under wave breaking, with analysis of the effect of significance of wave impact events. Discussions and conclusions of the of the experimental programme and analysis procedures is provided in Chapter 7. Finally Chapter 8 presents recommendations for future work in the field of study.

# Chapter 2

# Processes that Shape Gravel Beaches

Morphological change of beaches in the nearshore is controlled by a wide range of processes and parameters, but generally the nearshore hydrodynamics of gravel beaches are controlled by the swash zone (Buscombe and Masselink 2006). The importance of the surf zone can become more prevalent for shallower-sloped sand beaches, or on steep-sloped gravel beaches during storm events with a more active sea state.

The swash zone is defined by the area of the beach enclosed by the run-up limit of the swash and the run-down limit of the backwash (Figure 2.1). As the water level varies throughout a tidal cycle and the wave conditions vary, the location of the swash zone constantly changes, causing continual alteration of the beach profile. This area is highly important for the transportation of sediment, and it is therefore highly desirable to understand the processes taking place and to model them accurately. Pedrozo-Acuña (2005) concluded that the majority of the profile change occurs in the swash zone, both above and below Still Water Level (SWL).

The surf zone is the area between the wave breaking point and the swash zone, and experiences the transfer of irrotational motion of deep water waves to a variety of different wave motions, such as swash uprush and backwash, edge waves, and undertow, through wave breaking.

The sediment that forms a beach plays a significant role in the specific beach profile, and

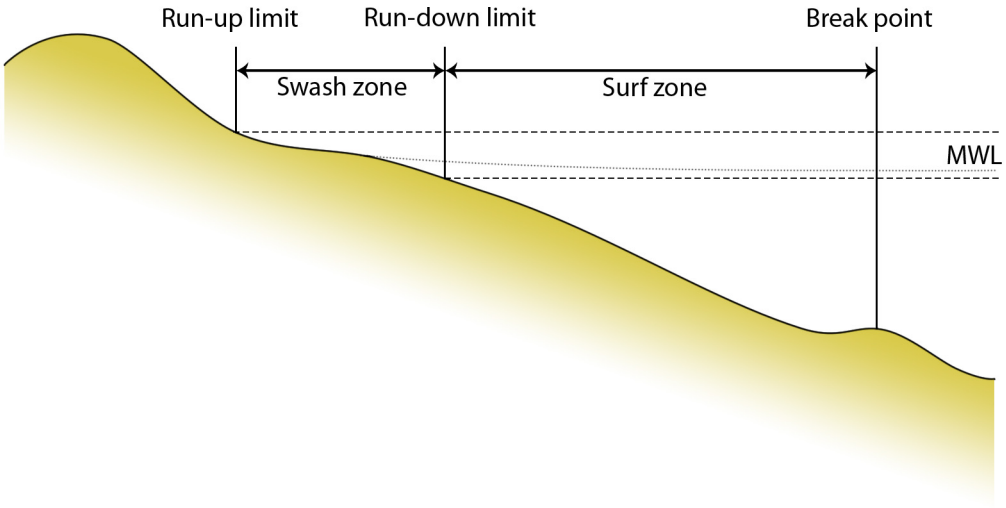


*Figure 2.1:* Swash and surf zone definition.

the location and size of the surf and swash zones. Beaches can be divided into four broad categories (Simm et al. 1996): sand, gravel/sand mixed (spatially uniform distribution for sand and gravel components), gravel upper/sand lower (gravel forming a steep slope on the upper foreshore overlying sand on a shallow sloping lower foreshore), and purely gravel. Each of these beaches forms significantly different equilibrium profiles in the natural environment, as follows:

- sand beaches form a shallow slope that encourages wave breaking over a large area (beach slope, $\tan\beta$, between 0.01 and 0.1)
- sand/gravel beaches form an intermediate slope ($\tan\beta$ between 0.04 and 0.12) (Jennings and Shulmeister 2002)
- gravel upper/sand lower beaches has two distinctly different components with a shallower sand slope in the lower region ($\tan\beta$ between 0.03 and 0.1), and a steeper gravel slope on the upper beach ($\tan\beta$ between 0.1 and 0.15)
- gravel beaches form very steep slopes ($\tan\beta$ between 0.1 and 0.25)

Each of these beach types will experience different hydrodynamic conditions and breaking locations. According to the general relationship proposed by McCowan (1894) the ratio of wave height and water depth at the breaking location, $H_b$ and $h_b$ respectively, is generally assumed constant,

$$\gamma = H_b/h_b = 0.78. \tag{2.1}$$

However, $\gamma$ can vary depending on other parameters such as beach slope and wave steepness, though generally retains a value between 0.7 and 1.3. The shallower slope created by finer sediment sand beaches will encourage wave breaking to occur relatively further offshore than steeper sloped beaches. Any variation in individual wave heights will cause a variation in the breaker location, and will result in waves breaking over a wide area. The intermediate slope of sand/gravel beaches causes waves to break closer to the shoreline than the finer sand slopes, with a more consistent breaker location. The steep slope present in gravel beaches shortens the area in which waves of different height break, providing a consistent breaking location close to the shoreline. The gravel upper/sand lower beaches exhibit a more complicated wave breaking regime, dependent on tides and wave conditions. During lower tides the beach will act similarly to the pure sand beach with a wide breaking area far from the shoreline, while at higher tidal levels, the breaking tends more towards a gravel beach scenario.

Mixed sand and gravel (MSG) beaches cannot be simply characterised by a single sediment parameter (such as $d_{50}$) as occurs in many numerical models, and they possess a relatively lower porosity than either sand or gravel beaches as the voids between the larger particle constituents can become filled by the finer sand component. There is a difference in the hydrodynamic conditions and transport processes between MSG and gravel beaches, therefore the study of MSG beach environments are outside the scope

of this work.

The majority of the previous research conducted regarding profile evolution pertains to sand beaches, largely due to the simpler internal flow regime and wave conditions (Dean 1991; Butt and Russell 2000; Holland and Puleo 2001; Butt et al. 2002; Jayaratne and Shibayama 2011). Recently attention to gravel beaches has increased (Pedrozo-Acuña 2005; Austin and Masselink 2006*a*; Jamal 2011; Kobayashi et al. 2011) with modelling accuracy showing incremental improvement. Accurate modelling of gravel beach morphological change is dependent on an understanding of the processes taking place in the swash zone.

## 2.1 Nature of swash

The hydrodynamics of the swash zone can be broadly described as a series of swash cycles, each composed of two phases, with variation in the depth of water above the beachface, or swash lens. The first phase of each cycle, the uprush, is the onshore directed swash lens, while the second phase, the backwash, is the down-slope swash movement in an offshore direction (Hughes and Baldock 2004). These swash flows follow a generally oscillatory pattern driven by the incident wave conditions, with flow deceleration and acceleration during the two phases.

The uprush phase is characterised by a high degree of turbulence due to bore collapse, and experiences deceleration in flow velocity as the swash lens propagates onshore. The high level of turbulence in the uprush phase helps retain and entrain sediment within the water column, increasing the suspended sediment load during this phase of the swash cycle. After flow reversal and the commencement of the backwash phase, the bore turbulence has largely dissipated and, along with a reduction in the swash volume through infiltration, the swash returns seaward through an accelerating sheet flow, producing a more bedload dominated flow (Masselink and Puleo 2006). This general tendency can

be affected by fluctuations in wave energy during storm events or higher groundwater levels, which alters the hydrodynamics and can lead to erosion above the SWL.

A crucial observation at this stage is that the backwash is not a simple reverse of the uprush, creating an asymmetrical process (Hughes et al. 1997). This asymmetry helps to drive the asymmetric cross-shore transport rates on beaches of all types, however it is the specific details of how this asymmetry is exhibited that produces the variation in profile development across a range of sediment sizes. If the backwash is the more dominant phase of transport, erosion may occur above the SWL with deposition below, while on steeper beaches the uprush can dominate leading to erosion below and accretion above the SWL.

### 2.1.1 Sediment transport

Sediment transport is broadly separated into two alternative transport modes; suspended sediment transport and bed load transport, although sheet flow is sometimes counted as a separate transport form from bed load. Suspended sediment is the transportation of individual particles held in suspension within the water column. Clearly to entrain sediment either the particles must be small, or the flow rate must be high. This form of transport therefore plays a significant role on sand beaches where the particle size is sufficiently small (Reeve et al. 2004), however on gravel beaches the individual particles are often too heavy to be held in suspension for a significant period of time.

The predominance of different transport modes in different phases of a swash event was noted by Horn and Mason (1994), who observed an increased prevalence of bed load transport in the backwash phase. Bed load transport was also the overall dominant mode of transport in the majority of the limited beaches investigated in this work.

A description of the transport modes and what influences them is given in the following

sections.

#### 2.1.1.1 Suspended sediment transport

Pritchard and Hogg (2005) investigated suspended sediment transport, concentrating their efforts on addressing an observation of net onshore transport despite the tendency for offshore transport created by the difference in onshore and offshore flow velocities. Two main mechanisms of increasing onshore transport were identified and explored; pre-suspended sediment entering the swash zone from bore collapse, and settling lag. While for coarse-grains the relevance of settling lag is diminished, pre-suspended sediment can play a key role, particularly as the steeper sloped beaches formed by this coarse sediment induces breaking with higher turbulent energy levels. Pre-suspended sediment is likely to settle before the commencement of the backwash, contributing to the observed difference in transport modes in uprush and backwash phases.

Suspended sediment within the swash zone can be separated into sediment derived from two sources: pre-suspended sediment from the surf zone, advected into the swash zone; and locally suspended sediment within the swash zone due to the swash-swash interaction. While sediment particles remain in suspension they are transported in the direction of swash flow.

Reeve et al. (2004) indicated that the settling velocity is a useful parameter in determining whether particles are transported as suspended load or as bed load. On steep gravel beaches, the large sediment particles tend to have a high settling velocity so they can only stay in suspension if the turbulent energy level and the flow rate are high. As the uprush propagates up the beachface the flow decelerates and the fluid volume is reduced, encouraging the particles to fall out of suspension. During the backwash phase, the flow accelerates with an increasing turbulence level throughout, which in turn increases the potential for suspended transport. However, the lack of suspended

sediment at the start of this phase means that the total suspended volume remains low.

At present it is not possible to quantify the volume of suspended sediment advected into the swash zone due to bore collapse, though developments are being made in this area (Jensen et al. 2010). As the onshore distance this sediment is transported is also unclear, most researchers consider the volume of sediment to be negligible on gravel beaches and consider swash zone transport to occur through the bed load mode.

#### 2.1.1.2 Bed load transport

Bed load transport is transport of material through sliding, rolling, and jumping (saltation) of sediment, where the particles are in contact with the bed surface during movement (Fredsøe and Deigaard 1992). Sheet flow occurs when turbulent fluid flow generates sufficiently high shear stresses to overcome the local morphological character of the beach and transports a large, highly concentrated, volume of sediment in a fluid-like flow (Hsu et al. 2004).

Incipient motion of near bed sediment can be parametrised with the Shields parameter, $\theta$, (Shields 1936), defined as

$$\theta = \frac{\tau}{(\rho_s - \rho) g d_{50}}, \tag{2.2}$$

where $\tau$ is the instantaneous bed shear stress, $\rho_s$ is the sediment density, $\rho$ is the water density, $g$ is the acceleration due to gravity, and $d_{50}$ is the mean grain diameter of the beach sediment.

The relationship presented characterises the sediment with a single parameter, $d_{50}$, which introduces the possibility of underestimation or overestimation of the threshold

of motion depending on the specifics of the grain size distribution. Further, the Shields parameter was initially derived for steady, unidirectional flow, and therefore may not accurately represent peak flow rate in a bidirectional environment.

Despite these concerns, the Shields parameter has proven useful, and is often adopted in bed-load sediment transport models to determine incipient bed motion. When the instantaneous shear stress exceeds a critical value, the Shields parameter exceeds a threshold value ($\theta > 0.03 \sim 0.06$) and the motion of the sediment commences (Zyserman and Fredsøe 1994). Further increase beyond this initial threshold results in the development of morphological features such as ripples, while exceedance beyond a second threshold value ($\theta > 0.8 \sim 1.0$) leads to the onset of sheet-flow transport (Foster et al. 2006).

The critical Shields parameter is the effective Shields parameter at which point sediment begins to move, and can be calculated according to Equation 2.3. This relationship is applicable for steady flow, with finer sediment material, however the coastal environment has a significantly more complicated flow regime due to the oscillatory swash flow and bore turbulence (Fredsøe and Deigaard 1992).

$$\theta_{cr} = \frac{\tau_{cr}}{(\rho_s - \rho) g d_{50}} \tag{2.3}$$

The critical Shields parameter was related to a dimensionless grain diameter, $D_*$ (Soulsby 1997)

$$D_* = \left[\frac{g(s-1)}{\upsilon^2}\right]^{1/3} d_{50}, \tag{2.4}$$

where $s = \rho_s/\rho$ is the relative density, and $\upsilon$ is the kinematic viscosity of water. The threshold of motion of sediment under a series of wave and current conditions were

investigated, and an expression for the Shields threshold curve for this data based on the dimensionless grain parameter was presented by Soulsby and Whitehouse (1997):

$$\theta_{cr} = \frac{0.3}{1+1.2D_*} + 0.055[1 - exp(-0.02D_*). \tag{2.5}$$

Unfortunately the bed slope remains unaccounted for in these works, and while its role on fine-grained shallower slopes may be negligible, the significance of the slope plays a key role in sediment motion on rippled beds and steeper gravel beaches. The modification presented in Equation 2.6 can be introduced to account for the influence of the bed slope on the critical Shields parameter.

$$\frac{\theta_{\beta cr}}{\theta_{cr}} = \frac{\tau_{\beta cr}}{\tau_{cr}} = \frac{\sin(\phi i \pm \beta)}{\sin \phi i} \tag{2.6}$$

where $\theta_{\beta cr}$ is the slope corrected critical Shields parameter, $\tau_{\beta cr}$ is the slope corrected critical shear stress, $\phi_i$ is the angle of repose of the sediment and $\beta$ is the beach slope angle. The $\pm$ sign in Equation 2.6 indicates the direction of motion, with positive sign adopted for sediment moving up slope, and minus sign used for sediment moving down slope.

This slope-corrected Shields parameter is used to determine the dimensionless cross-shore transport, $\Phi_x$, given by $\Phi_x = max(\Phi_{x1}, \Phi_{x2})$, with $\Phi_{x1}$ and $\Phi_{x2}$ given by Soulsby and Damgaard (2005).

$$\Phi_{x1} = C_t \theta_m^{0.5} (\theta_m - \theta_{\beta cr}) \tag{2.7}$$

and

$$\Phi_{x2} = C_t (0.9534 + 0.1907 \cos 2\alpha) \theta_w^{0.5} \theta_m, \tag{2.8}$$

where $C_t$ is the sediment transport coefficient based on sediment material, $\alpha$ is the an-

gle between current flow and wave propagation (taken as 0°), and $\theta_m$ and $\theta_w$ are the dimensionless Shields parameters for the mean shear stress and the wave shear stress, respectively.

Finally $\Phi_x$ can be used to quantify the sediment transport, estimated according to equation

$$Q_b = \Phi_x[g(s-1)d_{50}^3]^{0.5} \tag{2.9}$$

The approach described above, outlined by Soulsby and Damgaard (2005) and adopted by Jamal (2011), allows determination of the conditions necessary for motion on a sloped coarse-grained beach, and the subsequent sediment transport. It is clear that the specific characteristics of the sediment particles, the shear stress exerted on them, and the local beach slope are crucial in determining whether sediment is transported as bed load.

Bakhtyar et al. (2009) highlighted that while the application of Shields-based models are accurate for unidirectional flow, they do not include the inertial forces of the sediment particles that may be large for gravel material (Baldock and Holmes 1997). Some researchers have made attempts to include these additional complexities in bedload transport (Jenkins and Hanes 1998; Hsu 2002; Hsu and Hanes 2004), however the significance of the inertial forces have also been questioned (Soulsby and Damgaard 2005).

### 2.1.2 Interactions with porous beds

The processes responsible for the formation and morphological change of gravel beaches are not fully-understood, with additional work necessary to provide this further understanding (Masselink and Buscombe 2008). While the main concern for this project involves the interactions within the swash zone, it is well reported that transport can occur across a much wider nearshore zone. During calm conditions the sediment trans-

port is largely restricted to the inner surf and swash zone, yet during more active storm conditions the transport widens into the full surf zone.

Surf and swash zone processes have been reviewed a number of times by a range of different researchers (Butt and Russell 2000; Mason and Coates 2001; Elfrink and Baldock 2002; Masselink and Puleo 2006; Bakhtyar et al. 2009) with good agreement over which processes are important to morphological change.

Work by Masselink and Hughes (1998) investigated the flow velocity and sediment transport on a natural beach. The sediment load and time-averaged velocity cubed displayed a strong relationship, consistent with bed-load transport equations. Masselink and Hughes (1998) concluded that sheet-flow transport predominates in the swash zone, and attributed the difference in uprush and backwash transport to the difference in processes active in each phase. The processes considered to be relevant were: the differences caused by accelerating and decelerating flow, interactions between swash and groundwater, and the higher suspended sediment concentrations not included in the adopted models.

Previously conducted field investigations on high and low energy beaches were reviewed by Butt and Russell (2000), who highlighted that swash on steep reflective beaches is dominated by high frequency oscillations. They indicated that suspended sediment transport concentrations are 3 to 9 times higher in the swash than in the inner-surf zone on such beaches, and recognised the importance of groundwater interactions on gravel beaches.

Elfrink and Baldock (2002) identified four main criteria of the swash hydrodynamics that affect sediment transport:

- Boundary conditions
- Swash zone characteristics, forcing mechanisms and shoreline oscillations
- Internal flow kinematics and turbulence
- Bed boundary layer, percolation and groundwater

The specifics of whether the swash zone is dominated by infragravity energy or short wave energy is determined by the long and short wave energies in the surf zone, which are in turn determined by the offshore wave conditions. The boundary conditions, taken at the inner surf zone, are therefore dependent on the saturation level of the surf zone and how the relevant wave components are affected as they propagate shoreward. Elfrink and Baldock (2002) proposed that the transition between saturated and unsaturated surf zones may be approximately defined with use of $\xi_b$.

Shoreline oscillations are mainly driven by non-breaking standing waves at infragravity frequencies, and broken short waves (bores) at wave frequencies, with the magnitudes largely governed by $\xi_b$ (Madsen et al. 1997). However, Elfrink and Baldock (2002) noted the complication that infragravity wave amplitude is generally linearly related to the incident wave height and therefore may not be determined by $\xi_b$, instead precipitating a more site-specific relationship between infragravity swash oscillations and $\xi_b$. Elfrink and Baldock (2002) further noted that for monochromatic waves, the lack of infragravity energy causes all cases to be dominated by short wave energy, irrespective of $\xi_b$.

The flow kinematics during swash events are typified by high flow velocities in both the uprush and backwash phases. Masselink and Hughes (1998) showed that although the peak and mean velocities were similar in both phases of a swash event, the duration of the uprush phase is shorter than the backwash, as divergent flow commences before the maximum run-up level is reached, thus increasing the duration of the backwash and causing a disparity in the durations of transport in opposing directions. If the duration

of the uprush and backwash event is larger than the incident wave frequency, significant interaction between subsequent swash events can occur. This swash-swash interaction introduces significant turbulence and is responsible for the formation of the submerged beach step.

The exchange of water between the ocean and the groundwater within the beach matrix influences the transport of sediment by introducing asymmetries between the conditions in the uprush and backwash phases of the swash through a number of potential processes. These processes are discussed in detail later.

Masselink and Puleo (2006) highlighted the differences that are present in the uprush and backwash phases of the swash. The uprush is dominated by the dissipation of bore and swash-swash generated turbulence, while the backwash is dominated by boundary layer induced turbulence. The different turbulent dissipation in the uprush and backwash phases causes sediment to be transported through different modes in each phase, with increased suspended sediment transport during the uprush, and a bed load dominated backwash transport.

Masselink and Puleo (2006) also identified a number of parameters that may partially account for the dominance in offshore swash transport in numerical models caused by the offshore directed velocity skewness, which required further investigation. These included in/exfiltration effects, flow acceleration, bore turbulence, settling lag, scour lag and sediment advection from the surf zone. Although these processes have been subsequently studied to various degrees, there remains uncertainty in the comparative contribution of these effects.

A recent full scale experimental programme was conducted to investigate the physical behaviour and response of a barrier beach to a range of hydrodynamic conditions

(*BARDEX - editorial* 2012). A large homogeneous barrier beach was constructed from gravel material at the Delta Flume in the Netherlands, and subjected to random wave conditions with various water elevations and tidal influences (Williams et al. 2012a). A range of measurements were recorded, including turbulence, run-up, bed morphology, and groundwater table.

The data collected in this experimental programme was used in a number of studies and analysed by a range of researchers. This subsequent analysis is discussed in the following sections.

In summary there are have been a number of reviews and studies over the previous decade that have drawn attention to the processes relevant to sediment transport and morphological change on gravel beaches. These processes are handled individually in the following sections.

#### 2.1.2.1 Turbulence and Wave Breaking

A measure of the degree of turbulence in the swash zone can be provided through consideration of the turbulent kinetic energy (TKE), the mean kinetic energy per unit mass associated with eddies. Elfrink and Baldock (2002) and Masselink and Puleo (2006) describe multiple sources of turbulence within the swash zone, acting in both onshore and offshore directions. The most obvious source of turbulence is generated by bore collapse due to wave breaking, propagating in a shoreward direction. There is also turbulence generated at the bed through frictional processes, and the possibility of offshore advected turbulence through generation of hydraulic jumps at the base of the swash zone.

Laboratory experimentation has enabled study of turbulence within the swash zone, for example Yeh et al. (1989), where it has been observed that turbulent energy advection operates in a net onshore direction. Bore-generated and bore-advected turbulence dom-

inates the uprush phase of swash motion, while the backwash phase is dominated by turbulence created by the growing boundary layer.

Field studies have also provided evidence of the significance of turbulence in the swash and surf zones. Flick and George (1990) measured high frequency oscillations, and found that the turbulence length scale is related to the bore height as well as the local water depth. Butt et al. (2004) estimated suspended sediment concentrations and TKE during bore propagation, observing almost simultaneous peak levels in both records, suggesting bore turbulence is responsible for suspension of sediment. However the suspended sediment concentration were significantly reduced after peak TKE, which was interpreted to indicate a rapid settling of sediment behind the bore. It is also possible that advection of the suspended sediment to a more onshore location could have occurred.

As mentioned in chapter 1, the specific details of the wave breaking process is determined by the incident wave conditions and the beach slope, and these parameters can be used to classify the type of breaking through the Iribarren number, $\xi_b$ (Equation 1.1). Incident waves are not completely dissipated by the wave breaking process, with a portion of the wave energy reflected seaward. The degree of reflection is dependent on the type of wave breaking and therefore the beach slope and beach sediment.

As previously mentioned, sand beaches typically form very shallow slopes which encourage wave breaking across a very wide area. The very shallow slope of the sand beach means wave breaking tends to occur through spilling breakers, resulting in a small decrease in wave height. The smaller wave subsequently also becomes depth limited, and experiences further breaking through the spilling mechanism. This process continues until the wave reaches the shoreline. This continuous breaking across a large area provides only a small opportunity for reflection of energy.

The steep slope typical of gravel beaches permits the fulfilment of the depth limited breaking condition only at locations close to the shoreline. This narrow breaking area offers less opportunity for dissipation of wave energy, allowing generation of larger reflected waves. According to Equation 1.1, steep beaches will provide larger Iribarren numbers and thus exhibit breaking through non-spilling breaker types.

Research regarding turbulence within the surf zone has been widely considered in recent decades (Stive 1980; Mizuguchi 1986; Ting and Kirby 1994, 1995) indicating the level of turbulence is dependent on the type of breaking present. This turbulence, present throughout the surf and swash zones, complicates the hydrodynamics and plays a significant role in sediment transport. The turbulence velocities can be calculated through Particle Image Velocimetry, and this allows the determination of the TKE distribution (Chang and Liu 1997).

Ting and Kirby (1995) utilised a phase-averaging approach, which was used to investigate the horizontal turbulence velocities throughout the water column. This approach indicated that for spilling breakers the horizontal turbulence velocities varied strongly in time close to the trough region, yet remained fairly stable throughout the lower portion of the water column. For plunging breakers, however, the horizontal turbulence velocities varied in time throughout the entire water column, suggesting the plunging jet penetrates a significant distance beneath the water surface, and introduces turbulence throughout the entire depth. This finding again underlines the potential significance of the plunging breaker type to sediment mobilisation and transport.

Turbulent energy is higher in the uprush than in the backwash, as the collapse of the incoming bore of a wave introduces a significant amount of turbulence, which remains present in the uprush but has begun to dissipate in the backwash (Puleo et al. 2000).

Further, the interaction between the backwash of one wave and the uprush of the subsequent incoming wave generates a high level of turbulence, and this helps in the mobilisation of sediment, and will therefore play an important role in sediment transport and the development of the cross-shore beach profile.

Chanson and Jaw-Fang (1997) conducted a series of experiments in a two-dimensional flume, investigating the characteristics of the plunging jet caused during plunging breakers, and the entrainment of air bubbles during these events. They catalogued air bubble entrainment at depths of up to twice the wave amplitude below the water surface, and highlighted the tendency for bubbles to be temporarily trapped due to vortical motion before motion toward the surface due to buoyancy. With consideration of Equation 2.1 this research indicates turbulence is likely to propagate to the bed and may be responsible for the entrainment of sediment into suspension.

Puleo et al. (2000) studied the effect of turbulence on sediment transport within the swash zone of a shallow-sloped sandy beach. This work indicated that turbulent effects from wave breaking were transmitted in the uprush phase to the seabed, and helped to maintain high suspended sediment concentrations. Although the beach material in the work was finer than the coarse-grained material studied here, the findings may still be relevant to coarse-grained beaches. The turbulence will be transmitted to the seabed irrespective of the type of bed material and, though the coarse particles are larger and less susceptible to suspended sediment transport, the turbulence will help to maintain any sediment already in suspension, and aid the motion of sediment through saltation or rolling.

#### 2.1.2.2 Groundwater dynamics

The beach groundwater level is defined as the mean surface within the beach material where the mean porewater pressure is zero (Nielsen 1997). The groundwater level of

the beach is a highly important interface that influences the response of a beach to wave action. Incoming waves contribute to groundwater level fluctuations in two ways. Firstly there is an instantaneous water level change generated via the pressure transfer through saturated sediment, and secondly a delayed groundwater level increase due to the infiltration/exfiltration of swash run-up.

The instantaneous change in groundwater elevation has been well documented and was observed in the mid-1970's (Waddell 1973), while the second, lagged fluctuation was observed much later (Hegge and Masselink 1991). The exit point of the beach is the point at which the groundwater level meets the beach surface. Hegge and Masselink (1991) proposed that the dominance of pressure forces or the lagged infiltration is determined by the location of the exit point. Below the exit point the transfer of pressure for an incoming wave is passed directly to the water within the beach, and causes an increase in the groundwater level. In the area above the exit point, water infiltrates into the beach, preventing an instantaneous increase in groundwater level, resulting in a time differential between maximum uprush and maximum groundwater level. The delay between the maximum uprush and the increase in groundwater elevation was of the order of 4-5s and was attributed to the time taken for the water to flow through the beach (and slowed due to the friction with sediment particles). It is clear that the lower the groundwater level within the beach the more the second lagged response will dominate the overall groundwater response. The measurement of the exact position of the watertable was not possible in these experiments, instead the location was estimated with the use of pressure transducers spaced along the cross-shore profile. Nielsen et al. (1997) highlighted a deficiency in this approach by indicating that the pressure measurement does not represent the watertable in unsaturated conditions, but instead provides a measure of the non-hydrostatic pressure at the depth of the transducer. The non-hydrostatic pressure is attenuated through the dynamic interaction with the porous beach material.

The decoupling of the swash front and the watertable within the beach has been discussed by a number of researchers (Turner 1993; Baird et al. 1998; Horn 2002), with a useful graphical representation provided by Austin and Masselink (2006*b*), who also identified two pathways through which water can enter the beach and impact the watertable. Figure 2.2 shows a series of images indicating the alternative pathways for infiltration of swash water into the unsaturated section of the beach.

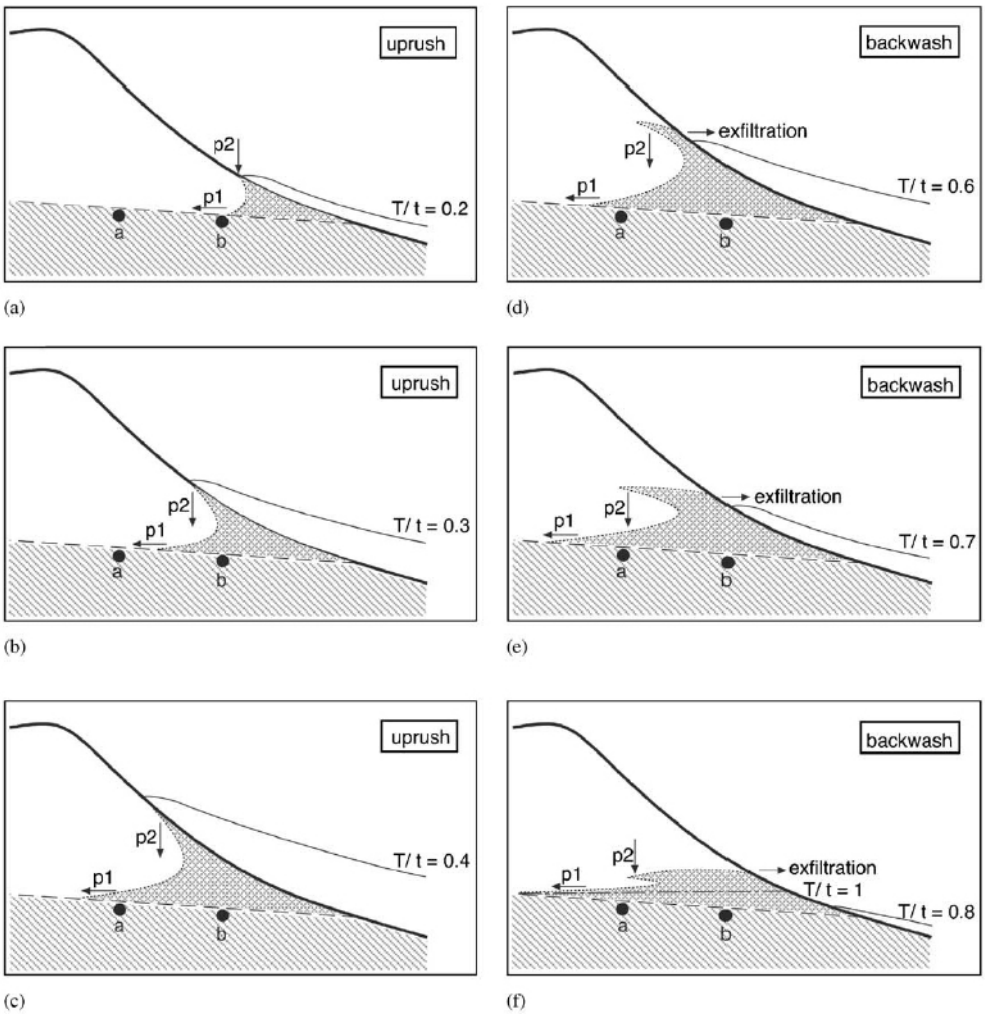


*Figure 2.2:* Swash water infiltration through pathways 1 and 2 (Austin and Masselink 2006*b*).

Pathway 1 occurs on the lower section of the beach where decoupling of the exit point and the swash edge occurs. As water flows up or down the beach it creates a difference

in elevation between the swash and the watertable, generating a difference in head and inducing the exchange of water, which progresses inland along the phreatic surface (the location where the pore water pressure is under atmospheric conditions). This continues until the exit point and the swash front reconnect and the flow of water between the two bodies ceases. Austin and Masselink (2006*b*) state the fluctuations resulting from this behaviour cannot be the result of vertical infiltration of the beach as there is no synchronous swash overtopping with the watertable fluctuations.

Pathway 2 occurs in unsaturated conditions. As the swash front runs up, the beach water enters the beach through pathway 1. However, the frictional resistance provided by the beach material causes disconnection of the swash front and the watertable which remains until the end of the uprush when they reconnect. The flow reverses and the swash front and watertable again disconnect, leaving a volume of water suspended in the beach that flows vertically into the beach towards the watertable. This second pathway only occurs under large swash events where the development of the suspended tongue of water is generated. Austin and Masselink (2006*b*) further highlighted that these pathways are not yet confirmed as the water elevations cannot be directly measured over the large area by pressure transducers.

It is well noted that beaches act as low-pass filters permitting only lower frequency wave components to impact the watertable within the beach. This filtering effect allows only the longer period swash events to be transferred through the beach matrix and affect the groundwater behaviour further landward.

It is not entirely clear what influences the presence or frequency of the filter behaviour, though Hegge and Masselink (1991) proposed the beach face slope, hydraulic conductivity, tidal stage and observation point (relative to the shoreline) would all play a significant role in determining the cut-off frequency of the filter.

It is also widely accepted that groundwater response on coarse-grained beaches occurs principally at incident frequencies on the lower beach yet shifts to lower frequencies moving inland, consistent with observations made on sandy beaches (Emery and Gale 1951; Waddell 1973; Hegge and Masselink 1991; Horn 2002).

Turner and Masselink (2012) described the importance of back-barrier lagoon level in the determination of the beach watertable and the net flow through the beach. A raised water level in the lagoon was observed to increase water flux through the beach towards the ocean, while a transition to lower lagoon level created a reduction and subsequent reversal in fluid flow direction. With wave action, and initially equal ocean and lagoon water levels, a mounding of the groundwater was observed with a net shoreward flow. As the through-flow of water adjusted the seaward interface location, and hence setup, Turner and Masselink (2012) concluded that when determining the seaward boundary conditions while modelling the groundwater flow within beaches, it is not appropriate to adopt simple fixed-head condition defined by an empirical relationship dependent on wave conditions only.

#### 2.1.2.3 Infiltration and exfiltration

Bagnold (1940) suggested that infiltration plays a significant role in sediment transport and morphological change. Since his seminal research, the role of infiltration in these areas has been investigated further, and it is widely recognised that it it plays a key role in the asymmetry of swash transport.

Infiltration on a beach is most likely to occur during a rising tide. Prior to an increase in water elevation during a rising tide, a beach possesses a relatively low groundwater level and therefore has the capacity to accommodate additional water, resulting in an increase in the groundwater level. During a falling tide the capability of the beach to ac-

commodate additional water is much less and therefore infiltration is likely to be lower. Obviously the difference in elevation between the groundwater level and the water level of the incoming swash is not the only factor in determining the rate of infiltration. It is well documented that sediment size (and associated hydraulic conductivity) plays an important role in determining the rate and amount of water infiltrating the beach.

Infiltration also occurs on the saturated section of the beach, though depending on the phase of the uprush/backwash cycle, exfiltration can also occur in this area. Infiltration and exfiltration of this nature has undergone significant research recently, while direct infiltration above the exit point has received very little. This is mainly due to the technical difficulties with measuring the volume of water entering the beach above the exit point. Measurement of infiltration and exfiltration below the exit point has traditionally been carried out on fine-grained beaches, and involves the measurement of vertical pressure gradients with a vertical array of pressure transducers. Flow is assumed to adhere to Darcy's Law of flow through a porous medium. This is an expression of the conservation of momentum, and Darcy's equations are adopted to estimate the infiltration and exfiltration rates, along with the vertical flow velocity. This technique has proved reasonably successful for application on fine-grained beaches, however when applied to coarse-grained beaches the assumption of Darcian flow can break down. Due to the low rate of flow within fine-grained beaches the areas of saturation remain fairly constant, however large regions of a coarse-grained beach can repeatedly change between saturated and unsaturated. This change means the pressure transducers record the movement of the 'wetting front' as opposed to the actual variation in the watertable (Austin and Masselink 2006*b*).

Nielsen (1992) highlighted the influence of infiltration/exfiltration on the near-bed hydrodynamics. The bottom boundary layer was defined as the layer of water inside which the flow is significantly influenced by the bed, and infiltration and exfiltration on per-

meable beds can affect this boundary layer.

Infiltration into the permeable bed causes a shift in the flow streamlines closer to the bed surface, reducing the flow velocity and causing a thinning of the boundary layer, causing larger bed mobility (Conley and Inman 1994). The infiltration into the bed has a stabilising effect on the permeable bed, because it increases the effective weight of sediment particles, thereby reducing the likelihood they will be involved in sediment transport.

Cheng and Chiew (1998) found that the bottom shear stress increases during infiltration, and that it decreases during exfiltration, although the reduction was determined to be less significant for rough sediment particles. Rao and Sitaram (1999) conducted a series of experiments that indicated that velocity and turbulence is increased during infiltration, while exfiltration causes a reduction in velocity and turbulence. This change in near-bed velocity and turbulence increases the potential of sediment mobilisation. Finally the infiltration of water into the beach reduces the volume of water able to participate in the backwash, reducing the potential suspended sediment load in this phase.

Exfiltration on a beach occurs predominantly during the backwash phase when the groundwater level of the beach is higher than the still water level. Exfiltration has the inverse effects of infiltration, and causes a shift in streamlines away from the bed surface, thickening the boundary layer. Exfiltration also reduces the effective weight of the sediment particles, reduces the bed shear shear stress, and reduces turbulence. The balance of these infiltration and exfiltration effects contributes to swash transport asymmetry, and a net onshore directed transport on coarse grained beaches.

Most of the previous research carried out was conducted on sand beaches. Fine-grained material forms a very shallow sloped beach, and the sediment also has a low hydraulic

conductivity. These two factors combined to make infiltration in the swash zone a minor concern for this type of beach; however, with consideration of coarser material, the effect of swash infiltration is increased due to the increased hydraulic conductivity and the steeper slope.

It is important however to recognise that although infiltration takes place on all beaches to a limited extent, not all beaches experience this asymmetrical transport. It is estimated that only approximately 2% of the total water in a wave cycle need infiltrate the beach for asymmetrical transport to occur (Masselink and Li 2001).

Butt et al. (2001) proposed a fundamental change in sediment transport behaviour at a critical grain size based on field work conducted at Perranporth Beach in the U.K. ($H_s = 2.0$m, $T_s = 8.0$s, and $\beta = 0.82^o$). For fine material smaller than the critical grain size, the sediment transport is asymmetric with a dominant offshore direction, while for coarse material larger than the critical grain size the transport is asymmetric with a dominant onshore direction. The critical grain size was estimated as 0.24mm. The difference between the transports was explained by a change in the dominant effect of infiltration. For fine-grained beaches, the increase in effective weight caused by infiltration dominates the alteration in the bed shear stress caused by thinning and thickening of the swash layer, while the reverse is true of coarse grained sediments.

Masselink and Li (2001) proposed the presence of a second critical grain size of 1.5mm where the backwash volume reduction from infiltration becomes a significant factor and begins to contribute to the swash transport asymmetry.

Horn (2002, 2006) provided reviews of the research conducted by a wide range of researchers into the groundwater effects on sediment transport, particularly the significance of infiltration and exfiltration on gravel beaches. Despite the fewer number

of investigations on coarse-gravel beaches, there seems to be common agreement that infiltration is significant to onshore-directed transport on gravel beaches, while on finer-grained beaches, infiltration plays a negligible role in sediment transport.

In the recent BARDEX project, Masselink and Turner (2012) provided significant evidence supporting the idea that swash-zone sediment transport and beach morphology are dependent upon the beach groundwater level. Low groundwater levels were responsible for driving onshore transport, while high groundwater levels were responsible for driving offshore transport. The contributing processes to the opposed morphological response of beaches with alternative groundwater levels were investigated, driven by variation of a lagoon level behind the beach. The change in swash hydrodynamics created by the increased infiltration into the unsaturated portion of the beach was unable to account for the differences in observed profile evolution, with the infiltration remaining fairly constant despite a change of 2m in the lagoon level. Masselink and Turner (2012) also applied a sediment transport model that accounted for infiltration/exfiltration effects. This indicated that the onshore sediment transport in the low-lagoon tests were mainly caused by enhanced bed shear stresses during uprush due to infiltration into the unsaturated beach.

#### 2.1.2.4 Flow acceleration

Early research into the effects of fluid acceleration by Nielsen (1992) were based on the assumption that the acceleration caused delayed development of the bed boundary layer. This permits higher velocities close to the bed, leading to the potential for higher sediment transport. Elgar et al. (2001) related sandbar morphology and flow acceleration within the surf zone of a beach, displaying good correlation between sandbar migration and peak velocity skewness in the surf zone.

Fluid accelerations become more pronounced in the swash zone, with large onshore

acceleration values caused by bore propagation and offshore fluid acceleration during backwash. Investigation of the role of acceleration in sediment transport has been made by a number of researchers (Cox et al. 1991; Nielsen 2002; Puleo et al. 2003; Pedrozo-Acuña et al. 2007). While investigating sediment transport on a steep, high energy beach, Puleo et al. (2003) recorded peak sediment transport occurred in the uprush during high onshore acceleration. Peak offshore transport occurred during decelerating flow, likely caused by adverse pressure gradients generated by the subsequent uprush event. A key conclusion drawn in this work was the necessity to include fluid acceleration in sediment transport models, to improve morphological evolution prediction. Terrile et al. (2006) conducted a series of laboratory experiments that confirmed the importance of fluid acceleration on the initiation of sediment transport for coarse-material.

Field work by Baldock et al. (2006) observed total fluid acceleration to be in a predominantly offshore direction throughout the swash cycle, producing an adverse pressure gradient during uprush, and a beneficial pressure gradient during backwash. Puleo et al. (2007) conducted numerical simulations of idealised swash events on a plane beach which supported these observations, highlighting the acceleration acting in an onshore direction occurred for only short durations (typically less than 22% of the swash space-time history) and generally in the lower swash zone at the beginning and end of swash events.

Pedrozo-Acuña et al. (2007) detailed the investigation into the relative importance of flow acceleration to sediment transport and consequent morphological change. The work included a comparison of results from a numerical model, containing an acceleration term in the sediment transport equation, with near full-scale experimental data for gravel and mixed sand-gravel beaches. A parametric sensitivity analysis was conducted, which suggested that although fluid acceleration contributed to the onshore movement of sediment, it alone was not able to account for the disparity between modelled and observed morphological change. Some of the other processes that were

highlighted as potential contributors to the predominance of onshore transport were infiltration/exfiltration effects, and the impact of the plunging breaker and its role in mobilising additional sediment for subsequent transport.

#### 2.1.2.5 Bottom friction

Bottom friction is an important beach and sediment characteristic when considering swash zone morphology (Hughes 1992), and, due to its effect on shear stress, it impacts both the swash hydrodynamics and the sediment transport.

Although there has been recent measurement of the direct bed shear stress at field locations (Conley and Griffin 2004) and during laboratory investigations (Barnes and Baldock 2007), most values of the bed shear stress are derived indirectly from measurement of the boundary velocity profile. This remains the case for the majority of numerical models where the hydrodynamic data is used to generate bed shear stresses at each time step. The bed shear stress is traditionally determined through utilisation of a quadratic drag law (Hsu and Raubenheimer 2006), with the introduction of an empirical friction factor:

$$\tau_b = \frac{1}{2}\rho f_w U(t)|U(t)| \tag{2.10}$$

where $\tau_b$ is the bed shear stress, $f_w$ is the friction coefficient, and $U(t)$ is the free stream velocity. The friction factor is a complicated parameter to quantify due to its relationship to both swash hydrodynamics and sediment transport. However, accurate approximation is important to ensure good morphological prediction is achieved in the later stages of numerical modelling.

Cox et al. (2000) found adoption of a quadratic drag law provided good estimation of bed shear stress in the surf and swash zone of a rough impermeable bed. Generally

larger friction coefficients were observed in the uprush compared with the backwash, and the authors suggested improvement of the estimation through adoption of different friction coefficients during different phases of a swash event.

Over the past decade a number of studies have been made regarding bed shear stress and the adoption of friction coefficients. Using data from two sandy beaches, Puleo and Holland (2001) estimated friction coefficients in the backwash may be up to three times larger that coefficients in the uprush. Raubenheimer et al. (2004) estimated similar friction coefficients in the uprush and backwash phases. Conley and Griffin (2004), using direct measurement of the bed shear stress, reported larger friction coefficients in the uprush than the backwash, broadly in agreement with Cox et al. (2000). Recent work by Puleo et al. (2012) on sandy beaches provided friction coefficient estimates slightly larger in the backwash than the uprush phase. Barnes et al. (2009) partially attributed the contrast in these observations to different methods in estimation, experimental conditions, and measurement locations.

Debate within the research community remains alive with regards to application of friction factors in the different swash cycle phases. While on its own the variation in the friction coefficients has not been able to reproduce the prediction of berm features in recent morphological prediction models (Pedrozo-Acuña et al. 2007), the prediction was significantly enhanced. Barnes et al. (2009) however recommended application of constant friction factors throughout the swash cycle.

As discussed previously, friction coefficient variation in the swash zone may be attributed to infiltration and exfiltration effects (Cheng and Chiew 1998). The vertical flow into the beach during infiltration causing an increase in the bed shear stress would result in increased sediment entrainment and higher transport rates, while the reverse would occur in the backwash.

### 2.1.3 Plunging wave impact pressure response

Pedrozo-Acuña et al. (2007) identified the potential influence of plunging breaker types on the morphology of gravel beaches, indicating its absence from numerical modelling frameworks. The high pressure impulse experienced at the impact location on steep beaches may result in increased mobilisation of sediment and higher transport rates.

Bullock et al. (2007) investigated the pressure response under plunging impacts on vertical and sloping walls. They identified a characteristic 'church-roof' signal (Figure 2.3) containing a sharp localised pressure spike associated with the initial plunging impact, followed by a quasi-hydrostatic pressure associated with the passage of a lens of water passing over the pressure transducer.

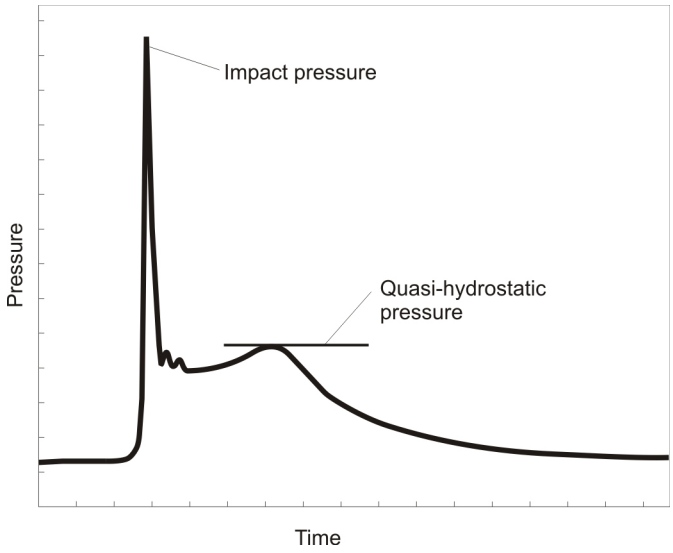


*Figure 2.3:* Schematic representation of a plunging impact after (Bullock et al. 2007).

This pressure response has since been observed to occur in gravel beaches during full-scale testing (Pedrozo-Acuña et al. 2008), and although the pressures acting on a sloping granular beach are less than on a vertical or near vertical walls, the impulse of a breaking wave is still sufficient to transport material (Cox and Cooker 1999).

## 2.2 Cross-shore profile evolution modelling

The modelling of the cross-shore profile of beaches has long been considered a desirable skill for engineers interested in protecting stretches of the coast. Early morphology models provided a simplistic relationship that predicted the long-term equilibrium profile of beaches (Bruun 1956; Dean 1991). While this has some use, the particular response of beaches to specific wave conditions is necessary in order to estimate the level of protection offered. Roelvink and Brøker (1993) reviewed a number of the then existing cross-shore profile evolution models. All were regarded as limited due to the computational restrictions, lacking multiple swash zone processes.

Li et al. (2002) utilised a process-based model to investigate the influence of swash infiltration/exfiltration on sediment transport and profile development. With introduction of lower groundwater levels this model reproduced the accretionary characteristics often observed on coarse beaches. Horn and Li (2006) compared field site data from a gravel beach to numerical prediction with the same model. The importance of infiltration to profile response was high, and the model was shown to be sensitive to a range of parameters (beach hydraulic conductivity, friction coefficient, and the ratio of uprush and backwash sediment transport rate) indicating their importance to profile prediction, however it was highlighted that uncertainties exist over the values of these parameters.

Pedrozo-Acuña (2005) and Pedrozo-Acuña et al. (2006) utilised a higher order Boussinesq hydrodynamics model, with moving shoreline boundary, coupled with a bed-load transport model to investigate gravel beach processes. Adoption of different friction coefficients during uprush and backwash improved prediction of cross-shore beach profile, however significant discrepancies still existed between predicted and measured beach profiles. The sediment transport equation was also adjusted with a different sediment transport efficiency coefficient ($C$-value) in the uprush and backwash to improve profile

prediction.

The improvement in the predicted morphological response by the model with different coefficients in the uprush and backwash was attributed to the parametrisation of many processes not directly included within the simulations, such as infiltration effects, additional transport due to bore collapse, and accelerated flow in the uprush. Overall, the model simulated a net onshore transport of material, as observed in the comparative experimental tests. However, the specific profile response under-predicted the size and location of the berm above the SWL, and the extent and location of excavation below the SWL (Figure 2.4).

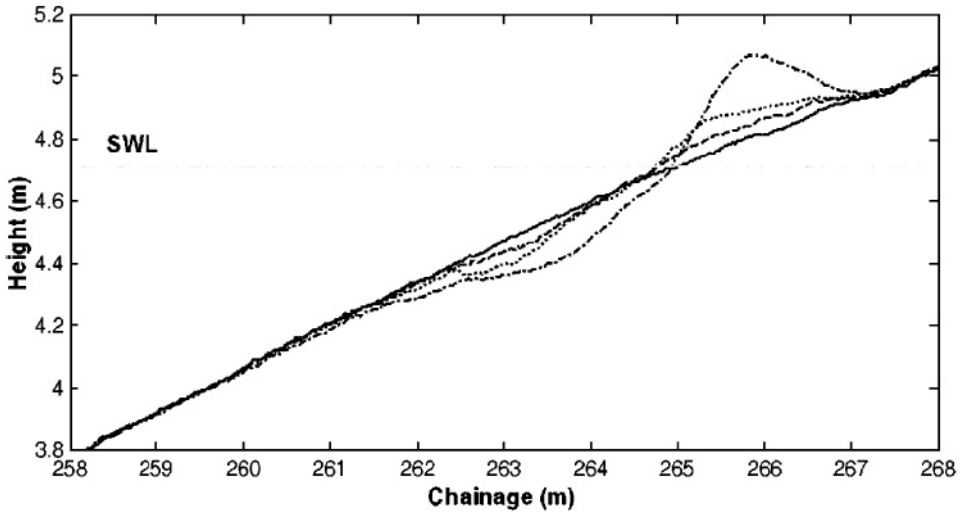


*Figure 2.4:* Gravel beach profile evolution; (solid line) initial profile, (dashed line) measured profile after 50 waves, (dotted line) measured profile after 100 waves, (dash dot line) measured profile after 500 waves (Pedrozo-Acuña et al. 2006).

Jamal (2011) utilised a modified XBeach model to simulate profile evolution on gravel beaches, and compared the numerical estimation with the same experimental values as Pedrozo-Acuña (2005). Again, variation in the friction coefficients during uprush and backwash was adopted, however inclusion of additional processes were made in an attempt to improve prediction capability.

A pragmatic method for handling infiltration was adopted, which essentially involved the removal of water from the swash above the bed surface in unsaturated regions, based on the permeability of the sediment. Exfiltration from the beach was ignored due to the reported lower significance to profile development. Morphological prediction was improved in comparison with Pedrozo-Acuña (2005) and Pedrozo-Acuña et al. (2006), with good localisation of the berm. However, the crest elevation and net sediment transport both appear to have been underestimated.

A further numerical model CSHORE was adapted for use on coarse-grained beaches by Hicks (2010). Provision for suspended sediment transport was included where the instantaneous flow velocity exceeded the particle fall velocity. However, the experimental data used for comparison adopted a gravel with fall velocity similar to the wave-induced oscillatory velocity, producing a transport environment governed almost entirely by bed load.

The cross-shore profile prediction was reasonable for extremely steep beaches ($\tan\beta = 0.5$), however for accretional tests the prediction within the swash zone was less successful, despite adjustment of bed load transport parameters to produce a closer fit.
Williams et al. (2012b) utilised XBeach to simulate the morphological response of both a gravel barrier beach during laboratory testing (*BARDEX - editorial* 2012), and evolution of a natural barrier beach at Slapton Sands in the Southwest of the UK. In both scenarios the modelled beach profile response demonstrated a strong dependence on the beach permeability, indicating the dominance of hydraulic conductivity in the swash hydrodynamics, supporting the work by Austin (2005) and Jamal et al. (2010). Best model performance was also obtained with the inclusion of beach groundwater levels and the associated implications for infiltration into the beach.

Williams et al. (2012b) concluded that the performance of the XBeach model in predicting the erosional characteristics of a gravel beach was good, however the prediction of the berm observed on gravel beaches was not well represented. This was attributed to the inability to accurately simulate the strong uprush, and weakened backwash after swash infiltration with the associated sediment transport.

One of the potential sources of inaccuracy in the modelling by some researchers is the reliance of transport by the bed load mode, assuming that sediment is locally entrained and that the total sediment transport rate is directly correlated to the bed shear stresses. It is widely recognised that the main mode of transportation on gravel beaches is bed load transport, and therefore some researchers (e.g. Pedrozo-Acuña (2005) and Jamal (2011)) adopted a bed load transport model by Soulsby and Damgaard (2005).

This model approach has proven to be reasonable at predicting morphological response of beaches, with discrepancies tending to occur around the berm region. The assumption of bed load dominance is reasonably likely during backwash phase when most turbulent energy has dissipated, and at times of lower flow rate and turbulent energy levels, which allows suspended sediment material to settle due to the higher settling velocities (Reeve et al. 2004). However large localised turbulence levels due to bore collapse during the uprush may allow transportation of suspended sediment during this phase. This form of transport would not be included within the numerical models used on gravel beaches.

Finally, a widely acknowledged difficulty with understanding morphological evolution stems from the net sediment transport being a balance in onshore and offshore transport. Both are significantly larger than net change, and neither of can be easily measured.

## 2.3 Summary

In summary, gravel beach environments are very important areas of interest to a wide range of stakeholders, and often act as a primary line of defence to many valuable regions. Understanding of these environments will allow more effective management in the coming years.

Due to the technical difficulties in producing accurate measurements within the swash zone, the investigation of the processes taking place there, and the modelling of those processes have been slower than in areas with simpler flow regimes. The continued increase in computing power of the last decade has allowed for a greater prevalence of numerical models capable of handling highly turbulent flow regimes present in the swash zone (e.g. Puleo et al. (2007)). The continual technological development also provides additional equipment that is beginning to make the swash region more accessible. For example, Puleo et al. (2012) utilised new high-resolution acoustic Doppler current profilers to quantify the vertical structure of cross-shore fluid velocities in the swash zone.

Sediment can be transported either in suspension or as bed load, including sheet flow. Bed load transport occurs when the local shear stress exceeds a critical threshold value, typically caused by high flow velocity. However, the threshold value for motion is different in the uprush and backwash phases of the swash on gravel beaches, as the effect of the steep slope plays a significant role. It is widely considered that bed load transport is the dominant transport mode within the swash zone of gravel beaches, due to the high settling velocity of the sediment particles making suspended transport difficult for prolonged periods.

A wide range of processes and parameters have been found to affect sediment transport on gravel beaches, and the subsequent morphological response. Many of these have been examined by researchers and in some cases the influence that they have on sediment

transport has been considered.

Cross-shore profile modelling has improved over the last decade, with integration of improved swash hydrodynamic models to, predominantly, bed load sediment transport modules. Modelling by Pedrozo-Acuña (2005) included variation of a sediment transport efficiency coefficient during the uprush and backwash phase to improve morphological prediction performance. Variation of this coefficient was presumed to parametrise some of the processes not specifically included in the model.

Infiltration effects were introduced to profile evolution prediction by both Jamal (2011) and Williams et al. (2012b) indicating good agreement between experimental and modelled profiles. Despite the improvements made, there are still discrepancies in the prediction of the gravel beach berm, likely due to a remaining processes not included within the model that contribute to the strong net onshore transport of sediment.

Horn (2002) identified a number of areas that required further investigation to improve modelling performance of sediment transport in the swash zone. These included, but were not limited to, the excess suspended sediment present during the uprush due to bore collapse, and intensity levels and vortex structure of turbulence in swash flows. These remain relatively untested. Pedrozo-Acuña et al. (2007) also suggested a number of processes that may be responsible for the disparity in numerically modelled and experimentally observed morphological change on gravel beaches. The impact of plunging breakers in mobilising additional sediment was identified as one of the processes that remains unaccounted for in the numerical modelling, and is worth additional investigation.

## 2.4 Project Aims

The over-arching aim of this programme is to conduct a series of experiments to extend the knowledge of how the cross-shore beach profile of a coarse-grained beach evolves under breaking wave action. The experimental project aims include:

1. To create a unique detailed set of data with beach profile at the plunging location recorded throughout the experiment
2. Monitor the beach profile evolution, and estimate sediment transport for various wave conditions
3. To investigate violent plunging wave impacts on the beach face, and assess whether this process may contribute to the discrepancy observed in numerical prediction of gravel beach profiles.

A controlled set of laboratory experiments, investigating a wide range of wave conditions, will be conducted to provide a detailed record of pore-water pressures induced by wave action within the beach. The beach profile will also be monitored, which will enable a sediment transport rate to be estimated at specific intervals.

The recorded pressure and incident wave conditions will be used to investigate the relationship between impact pressure and breaker-type. This will help inform the importance of the large pressure induced by plunging impacts on sediment mobilisation and transport asymmetry.

To enable the analysis of the recorded pressure responses within the porous beach medium, a new analytical approach will be developed and applied to correct the pressure record of swash events containing plunging impacts.

# Chapter 3

# Experimental procedure

The data used in this study were collected during a laboratory investigation, in which the author was a member of the laboratory team, comprising students and staff from Universidad Nacional Autónoma de México (UNAM) and the University of Plymouth (UoP).

The experimental programme aimed to provide a comprehensive set of data for plunging impact pressures and morphological response of a coarse-grained beach. This allows a more detailed study of the processes controlling beach response than is possible with the existing available data. To achieve this it was necessary to monitor the incident wave conditions and the pore-water pressure generated under impacting events, along with the cross-shore profile at intervals.

The following chapter introduces the facilities utilised, and provides details of the instrumentation adopted for the various measurements. The sediment characteristics are presented to provide a detailed understanding of the material forming the beach. Discussion of the calibration procedure for the measurement instrumentation is included, and finally the wave conditions are discussed.

## 3.1 Facilities

Large-scale facilities offer the opportunity to reproduce the real world environment with fewer difficulties associated with scaling effects, and with an opportunity to deploy a

significant amount of recording equipment in a comparatively small area. However, large scale facilities are often used in large collaborative ventures with significant funding and investigation into a very wide variety of processes. The limited number of such facilities, and the demand for their use, means access to large-scale testing facilities is somewhat restricted.

Smaller-scale laboratory testing allows a more flexible regime, with solutions to difficulties encountered during testing more easily accommodated. The opportunity for greater observation of the beach cross-section throughout the test duration, permitted by observation windows or glass-panelled channels, provides additional information that can be of tremendous importance in identifying difficulties, particularly at a preliminary stage.

Considering the advantages and constraints offered by these two options the small-scale facilities were determined to be preferential for this project due to:

- Lower operational costs
- A larger number of facilities offering greater accessibility
- Typically longer duration of availability provides an opportunity for adjustments and retesting if necessary
- More rapid experimental adjustments, and faster turn-around time between experiments, due to less material transportation during testing
- Retaining the capability to deploy equipment within necessary regions

As such the Wave Laboratory at UNAM in Mexico City was used to collect all experimental data used in this work, during a laboratory investigation of Summer and Autumn of 2008. The wave facilities have been used for a number of experimental programmes investigating beach morphological response and structural response to wave action (Mendoza-Baldwin et al. 2010; Pedrozo-Acuña et al. 2011). Measurements in this

work included: water surface elevation, cross-shore beach profiles, internal pore-water pressure at multiple cross-shore locations, and video imagery at pressure transducer locations to help quantify profile evolution in these areas.

The wave channel measures 37.0m long, 1.2m deep, and 0.9m wide, with a piston-type wave paddle permitting generation of 0.3m wave height with periods varying between 0.2s to 4.0s. It incorporated an active absorbing system by monitoring wave height at the paddle and adjusting the motion in real-time to reduce reflection from the paddle.

*Figure 3.1:* Wave flume at the UNAM facility.

## 3.2 Sediment characteristics

The specific area of interest in this work is investigation of gravel beach behaviour, however the term 'gravel' according to the Udden-Wentworth scale applies to sediment ranging from 2mm to 64mm, therefore a discussion regarding the selection of suitable sediment is necessary.

Data analysed by Pedrozo-Acuña et al. (2008) was collected at a full-scale testing facility (GWK) with wave heights of $H_s$ = 1.0m and the sediment utilised had a mean diameter of $d_{50}$=21mm (López de San Román-Blanco et al. 2006).

To move larger gravel requires a larger force, and therefore comparatively larger wave height. The wave period also has significant implications on sediment transport occurring on a beach, with larger period waves exhibiting higher wave run-up and run-down limits, and thus permitting morphological change over a wider area. The capabilities of wave generation within the flume in the wave laboratory at UNAM offers lower wave heights and shorter wave periods than those adopted during the work by Pedrozo-Acuña et al. (2008). Smaller gravel than the $d_{50}$=21mm used at the GWK facility was therefore adopted to ensure that sufficient transport occurred. Larger particle size also introduces the potential for error in beach profile measurement and subsequent transport rates. The beach elevation at a particular cross-shore location may fluctuate based on the presence of a large gravel particle or a large pore space between particles. This could potentially introduce a change in the cross-shore elevation between measurements, and indicate increased or reduced sediment transport at that location. While this is still a consideration for smaller gravel, the reduced particle size and pore spaces reduces the possibility of affecting measurements. It is possible to prevent measurement within a pore space with application of a plate to the base of the measurement equipment. However, due to the adopted profile measurement technique, discussed in Section 3.3, this would have introduced additional risk of the equipment modifying the profile during measurement.

To ensure transportation of the sediment particles occurred during testing, and to minimise the complications described relating to the measurement of accurate cross-shore profiles, a fine gravel (based on the Udden-Wentworth scale - 4mm to 8mm), was adopted for all tests. The beach was therefore constructed from well-rounded alluvial gravel with a median diameter of $d_{50}$ = 6mm, and was constructed to form an initial profile shown

in Figure 3.2.

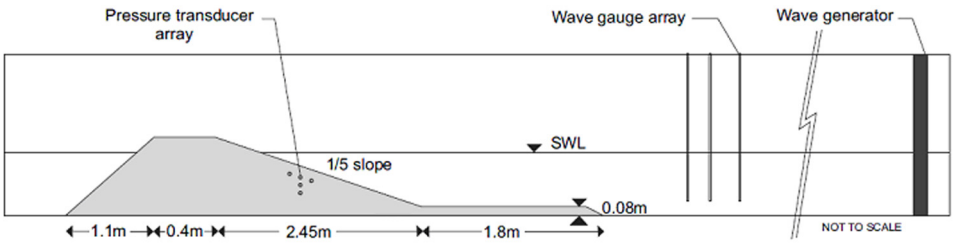


*Figure 3.2:* UNAM experimental equipment arrangement.

The sediment was sieved and thoroughly washed to remove particulate from the sample, to ensure a consistency of material, and to prevent discolouration of the flume water adjusting visibility and potential affecting characteristic properties of the water. After sieving and cleaning, the gravel was carefully mixed, both immediately after cleaning and during beach construction within the flume to ensure a homogeneous material. The sediment density of the final sample used for this work measured as $2591.6 kg/m^3$, the porosity was 0.403, while the critical angle of repose was approximately 25°.

Although alluvial gravel is generally not as rounded as that found on natural coastal beaches, it was considered to fall within acceptable angularity limits, which is supported by the measured angle of repose.

Sediment grain size distribution obtained through sieve analysis is included in Figure 3.3 and indicates a $d_{50}$ of 6mm. The details of how these values were derived can be found in Appendix A.

## 3.3 Instrumentation

To enable the investigation of the pressure response of plunging breakers on a gravel beach, it is necessary to monitor a range of parameters during each test. The mea-

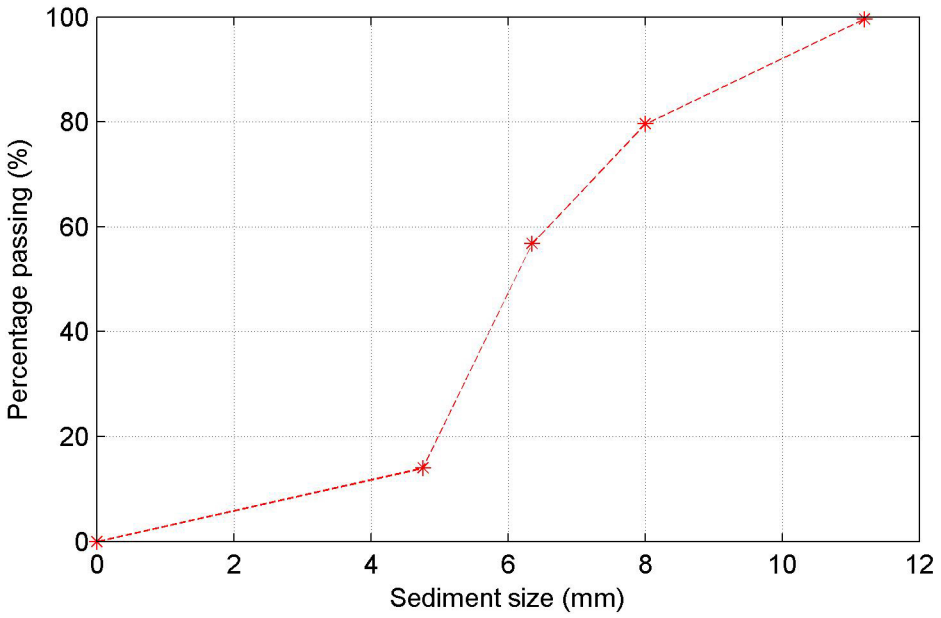


*Figure 3.3:* Sediment grain size distribution of the gravel beach.

surements required for further analysis include: the incident wave conditions which are responsible for each wave impact; the pressure response at the impact location, to assess the magnitude of each impact event; and morphological change at intervals throughout the tests to assess sediment transport rates.

To monitor the incident wave conditions the water surface elevation was measured at multiple locations close to the beach. Five resistance-type wave gauges were located within the wave channel to allow for the recording of the surface water elevation at different positions along the channel. Three wave gauges were located along the centre line of the wave channel close to the beach to permit separation of incident and reflected wave data, through application of a frequency domain analysis process (details in Section 4.1). The location of this three wave gauge array is indicated in Figure 3.2. One wave gauge was located landward of the beach to monitor the water surface elevation and one wave gauge was located an intermediate distance between the beach and the wave generator. Fuller details of the locations of the equipment are presented later in

Table 3.1.

One of the key requirements was to monitor the pressure at the plunging impact location, however monitoring this directly is very difficult. If a pressure transducer is located at the bed surface several difficulties are encountered throughout the duration of a test. Firstly the variation in the bed surface level due to sediment transport at the impact location will expose the transducers, resulting in measurement error. Secondly, exposure of the transducers at any point in the experiments may lead to scour around the transducers, affecting the cross-shore profile. Finally if the transducers are not buried to a sufficient depth, the presence of the transducers may still affect bed behaviour (for example the transducers may obstruct sheet flow transport). The pressure transducers must therefore be submerged in the beach to avoid these difficulties, with the attenuation of the pressure response subsequently accounted for.

The adopted pressure transducers had to be capable of recording the full pressure range expected during the testing regime, while also retaining fine detail of the pressure fluctuation. A fast response time was also desirable to ensure the rapid fluctuation under plunging impacts was captured. With these considerations five Druck PTX 1830 200mBar pressure transducers, henceforth referred to as UoP1-UoP5, were utilised during the testing regime at various locations to provide information on the pressure generated under impacting events.

Figure 3.4 provides a representation of the pressure transducer placement and orientation during experimentation. The transducers UoP1 to UoP5 were positioned within the beach sediment matrix close to the interface between the beachface and the SWL. A vertical array of horizontally co-located transducers (UoP1 to UoP3) provided information that allowed an estimate of the pressure attenuation experienced during pressure propagation through the sediment matrix. Two additional transducers (UoP4 and UoP5)

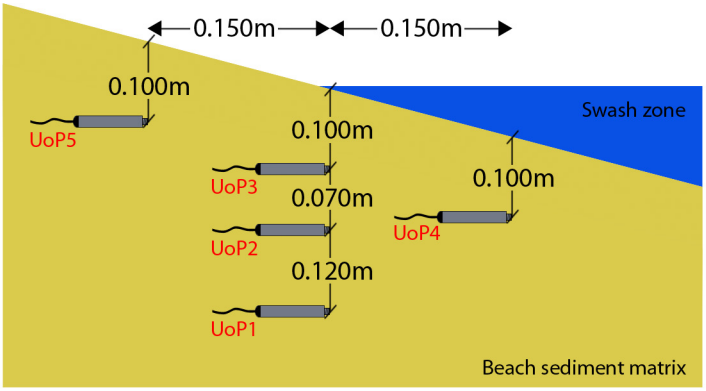


*Figure 3.4:* Schematic representation of the pressure transducer localisation during the testing at UNAM.

were located 150mm seaward and landward of the three transducer array respectively. UoP3, UoP4, and UoP5 were all buried to a depth of 100mm from the initial profile surface. This initial depth may appear large, however localised morphological change at the impact location caused erosion, lowering the depth of cover material to the transducers. A small initial depth of burial would risk exposure of the pressure transducers during wave action. Additional cover was also required to avoid introducing the transducers to movement during fluid bed conditions characteristic in sheet flow. The 100mm embedded depth was established during preliminary testing.

For determination of the beach profile a measurement guide was fixed across the centre line of the wave channel to ensure that the profile points were taken at consistent locations. Measurements were taken at initially 10cm intervals where little to no morphological change occurred, increasing to 5cm intervals in the more dynamically varying regions. Profiles were recorded with a Leica TCR series total station system and a prism reflector staff supported from above the flume and moved after each reading.

A video recording of the wave impact site was also maintained throughout all tests using a Casio Exilim EX-Z15, to allow monitoring of the approximate impact location, and permit additional monitoring of the sediment depth above the pressure transducers. This is crucial for a robust estimation of the signal attenuation that occurs between the beach surface and the pressure transducer, which evolves throughout each test as the sediment profile changes in response to wave action. Grid markings were made on the glass wall of the flume to allow assessment of the depth of burial of the pressure transducers.

Figure 3.2 indicated the experimental set-up adopted during the testing regime with the relevant positions of the wave gauges and pressure transducers outlined in Table 3.1.

| Equipment | Chainage from wave paddle flume end (m) | Equipment | Chainage from wave paddle flume end (m) |
|---|---|---|---|
| UoP1 | 29.50 | WG1 | 9.50 |
| UoP2 | 29.50 | WG2 | 24.10 |
| UoP3 | 29.50 | WG3 | 24.80 |
| UoP4 | 29.35 | WG4 | 25.20 |
| UoP5 | 29.65 | WG5 | 32.10 |

*Table 3.1:* Chainages of measurement devices.

To establish an appropriate sampling frequency during the experiments, a series of preliminary tests were conducted on an impermeable steep slope at Plymouth University. A plywood slope was fixed to a rigid frame and placed within a wave channel forming a slope of $\tan\beta = 0.2$, with a series of pressure transducers attached from the underside of the slope at regular intervals along the centre line of the beach. This formed a smooth impermeable slope with the pressure transducers recording the pressure response at the slope surface. A short series regular waves (H=0.08m T=1.25s) were directed at the beach, with the pressure response recorded.

The same pressure transducers as used in the UNAM tests were located along the cen-

tre line of the slope. A high sampling frequency of 2kHz was adopted and plunging breaker types were generated, producing a pressure-time curve characterised by the classic 'church-roof profile' (Figure 3.5).

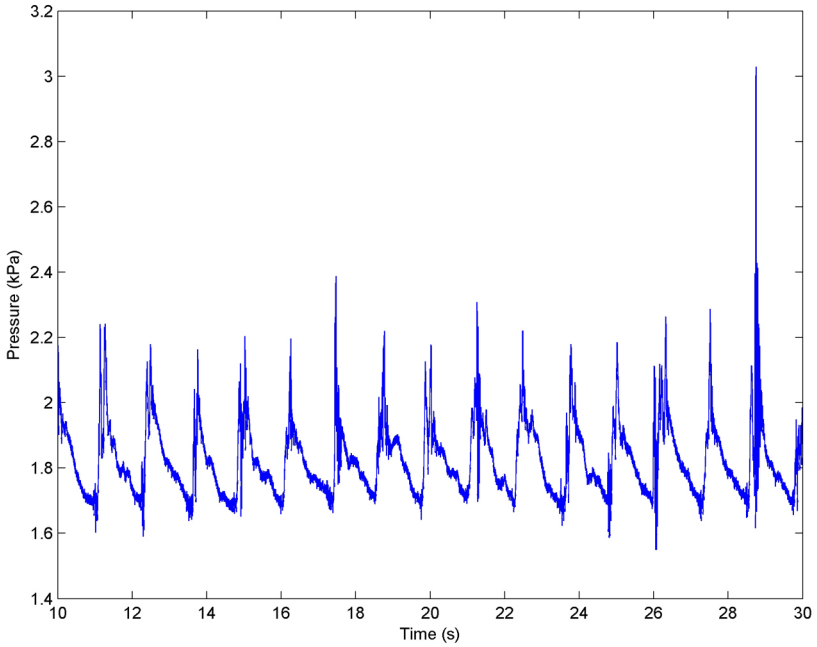


*Figure 3.5:* Pressure record for preliminary test.

Spectral analysis of the time series of this signal reveals the relevant frequency components comprising the signal. Figure 3.6 provides a single-sided amplitude spectrum of pressure-time series (0-100Hz is shown in detail as all amplitudes above 100Hz were effectively 0) which indicates the same pressure response could be resolved with a much lower sampling frequency.

Bullock et al. (2007) indicated that the church-steeple portion of the pressure response from impacting waves may exist for a very short duration, however the work by Pedrozo-Acuña et al. (2008) detected the church-steeple signature with a sampling frequency of 60Hz. A practical sampling frequency of 100Hz was chosen as a suitable compromise

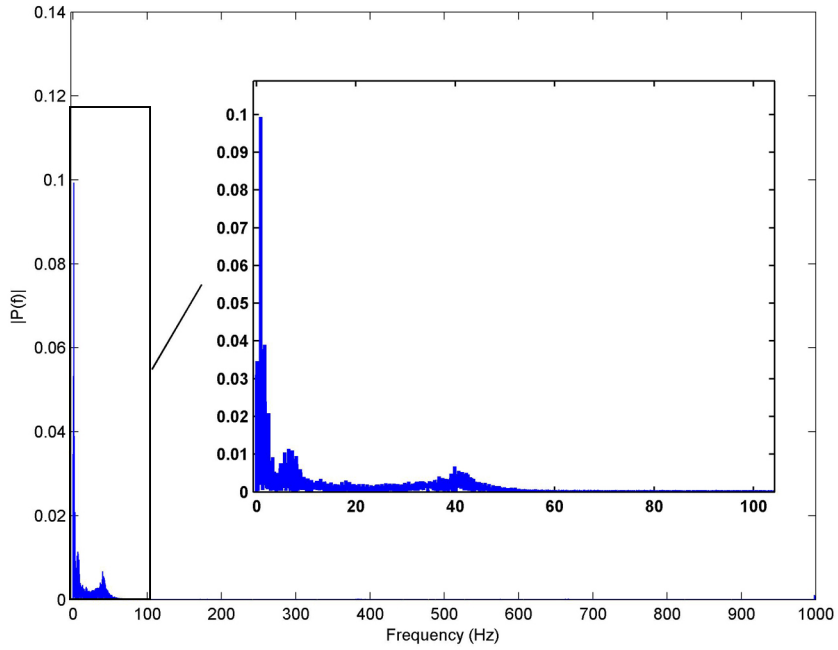


*Figure 3.6:* Single-sided amplitude spectrum of P(t) for preliminary test.

between providing a sufficiently high rate of data acquisition to resolve the sharp pressure impulse peak, with the size of the output files. Although this sampling frequency is less than the very high rate adopted by Bullock et al. (2007), 100Hz captures the vast majority of relevant frequencies indicated in Figure 3.6. Further, if all of the frequencies greater than 100Hz are excluded and an inverse Fourier transform is conducted, there is no aliasing between the original and reconstructed signal. Subsequent research by Pedrozo-Acuña et al. (2011) adopted a 100Hz sampling frequency for tests involving plunging impact pressure response, lending credence to the selection of the chosen sampling rate as suitable.

## 3.4 Calibration

Before each period of testing, the wave channel was filled with water to the correct water depth, with filling occuring at the beginning of each days testing. Further, after

each test was completed the SWL was checked, and if the level had fallen below 0.395m, additional water was added to the channel to return the SWL to 0.4m. Recalibration of the wave gauges took place each time water was added to the channel.

The Plymouth University transducers were calibrated at Plymouth before transport to UNAM with a Druck DPI603 pressure calibration unit. After shipping, the pressures transducers were recalibrated at the start and end of the testing by measurement of a variety of water elevations above the transducer aperture.

The beach profile measurements were calibrated to a fixed datum point next to the flume before each recording, and the sections of each test were then recorded before the data was downloaded to a computer and checked. Though it was not possible to collect all of the data without movement of the total station, due to limitations on storage space of the internal memory, this allowed for checking of the profiles to identify problems and allow for repeat experimentation if necessary.

## 3.5 Hydrodynamics

To monitor the beach profile evolution (and therefore estimate the sediment transport rate) it is necessary to separate each test into a number of shorter experiments, with beach profiles recorded between each experiment. Work by Blenkinsopp et al. (2011) indicated sediment transport of large individual swash events may be similar to the sediment transport for an entire tidal cycle. Sediment transport generated by irregular wave trains may therefore be affected by large individual events during short duration segments, generating unrepresentative profile change for the test as a whole.

Regular waves offer an approximately consistent wave energy level for consistent wave conditions, which allows for segmentation of each experiment without significant influ-

ence on morphological response by a single event.

To achieve the objectives of this work, set out in the previous chapter, it is crucial to encompass a wide range of surf-similarity parameters, as Pedrozo-Acuña et al. (2008) investigated a narrower variation in breaker type (mostly between $0.5 < \xi_b < 1.0$). As such a range of wave heights and wave periods were selected to create a variety of Iribarren values throughout the plunging wave breaking region (Table 3.2).

| breaking wave height (m) | Wave period (s) | | | |
|---|---|---|---|---|
| | 1 | 2 | 3 | 4 |
| 0.08 | 0.884 | 1.767 | 2.651 | 3.534 |
| 0.10 | 0.790 | 1.581 | 2.371 | 3.161 |
| 0.12 | 0.721 | 1.443 | 2.164 | 2.886 |
| 0.14 | 0.668 | 1.336 | 2.004 | - |
| 0.16 | 0.625 | 1.250 | - | - |

*Table 3.2:* Intended wave conditions and associated Iribarren values.

As mentioned earlier, each of the tests was separated into five smaller experiments to permit the measurement of the beach profile at stages throughout the specific wave conditions under test. The greatest sediment transport rate will occur early in each experiment as the beach is furthest from the equilibrium profile, and as such each experiment is divided into sections lasting one, two, four, seven and ten minutes. This quasi-logarithmic increase in test duration adopted here will capture the early rapid morphological response, while avoiding the necessity for repeated profile measurement as the equilibrium profile is approached.

An additional duration was recorded after active wave duration to record the slow down or the wave paddle and dissipation of wave energy within the flume. Data was acquired at 100Hz, therefore the 'Data required' is the product of the total duration of each experiment and the acquisition rate. Finally, the operation in place at UNAM recommended recording total data samples as a multiple of 256, therefore the actual data

samples recorded is also provided. Table 3.3 presents the data acquisition for each experiment.

| Wave duration (s) | Additional duration (s) | Total duration (s) | Data required | Data recorded |
|---|---|---|---|---|
| 60 | 30 | 90 | 9,000 | 9,216 |
| 120 | 30 | 150 | 15,000 | 15,360 |
| 240 | 60 | 300 | 30,000 | 30,208 |
| 420 | 60 | 480 | 48,000 | 48,128 |
| 600 | 60 | 660 | 66,000 | 66,048 |

*Table 3.3:* Test data recording details.

This experimental arrangement, and selection of hydrodynamic conditions should offer the data necessary for the analysis stage and investigation of the aims outlined in Chapter 2.

# Chapter 4

# Data handling for analysis

The raw data collected is not in a format that can immediately be used in analysis. Often, the most practical location for data collection is not the same location required for further calculations, for example the breaking wave height is often desirable but is difficult to monitor.

This chapter describes the calibration of the recorded data, and the translation of the data from the recorded locations to positions necessary for analysis in Chapters 5 and 6.

## 4.1 Wave height determination

For analysis where wave conditions are required, it is necessary to translate the recorded water elevation fluctuation to incident wave conditions, and address translation of the recorded wave heights to breaking wave heights. These procedures are explained in the following sections.

### 4.1.1 Incident wave separation

Wave reflection occurs when incident waves interact with a sloping beach and a portion of the energy is reflected by the slope, creating a reflected wave which propagates off-shore and interacts with the subsequent incident waves. The water elevation monitored is therefore a combination of incident and reflected waves and the interaction may form standing waves, which can result in the generation of currents, significantly altering the

flow regime around a beach and adjusting the bathymetry of the foreshore. Reflected waves are also present during experimentation within wave channels, requiring separation of the incident wave and reflected conditions.

Separation was achieved through application of the Separation of Incident and Reflected Waves (SIRW) method outlined by Friigard and Brorsen (1995). This approach assumes that a water elevation record is the composite of incident waves propagating towards the beach and reflected waves propagating towards the wave paddle. It is possible to apply this method to both irregular and monochromatic wave fields. The water elevation signals from two wave gauges are phase-shifted in a manner that results in the incident parts of the wave signal being in phase while the reflected parts of the signal are in mutual opposite phase. The consequence of this is the sum of the altered signals is proportional to, and also in phase with the incident wave signal. An amplification coefficient and the phase shift are calculated and applied to the wave signals to produce the final incident and reflected wave record, which is valid within the frequency domain. For translation to the time domain, digital filters are employed, acting as frequency dependent amplification and phase shift to the elevation signals.

Application of the digital filters introduces the possibility of singularity generation, however guidance is provided by Friigard and Brorsen (1995) in design of the filters to reduce potential difficulties with singularities.

Three wave gauges were deployed in an array close to the beach throughout the testing programme at UNAM. The method outlined by Friigard and Brorsen (1995) requires only two wave gauges, which permits the opportunity to conduct analysis multiple times with different gauge combinations, and variation in the wave gauge spacing allows control of the singularity placement.

### 4.1.2 Incident wave calculation

Power Spectral Density (PSD) analysis was conducted on the water elevation record closest to the beach to establish the High and Low frequency values necessary for the digital filter translation to the time domain. The Welch method was applied, utilising a Hamming window.

Data collection was initiated before wave generation commenced to ensure that all relevant data was collected. Elimination of the data before and after wave action was important to avoid inclusion of two sections with different reflection characteristics. A consequence of not accounting for this would be the derivation of a single erroneous reflection coefficient representative of the entire data set. This can be corrected by splitting the wave data into two shorter sections, one section that relates to the early incoming waves that have no reflected waves recorded at the wave gauge, and one longer section of data relating to the combined incident and reflected waves recorded at the wave gauge.

A further difficulty encountered during the processing of the data, is introduced by the 'warm-up' period of the wave generator. The first waves after wave generation commenced were less than the intended wave height as the generator required a short period of time before it was capable of operating at optimal conditions. This resulted in an increase in wave heights from 0m to the maximum wave height, therefore the first reflected waves detected will be generated during the period of increasing wave height and will thus also exhibit an increase in wave height. Optimal performance of the separation procedure occurs with steady wave conditions, as this will require the summation of fewer sinusoids to reproduce the detected signal. This is most relevant for short duration tests where the overall record is more easily affected by a small number of waves.

All wave data relating to periods of no reflection and increasing reflected wave heights were excluded from the analysis to provide consistency across the experimental programme and ensure that test duration was not an issue in reflection coefficient determination.

### 4.1.3 Comparison of wave separation techniques

Meneses Fernández (2009) produced a series of reflection coefficients for the same data set, utilising an alternative method for wave separation (Baquerizo 1995), which are presented in Table 4.1. Due to a discrepancy in the test order during the experimental programme, and to retain increasing wave height moving down the table, Test 7 appears before Test 6.

| Test | H (m) | T (s) | $K_{R-i}$ | $K_{K-f}$ |
|---|---|---|---|---|
| 7 | 0.08 | 2 | 0.476 | 0.257 |
| 6 | 0.10 | 2 | 0.437 | 0.310 |
| 8 | 0.12 | 2 | 0.402 | 0.313 |
| 9 | 0.14 | 2 | 0.356 | 0.293 |
| 10 | 0.16 | 2 | 0.397 | 0.319 |
| 11 | 0.08 | 3 | 0.461 | 0.411 |
| 12 | 0.10 | 3 | 0.446 | 0.319 |
| 13 | 0.12 | 3 | 0.429 | 0.320 |
| 14 | 0.14 | 3 | 0.422 | 0.315 |
| 15 | 0.08 | 4 | 0.738 | 0.517 |
| 16 | 0.10 | 4 | 0.705 | 0.523 |
| 17 | 0.12 | 4 | 0.659 | 0.522 |

*Table 4.1:* Calculated initial reflection coefficients ($K_{R-i}$) and final reflection coefficients ($K_{R-f}$) (Meneses Fernández 2009).

Tests one to five related to tests with 1-second period waves, but are not included here, due to vibration caused between the mounting of the wave maker and the wave channel. An adjustment to the wave maker mounting was made for subsequent tests, which eliminated this complication. This vibration caused discrepancies within the pressure records that could not be removed with post processing, therefore as further analysis was not possible, these tests were discarded.

Reflection coefficients were calculated in this work after application of the SIRW method. The results of this approach are presented in Table 4.2 (details of the reflection coefficient for each segment of each test are available in Appendix B). Wave reflection coefficients were calculated as $K_R = H_r/H_i$, where $H_r$ and $H_i$ are the reflected wave height and incident wave height respectively.

| Test | H (m) | T (s) | $K_{R-i}$ | $R_{R-f}$ |
|---|---|---|---|---|
| 7 | 0.08 | 2 | 0.226 | 0.431 |
| 6 | 0.10 | 2 | 0.185 | 0.386 |
| 8 | 0.12 | 2 | 0.175 | 0.338 |
| 9 | 0.14 | 2 | 0.163 | 0.277 |
| 10 | 0.16 | 2 | 0.105 | 0.326 |
| 11 | 0.08 | 3 | 0.366 | 0.522 |
| 12 | 0.10 | 3 | 0.356 | 0.615 |
| 13 | 0.12 | 3 | 0.309 | 0.617 |
| 14 | 0.14 | 3 | 0.330 | 0.594 |
| 15 | 0.08 | 4 | 0.372 | 0.549 |
| 16 | 0.10 | 4 | 0.346 | 0.546 |
| 17 | 0.12 | 4 | 0.303 | 0.498 |

*Table 4.2:* Calculated reflection coefficients ($K_{R-i}$: reflection coefficient for first part of the relevant test, $K_{R-f}$: reflection coefficient for final part of the relevant test) using SIRW method, by Friigard and Brorsen (1995).

Battjes (1974) proposed a simple relationship for estimation of the reflection coefficient (Equation (4.1)), while an alternative empirical relationship for reflection generated from coastal structures was proposed by Zanuttigh and van der Meer (2008) (Equation (4.2)).

$$K_R = 0.1\xi_0 \tag{4.1}$$

$$K_R = \tanh(a.\xi_0^b) \tag{4.2}$$

where $\xi_0$ is the Iribarren number, $a$ and $b$ are coefficients dependent on the material

used in the coastal structure.

It is apparent from both of these relationships that the Iribarren number, and therefore beach slope and wave steepness, plays a critical role in the level of wave reflection. Both relationships predict an increase in $K_R$ from an increase in beach slope, and decrease in $K_R$ as wave steepness increases.

Inspection of the reflection coefficients generated by the Friigard and Brorsen (1995) method (Table B.4) indicates a general increase in reflection as the profile evolves and the beach steepens, matching the expectations presented by Equations (4.1) and (4.2). As wave steepness increases (indicated here through an increase in wave height with constant wave period) the reflection coefficient decreases, again providing agreement with the empirical relationships.

The general agreement of the reflection coefficient with that expected under theoretical circumstances, provides confidence in the accuracy of the chosen method for incident and reflected wave separation.

The details of the analysis carried out by Meneses Fernández (2009) states only the use of the method proposed in Baquerizo (1995), and does not provide discussion of whether data was included before reflection was established. The results in some cases seem counter intuitive, displaying a reduction in the reflection coefficient as the beach profile steepens. Due to the uncertainty in the method utilised in calculating the reflection coefficients by Meneses Fernández (2009), these results are discarded.

### 4.1.4 Wave shoaling

Wave shoaling is the process by which waves increase in height as they propagate into shallower water. It is essential to account for wave shoaling to appropriately estimate the breaking wave height that occurred during testing, which is adopted during pressure analysis. Wave shoaling investigations commenced as long ago as McCowan (1894), however the most significant strides in its understanding were achieved in the 1970's and 1980's (Weggel 1972; Shuto 1974; Goda 1975; Svendsen and Hansen 1976; Van Dorn 1978; Peregrine 1983). Traditional methods for calculating shoaling are discussed below.

Shuto (1974) presented Equation (4.3) for estimation of the shoaling coefficient ($K_s$), based on the Korteweg-de Vries equation, assuming no wave refraction and no energy is added or removed from the system:

$$K_s = \frac{H}{H_0} = \frac{1}{\sqrt{2n\tanh(2\pi d/L)}}, \tag{4.3}$$

where $n$ is given by Equation (4.4):

$$n = \frac{1}{2}\left[1 + \frac{4\pi d/L}{\sinh(4\pi d/L)}\right]. \tag{4.4}$$

The breaking criterion (Equation (4.5)) outlined by Goda (1975) provides an alternative method, utilising the offshore wave conditions:

$$\frac{H_b}{L_0} = A\left\{1 - exp\left[-1.5\pi\frac{h}{L_0}(1 + B\tan^{4/3}\beta)\right]\right\}, \tag{4.5}$$

where $H_b$ is the breaking wave height, $L_0$ is the offshore wavelength, $A$ and $B$ are empirical derived constants (taken as 0.17 and 15 respectively), $h$ is the local water depth, and $\tan\beta$ is the beach slope.

The applicability of these approaches on various laboratory slope scenarios was investigated by Tsai et al. (2005). Three alternative slopes were examined: $\tan\beta = 0.1$, $\tan\beta = 0.2$, and $\tan\beta = 0.33$, with the intention to specifically look at the validity of the relationships to steep beach slopes. Tsai et al. (2005) concluded that the relationship proposed by Shuto (1974) provided good agreement with the shallow slope ($\tan\beta = 0.1$), however there are inconsistencies between the theoretical relationship and observed results for the two steeper slopes. As the beach slope adopted during the experimental procedures in this work is initially $\tan\beta = 0.2$ it is not appropriate to adopt Equation (4.3).

Comparison of the theoretical values derived from Goda (1975) and the practical data indicated good agreement across all three tested beach slopes, suggesting use of this empirical relationship to be suitable for this work.

Le Méhauté and Koh (1967) proposed a further relationship (Equation (4.6)) presenting the breaking wave height in terms of deepwater wave conditions.

$$\frac{H_b}{H_0} = 0.76(tan\beta)^{1/7}\left(\frac{H_0}{L_0}\right)^{0.25} \tag{4.6}$$

Again the applicability of this empirical relationship was investigated by Tsai et al. (2005). They indicated the relationship was in good agreement with additional experimental data for a 1/10 slope beach, however it overestimates $H_b/H_0$ for beach slopes of 1/5 and 1/3. A modification to Equation (4.6) was recommended to better represent the relationship for steep slopes.

$$\frac{H_b}{H_0} = 0.79(tan\beta)^{1/7}\left(\frac{H_0}{L_0}\right)^{-0.19} \tag{4.7}$$

The approach expressed by Goda (1975) (Equation (4.5)) and the modified empirical

formula of Le Méhauté and Koh (1967) (Equation (4.7)) both appear to provide a good fit for steeper beaches and therefore suitable for application in this work.

#### 4.1.4.1 De-shoaling recorded wave data

The water elevation was recorded during the test programme at a location a short distance from the toe of the beach. While this location can be useful, and is the most practical position to record water elevation data during testing, it is not suitable for immediate use in analysis. Deep-water wave conditions are widely used in calculations, however the wave height to water depth ratio ($H/d$) does not constitute deep-water wave conditions. Therefore, the equivalent deep-water parameters for the recorded waves will be calculated, before account of shoaling between deep-water and wave breaking is made.

The notion of deep-water conditions for wave channel testing is obviously a hypothetical situation. Effectively the wave channel represents the nearshore (intermediate and shallow water wave conditions), and the wave conditions present in the wave channel are representative of waves that have propagated from deep-water. As will be seen below the bathymetry of this propagation distance is not required for the calculations, therefore no assumptions are offered on this front. Assuming linear wave theory the deep-water wavelength can be calculated from Equation (4.8).

$$L_0 = \frac{gT^2}{2\pi} \tag{4.8}$$

The wavelength for intermediate water depth conditions can be calculated from Equation (4.9) using an iterative procedure until a stable value is achieved.

$$L_n = L_0 \sqrt{\tanh(2\pi h / L_{(n-1)})} \tag{4.9}$$

To determine the water depth that constitutes deep water wave conditions, Equation

(4.9) was used with an increase in the water depth until the calculated wavelength was equal to the deep-water wavelength determined with Equation (4.8).

#### 4.1.4.2 Sensitivity to beach slope

The determination of the deep-water wave height can be made through rearrangement of Equation (4.3). With the deep-water wave conditions established, it is now possible to account for shoaling between deep-water and the breaking location. Thus adoption of the relationship presented by Le Méhauté and Koh (1967) (Equation (4.7)), and determined as appropriate for the steep beach slope of $\tan\beta = 0.2$, was made.

#### 4.1.4.3 Wave shoaling sensitivity analysis

The final complication with regards to calculating the shoaling that occurred in the practical experimentation pertains to the beach slope. Initially the beach was constructed to a stable, constant slope of $\tan\beta = 0.2$, however under wave action the beach profile evolves, causing a steepening of the slope localised around the mean water level. The evolution of the profile was an ongoing process that took place on a wave by wave basis. However, the measurement of beach profiles was only possible while wave generation was inactive (permitting approximately six profiles for each set of wave conditions), therefore a decision of which beach slope to adopt in the calculations is necessary.

Despite the constant morphological evolution, the slope over which shoaling occurs remained fairly constant throughout each tests. Sediment transport is mainly confined to the surf and swash zones, with little transport occurring over the beach seaward of the breaking location. A simple sensitivity test was conducted to investigate the impact of variation in shoaling slope.

The calculation procedure described above was conducted for a selection of shoaling slopes to determine the degree of shoaling predicted, producing a breaking wave height

for each case. Comparison of the breaking wave heights, presented in Table 4.3, will allow assessment of the sensitivity of the calculations to the small variation in shoaling slope.

| Beach slope ($\tan\beta$) | $H_b$ (m) |
|---|---|
| 0.195 | 0.134 |
| 0.200 | 0.134 |
| 0.205 | 0.134 |

*Table 4.3:* Sensitivity analysis results for wave shoaling at various beach slopes for 20080624T164058 (Test 8 - part 2).

A fluctuation in the beach slope of 0.01 indicates a stable wave height transformation, with negligible change in predicted wave breaker height within the measurement accuracy of the water elevation apparatus. The initial slope of $\tan\beta = 0.2$ is assumed to provide a reasonable estimate of the slope over which shoaling occurs for all tests.

## 4.2 Surface pressure correction

To investigate the role of the plunging breakers, and the influence of the higher pressures generated by plunging impacts on morphological change, it will be necessary to observe pressure responses under bore collapse for varying breaker types. As discussed previously it was necessary to bury the pressure transducers within the beach matrix, necessitating the account for signal attenuation as the pressure wave propagates from the bed surface to the pressure transducer location.

Attenuation is the reduction in intensity of a flux as it passes through a medium. In this scenario it is the reduction in the amplitude of a pressure wave as it propagates through the sediment matrix. The attenuation of the pressure wave can occur through either absorption or scattering and is affected by multiple variables, including but not limited to: the frequency of the signal; the size of the sediment particles; the aeration level of the sediment matrix; and the density of the pore fluid.

The degree of attenuation is very dependent on the frequency of the signal, with high frequencies attenuated to a higher degree than lower frequency signals. This is easily identifiable phenomenon is the real world when music can be heard from an adjacent room. The higher frequency notes are attenuated to a greater extent while passing through a wall, while the lower frequency bass notes are attenuated comparatively less, resulting in a bass dominated sound. Many researchers have identified the same phenomena in wave propagation through porous media (e.g. Biot (1956*a*) and Chotiros (1995)).

The aeration level of the fluid within the sediment matrix can significantly adjust the attenuation of a signal. Each pocket of air has the potential to decrease the strength of the signal by absorbing some of the energy of the propagating pressure wave, due to the high compressibility of the air allowing deformation of the bubbles.

### 4.2.1 Attenuation in poro-elastic material

The seminal work by Biot (1941, 1956*a*,*b*) formulated linear multi-phase poro-elastic equations, which represented the fluid flow in a porous medium. The approach was developed to permit calculation of soil consolidation under a constant load, pertaining to fine sediment material, and was initially limited to one-dimensional scenarios, before expansion to two-dimensional consolidation.

The following assumptions are made for the original work:

1. Isotropy of the sediment material;
2. Reversibility of stress-strain relations under final equilibrium conditions;
3. Linearity of stress-strain relations;
4. Small strains;

5. The water contained in the pores is incompressible;

6. The water may contain air bubbles;

7. The water flows through the pores according to Darcy's Law.

For brevity the derivation of the original equations is not reproduced here, but a clear and concise explanation is available in both the original work, and a number of other resources (Wang 2000).

### 4.2.2 Wave attenuation

The work by Biot was extended by Yamamoto et al. (1978) where exact solutions were obtained for the closed form for the case of waves propagating over a submerged beach. Many defining characteristics are retained; the soil is assumed homogeneous and isotropic, while the soil skeleton is assumed to obey Hooke's Law and therefore has linear, elastic mechanical properties. Equation (4.10) presents the relationship developed by Yamamoto et al. (1978), which allows for the calculation of the pressure at depth $z$, $P_z$:

$$\frac{P_z}{P_0} = \left[1 - \frac{im\omega''}{-\lambda'' + i(1+m)\omega''}\right] e^{-\lambda z} + \frac{im\omega''}{-\lambda'' + i(1+m)\omega''} e^{-\lambda' z}, \tag{4.10}$$

where $m$, $\omega$, and $\lambda$ are derived from sediment parameters (porosity, $n$, permeability, $K$, Poisson's Ratio, $\nu$, and Shear modulus, $G$) as outlined in Yamamoto et al. (1978).

Yamamoto et al. (1978) concluded that the bed pressure response was highly influenced by permeability, the stiffness of the sediment matrix, and the compressibility of the pore fluid. It was particularly noted that when the stiffness of the sediment is much larger than the stiffness of the pore fluid ($G/E'_w) \to 0$, i.e. for partially saturated denser sediment), the pressure attenuates rapidly and the phase-lag increase linearly with increasing embedded depth.

Massel et al. (2004, 2005) continued research in this field with determination of a relationship for pressure attenuation within beds of a finite thickness. After significant mathematical handling, (Massel et al. 2005) presented the pressure ratio $P_z/P_0$ given as:

$$\frac{|P_z|}{P_0} = |\frac{cosh\,[\lambda(z-D)]}{cosh\lambda D}|, \tag{4.11}$$

where $z$ is the depth below the bed surface and $D$ is the thickness of the bed. $\lambda$ is the wavenumber within the porous media which is now a complex quantity, expressible as: $\lambda = \lambda' + i\lambda''$ or $\lambda = |\lambda|e^{i\theta}$, where:

$$|\lambda| = k\left\{1 + \frac{\omega^2(\rho g)^2}{k^4K^2}\left[\frac{n}{E'_W} + \frac{1}{G}\frac{1-2\nu}{2(1-\nu)}\right]^2\right\}^{1/4}, \tag{4.12}$$

and the argument:

$$\theta = \frac{1}{2}arctan\left\{-\frac{\omega(\rho g)^2}{k^2K}\left[\frac{n}{E'_W} + \frac{1}{G}\frac{1-2\nu}{2(1-\nu)}\right]\right\}. \tag{4.13}$$

In the above equations; $\rho$ is the density of fluid within the porous medium, $E'_w$ is the apparent bulk modulus of the pore fluid, $g$ is the acceleration due to gravity, $K$ is the permeability of the sediment, $n$ is the porosity of the sediment, $G$ is the shear modulus of the sediment, and $\nu$ is Poisson's ratio. The wavenumber, $k$, is calculated such that it satisfies the classic dispersion relation:

$$\omega^2 = \left(\frac{2\pi}{T}\right)^2 = gk\,tanh\,(kh)\,, \tag{4.14}$$

where $h$ is the water depth and $T$ is the wave period of the incident waves.

### 4.2.3 Attenuation of impacting event

The development of these previous pressure attenuation approaches was made for the case of waves propagating over a submerged beach. Accounting for pressure attenuation in a porous media under plunging impact events has not been a topic that has received study. Pedrozo-Acuña et al. (2008) accounted for pressure attenuation under plunging impact wave events through the direct application of Equation (4.11). This approach resulted in a single attenuation value (inverse of the pore-pressure ratio $P_z/P_0$) that was applied to the entire signal. The close proximity of a wave gauge within the flume allowed for the calculation of the theoretical surface pressure to be estimated assuming a hydrostatic situation based on the depth of the water lens above the transducer array.

There are a few limitations in this approach. Firstly the gravel used in the analysis by Pedrozo-Acuña et al. (2008) has a median diameter of $d_{50} = 21mm$. It is widely accepted that Darcian flow through sediment pores is observed in fine sediment material such as silt or sand, however as sediment size increases and moves into coarser material, the Reynolds number increases and the pore flow becomes more turbulent. Gravel with $d_{50} = 21mm$ is unlikely to experience Darcian flow through the pore spaces, thereby invalidating one of the key assumptions put forward by Biot (1941), Yamamoto et al. (1978), and Massel et al. (2004). Massel et al. (2005) also specifically states the case of high permeability should be treated with an alternative method.

The second error with applying the approach taken by Pedrozo-Acuña et al. (2008) to impacting waves pertains to the frequency adopted during the analysis. The wave frequency is adopted in calculations by Yamamoto et al. (1978) and Massel et al. (2004), as the purpose of these works is to investigate pressure fluctuations generated through wave propagation over a submerged beach. The pressure fluctuation is therefore directly related to the wave frequency. With consideration of impacting events however, the frequency of the pressure signal will differ substantially from that of a simple wave

oscillation, possessing a more complicated signal due to the abrupt pressure variation introduced by the impacting event. The pressure response of the impacting event is likely to contain a wider range of higher frequency components, invalidating the application of a single correction to the entire signal, due to the high sensitivity of attenuation to the signal frequency.

The final complication in the application of the chosen method by Pedrozo-Acuña et al. (2008) is the general applicability of the derivation to the case of impacting breakers. From the effective stress concept and Hooke's Law the following equilibrium equations can be derived:

$$\frac{\partial P}{\partial x} = G\nabla^2\xi + \frac{G}{1-2\nu}\frac{\partial \epsilon}{\partial x} \tag{4.15}$$

$$\frac{\partial P}{\partial z} = G\nabla^2\eta + \frac{G}{1-2\nu}\frac{\partial \epsilon}{\partial z} \tag{4.16}$$

The pore-water pressure satisfies the continuity equation

$$\nabla^2 P = \frac{\rho_w g}{K}\left[\frac{n}{E'_w}\frac{\partial P}{\partial t} + \frac{\partial \epsilon}{\partial t}\right] \tag{4.17}$$

where $\xi$ and $\eta$ are the $x$ and $z$ components of the soil displacement respectively, and $\epsilon$ is the volume strain such that:

$$\epsilon = \frac{\partial \xi}{\partial x} + \frac{\partial \eta}{\partial z} \tag{4.18}$$

This system of three partial differential equations was solved with consideration of appropriate boundary conditions (Massel et al. 2005). The bed surface provided the first location for known boundary conditions, where the pressure was determined from the sinusoidal variation in water surface such that:

$$P = \frac{\rho_w g H}{2} \frac{1}{\cosh kh} \tag{4.19}$$

It is clear that this approach was developed for sinusoidal variation in pressure caused by propagation of an unbroken wave, and is unrepresentative of the situation of a plunging impact pressure response. The direct application of this method to the entire record containing impacting events would generate an inappropriate output.

It is apparent through inspection of Figure 4.1, taken from Pedrozo-Acuña et al. (2008), that the attenuation adopted in this work was inappropriate. The four panels show pressure responses at four different depths, appearing to show a reduction in the peak impact pressures with increasing depth.

While the sharp, short-duration pressure spikes appear to become rapidly attenuated with depth, the almost-sinusoidal, lower-frequency, portion of the record is attenuated to a lesser extent. The application of a relevant single attenuation correction to the entire pressure record of each pressure transducer would provide different estimated surface pressures for the same impact event.

One potential solution to the difficulty in correcting impact pressure attenuation is the separation of the recorded pressure signal into constituent pseudo-sinusoidal and impulse components. The pseudo-sinusoidal component of the pressure record relates to the hydrostatic pressure variation caused by the change is water level above the pressure transducer, and is therefore analogous to the scenario described by Massel et al. (2004). Meanwhile the impulse pressure response can be handled as a separate process with each of the frequency components corrected by consideration of the relevant attenuation.

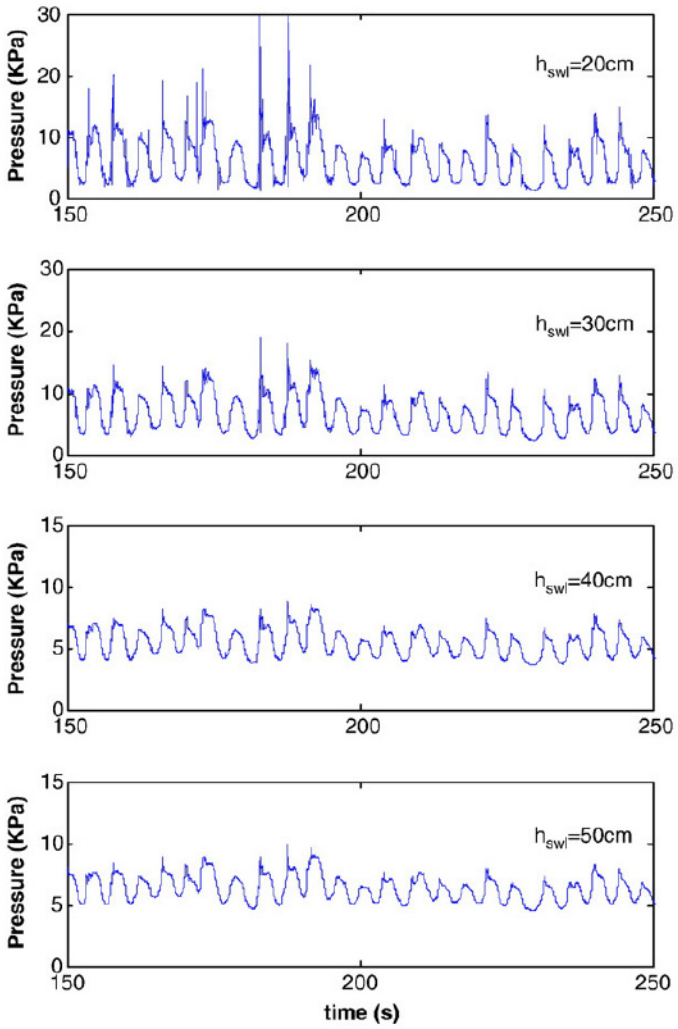


*Figure 4.1:* Pressure response from four co-located pressure transducers (Pedrozo-Acuña et al. 2008).

### 4.2.4 Pressure signal separation

Figure 4.2 indicates an idealised pressure signal representation of the recorded pressure response during testing, composed of an impulse component and hydrostatic fluctuation component. This idealised signal corresponds well with the schematic representation of a plunging impact provided by Bullock et al. (2007) (Figure 2.3), as well as observed pressure signals recorded in this work.

Conducting a fast Fourier transform (FFT) of these idealised pressure signal components

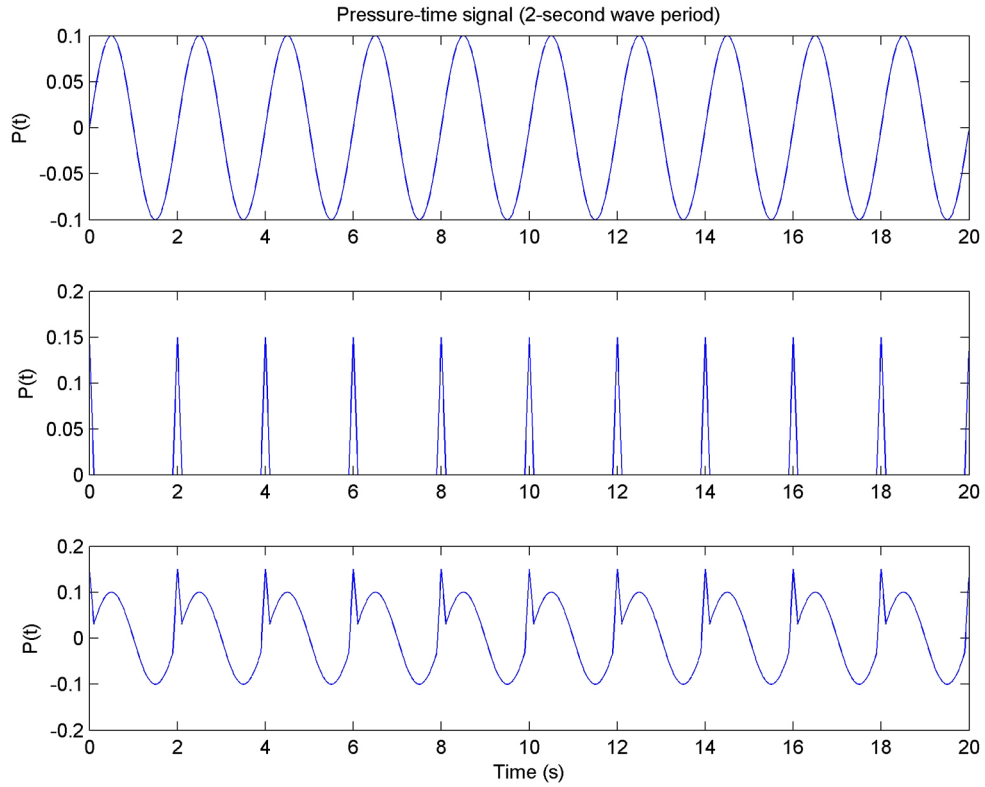


*Figure 4.2:* Idealised pressure response of plunging impact event. Top panel: sinusoidal component, middle panel: impact impulse component, bottom panel: combined pressure record

identifies the relevant frequencies that each component contain. Figure 4.3 presents the single-sided amplitude spectrum of each of the idealised pressure signals.

The top panel shows the hydrostatic pressure signal component has a single peak frequency of 0.5Hz (corresponding to the wave frequency). This outcome is self-evident, however the presence of a single peak frequency indicates the necessity for a single attenuation-correction for this component. The middle panel shows the impact impulse component is composed of a range of frequencies. As attenuation is strongly dependant upon the frequency of the signal, each of the frequency elements will be attenuated to a varying extent as the signal passes through the sediment matrix. The same event detected at different distances beneath the beach surface would provide characteristically

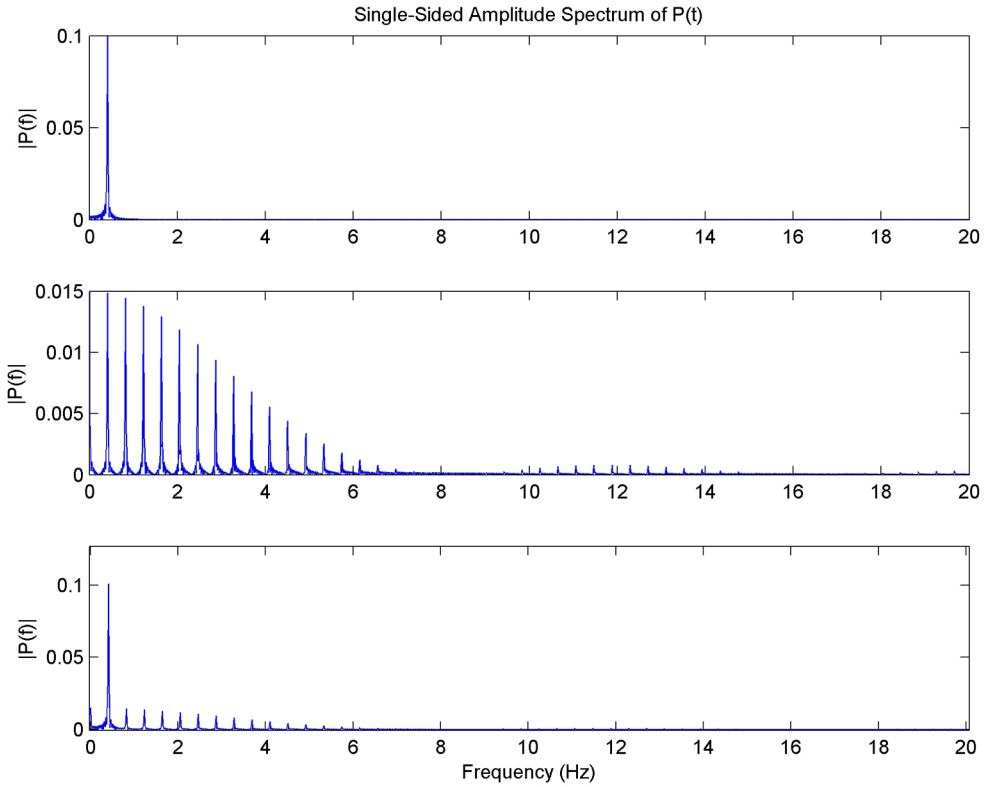


*Figure 4.3:* Single-sided amplitude spectrum of idealised pressure response. Top panel: sinusoidal component, middle panel: impact impulse component, bottom panel: combined pressure record

different Fourier spectra, with the deeper recorded signal showing diminished higher frequencies. The bottom panel indicates the combined pressure signal of the hydrostatic and the impulse components.

This image is similar to Figure 3.6 for impacting events on a impermeable sloped structure, suggesting similarity in this combined pressure response to experimental conditions.

However, analysis of a non-stationary signal such as that of an impacting wave event is not best handled through simple Fourier analysis, as this does not allow resolution

of frequency components within the temporal domain. It is possible to achieve this through application of Short-Time Fourier analysis, however this is limited by a constant window size throughout, permitting high resolution in either the frequency or time domain, but not both. Alternatively wavelet analysis offers a useful alternative that permits high resolution in both time and frequency.

#### 4.2.4.1 Wavelet analysis

Wavelet analysis (Combes et al. 1989) is a multi-resolution analysis, that allows expansion of a signal containing non-stationary components conducted in time-scale space. Derivation of the associated frequencies can be estimated, but requires further analysis. Wavelet analysis is similar to Fourier analysis in so much as it handles decomposition of signals in terms of basis functions. However, where Fourier analysis adopts trigonometric functions for the calculations, wavelet analysis adopts a family of wavelets, derived through translation, and dilation or compression of a *mother wavelet*.

A mother wavelet is a wave-like oscillation, varying in amplitude from zero, through some amplitude flux, and returning to zero. Each mother wavelet may be composed of multiple frequency components, therefore each scale, derived from dilation or compression of the mother wavelet, will also include multiple frequency components. It is common to calculate a *centre frequency* that characterises the dominant frequency of the wavelet. It is then possible to translate scale to frequency, through adoption of Equation (4.20), and knowledge of the mother wavelet.

$$F_a = \frac{F_c}{a.\Delta} \tag{4.20}$$

where $a$ is the scale , $F_a$ is the pseudo-frequency corresponding to scale $a$, $F_c$ is the centre frequency of the mother wavelet, and $\Delta$ is the sampling period.

There is not a clear formulaic process for the selection of an appropriate mother wavelet for the analysis procedure (Yaghmaei-Sabegh 2010), however consideration of the characteristics of the original signal, and the information required from the analysis will inform this choice. Also the choice of mother wavelet is often informed by previous work with wavelets in that particular field of study (Rafiee et al. 2009), with the most suitable wavelet typically reflecting the nature of signal characteristics.

Figure 4.4 indicates a trace for typical seismic event, and details the frequency components obtained after spectral analysis.

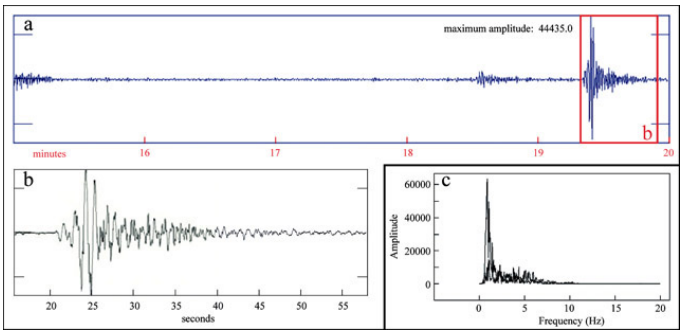


*Figure 4.4:* Panel a: Seismic trace for Telica event on 1 February 2011, panel b: zoom of highlighted section, and panel c: frequency components derived from spectral analysis (Instituto Nicaragüense de Estudios Territoriales 2012).

The rapid increase and decrease in amplitude notable in the zoomed trace in panel b exhibits similarity with the pressure response presented by both Bullock et al. (2007), Pedrozo-Acuña et al. (2008), and the data recorded during preliminary testing (Figure 3.5). The characteristic shape of the frequency components in panel c is similar to the equivalent output for the preliminary test provided in Figure 3.6. Seismic analysis tends to adopt the Morlet wavelet (Pyrak-Nolte and Nolte 1995) which is a reasonable approximation for dealing with wave impulse signals, therefore the Morlet wavelet was adopted throughout entire analysis section.

As with Fourier analysis, wavelet analysis has two broad forms, discrete and continuous. Discrete wavelet analysis present a discrete signal in a more redundant form. This allows storage of the original data in a more compressed form, and is therefore often used in digital communication, and the compression of images and videos.

Continuous analysis allows the ability to construct a time-frequency representation of the analysed signal, however retention of the additional information over discrete analysis provides a more detailed representation. Both discrete and continuous analysis have been used in wind, ocean, and earthquake engineering (Gurley and Kareem 1999). However, the ability to identify processes more readily in a detailed visual representation, makes continuous wavelet analysis more attractive in this case.

The continuous wavelet transform (CWT) of the function x(t) is defined by Equation (4.21).

$$X_w(a,b;x(t),\zeta(t)) = \int_{-\infty}^{\infty} x(t)\frac{1}{\sqrt{a}}\zeta * \frac{t-b}{a}dt \tag{4.21}$$

where $a$ is the scale parameter, $b$ is the position parameter, $\zeta$ is the wavelet function, and * denotes the complex conjugate.

Figure 4.5 presents a section of recorded pressure data for a 2-second test recorded at UNAM, including multiple sharp pressure fluctuations associated with plunging impact events, and the associated CWT spectrum for scales 1 to 250.

It is possible to identify the different features of the pressure response through inspection of the CWT spectrum. The information approximately between scales 100 and 190 applies to frequencies close to the incident wave frequency, and therefore relates to the oscillation in water depth above the pressure transducer. The rapid increase in pressure

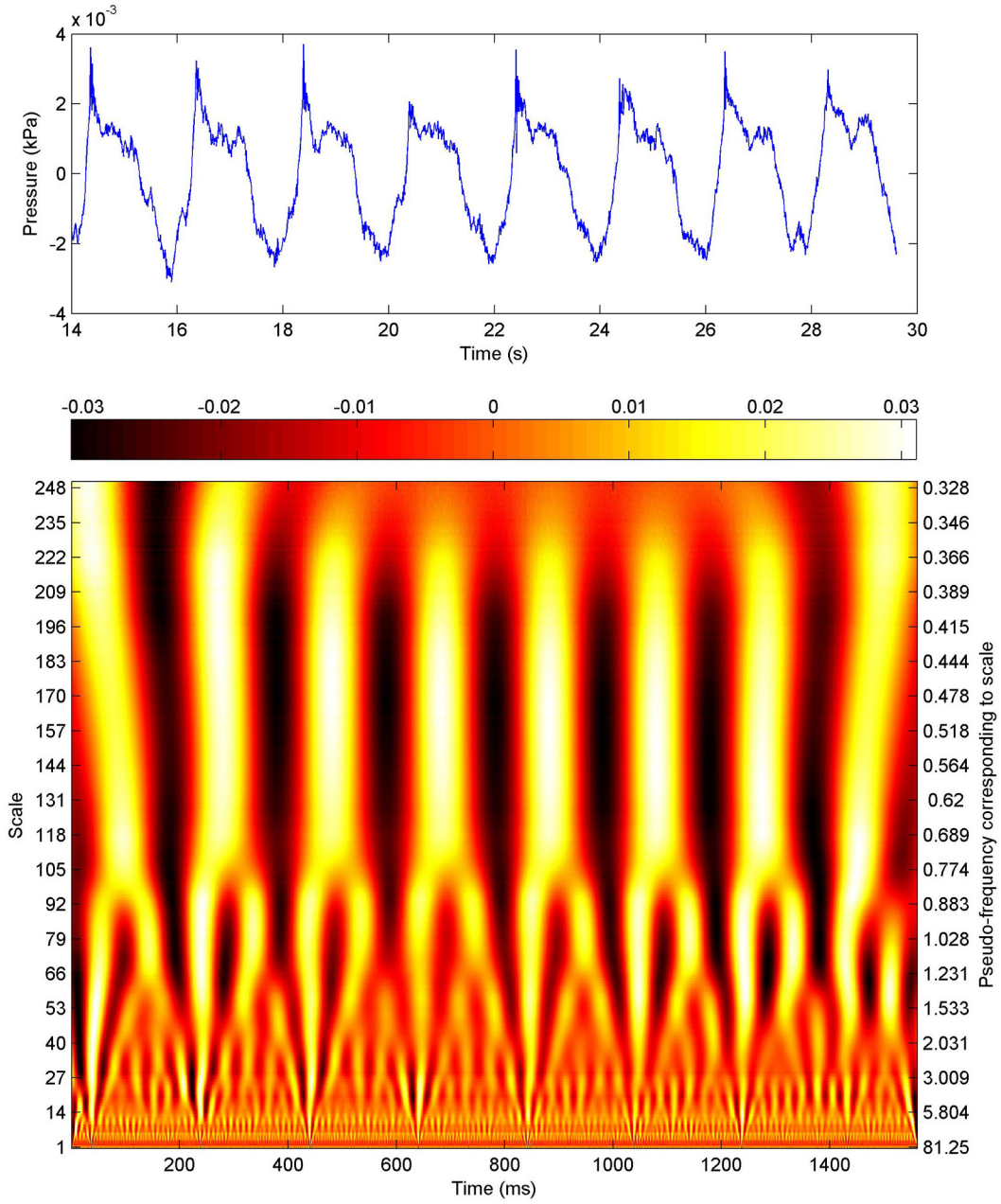


*Figure 4.5:* Top panel: Pressure response section including impact events recorded at UoP4 during test 20080624T164058 (plunging breaker). Bottom panel: Continuous wavelet transform spectrum for the selected pressure signal.

related to plunging impacts is identifiable in the CWT spectrum as a peak, before the incident wave frequency maximum, at scales less than 100. The peaks at similar scales occurring after this plunging impact provide additional detail to the pressure response,

describing the departure from an exact sinusoidal variation towards a pseudo-sinusoidal response.

Figure 4.6 presents an equivalent section of the pressure record for a 3-second wave test recorded at UNAM, and the associated CWT spectrum for scales 1 to 250. The waves in this record experienced breaking through a collapsing/surging process.

This image demonstrates a reduction in the clarity of the breaking impacts, with the CWT spectrum showing less distinct events than for plunging events in Figure 4.5. The relative magnitude of CWT coefficients at scales related to impacts (shown as colour intensity in Figure 4.6) is lower for collapsing/surging breakers than for plunging breakers, and for some events there is additional branching at low scales, indicating the impact may not have been localised at the transducer location.

In several cases an impact event for collapsing/surging waves can be identified in the CWT spectrum, but only those with a clear well defined impact were carried forward. This allowed identification of impact events not otherwise possible from simple inspection of the pressure-time record.

Unfortunately recovery of the pressure response from the CWT coefficients is not a simple matter, and adoption of an adapted transform is necessary. It is possible to define the CWT as the inverse Fourier transform of a product of Fourier transforms (Equation (4.22)), an approach called Continuous Wavelet Transform via the Inverse Discrete Fourier Transform (CWTFT) (Torrence and Compo 1998). This also allows an inverse operation, providing a reproduction of the original signal.

$$X(a,b;x(t),\zeta(t)) = \frac{1}{2\pi}\int_{-\infty}^{\infty} \hat{f}(\omega)\sqrt{a}\hat{\zeta}*(a\omega)e^{j\omega b}d\omega \tag{4.22}$$

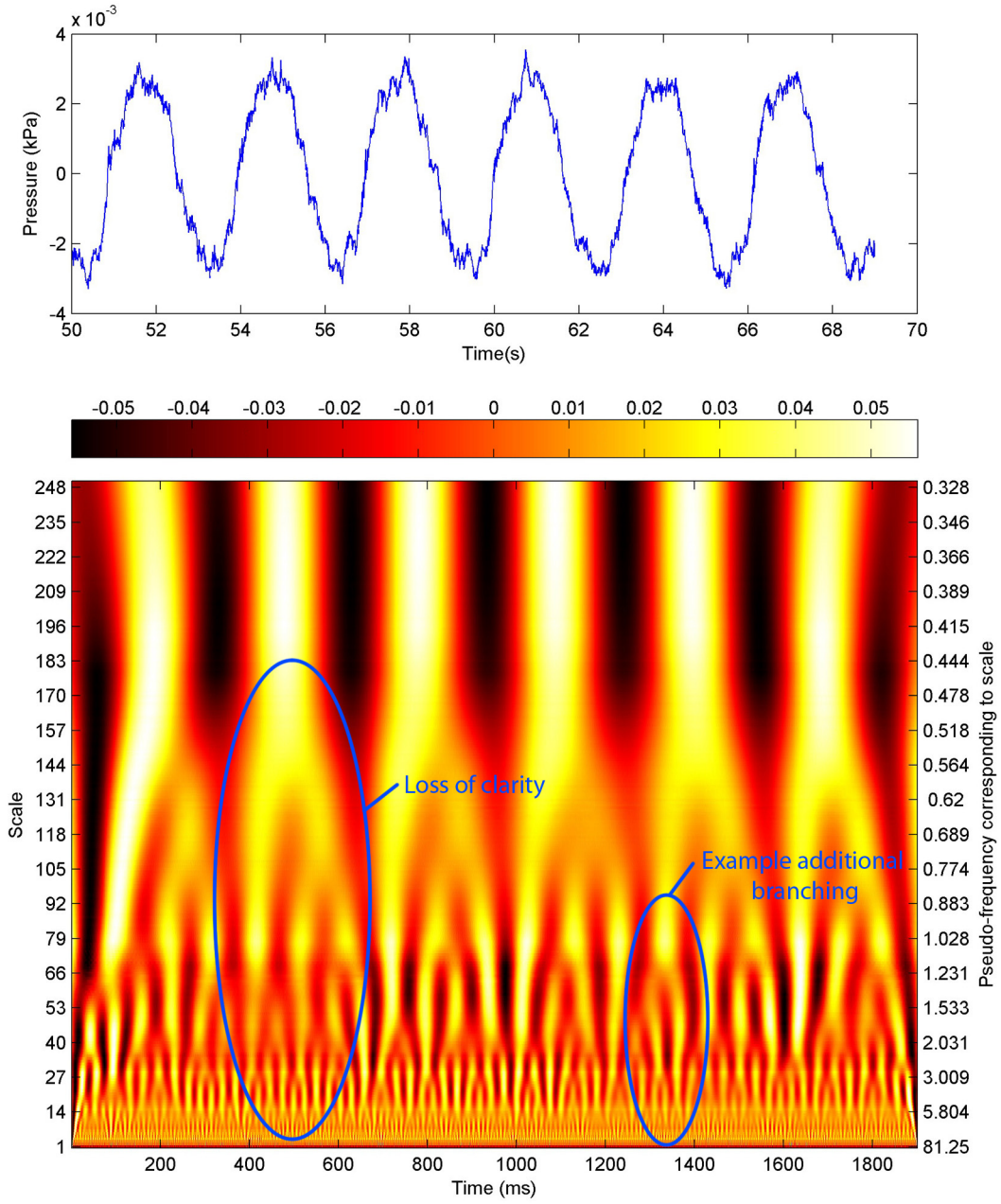


*Figure 4.6:* Top panel: Pressure response section including impact events recorded at UoP4 during test 20080703T131045 (collapsing/surging breaker). Bottom panel: Continuous wavelet transform spectrum for the selected pressure signal.

where $\hat{f}$ is the Fourier transform of the signal, $\hat{\zeta}$ is the Fourier transform of the wavelet, and $e^{j\omega b}$ is the analysing function used in the Fourier transform.

The inverse CWT (ICWTFT) utilises delta functions to reconstruct waveforms presented by Farge (1992) and, with some restrictions upon the nature of the mother wavelet, can be simplified to a single integral formula displayed as Equation (4.23), with a full derivation available in multiple locations, e.g. MathWorks (2012).

$$x_t = 2Re\left(\frac{1}{C_{\zeta_1,\delta}}\int_0^\infty < x(t)\zeta_1(t) > \frac{da}{a^{3/2}}\right) \tag{4.23}$$

where Re(...) is the real part, <...> denotes the inner product, and $\zeta_1$ is a wavelet introduced in the full derivation.

The two key criteria of the mother wavelet that must be met for this analysis to be valid are: the mother wavelet must have a real-valued Fourier transform, and the Fourier transform of the mother wavelet has support only on the set of non-negative frequencies. These conditions impose a restriction on the number of wavelets available for analysis, though the Morlet wavelet satisfies both conditions and is therefore suitable for use in further analysis.

A degree of error is introduced due to the computational procedure of application of a CWTFT to identify the pressure signal components, followed by an ICWTFT to reproduce the original signal. This error can be estimated through application of both transforms before provision for attenuation is included. Figure 4.7 displays the pressure response indicated earlier in figure 4.5, along with the reproduced pressure response after application of CWTFT and ICWTFT methods.

Both plots are almost coincident, however there is some discrepancy between the original and processed pressure responses. The standard deviation of the adjusted pressure response from the original pressure signal is 0.003kPa with pressure values fluctuating in a range of 0.681 kPa. With consideration of this standard deviation and some of the

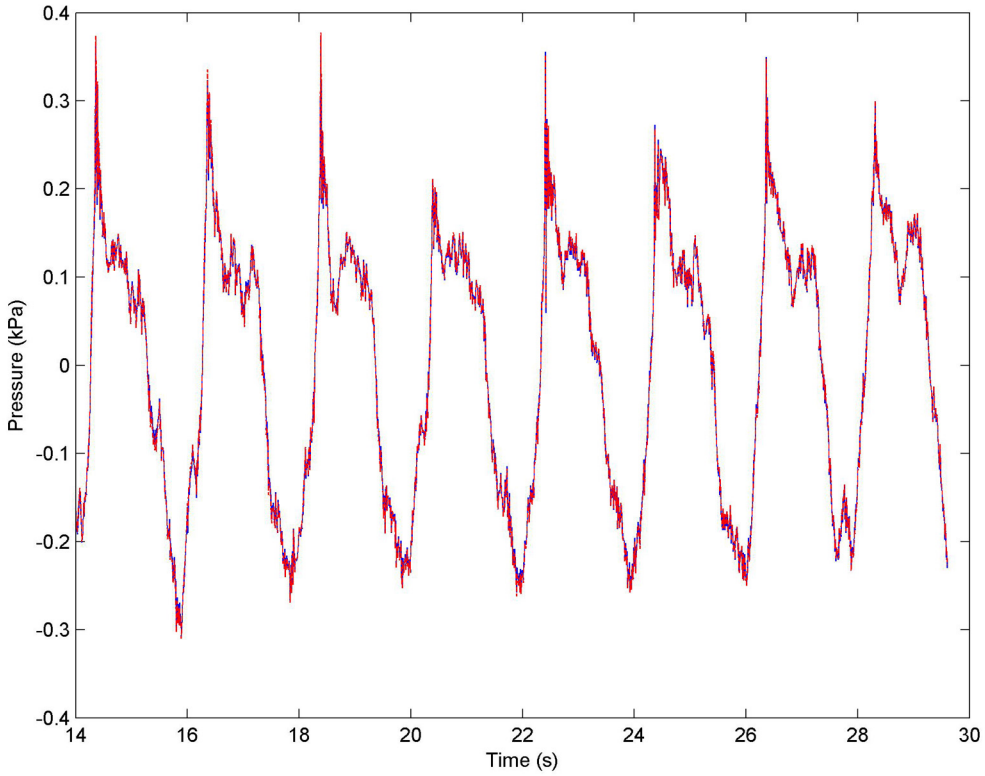


*Figure 4.7:* Pressure response section at UoP4 during test 20080624T164058. Blue solid line(—): original pressure response, red dashed line(- - -): adjusted pressure response.

uncertainties discussed below, the accuracy of this approach is adequate.

It is now possible to investigate the separation of the recorded signal into two components, through the manipulation of the matrix containing the wavelets coefficient values (used to generate the CWT spectrum). As previously discussed, it is possible to identify the temporal location and relevant scales of the impulse events when viewing the CWT spectrum. A series of polygons encircling the relevant sections can be constructed, creating a template allowing the separation of coefficients related to the impulses, and the coefficients related to the pressure generated by water elevation flux.

Adoption of this approach provided separation of the previously considered section of pressure record into constituent signals (Figure 4.8).

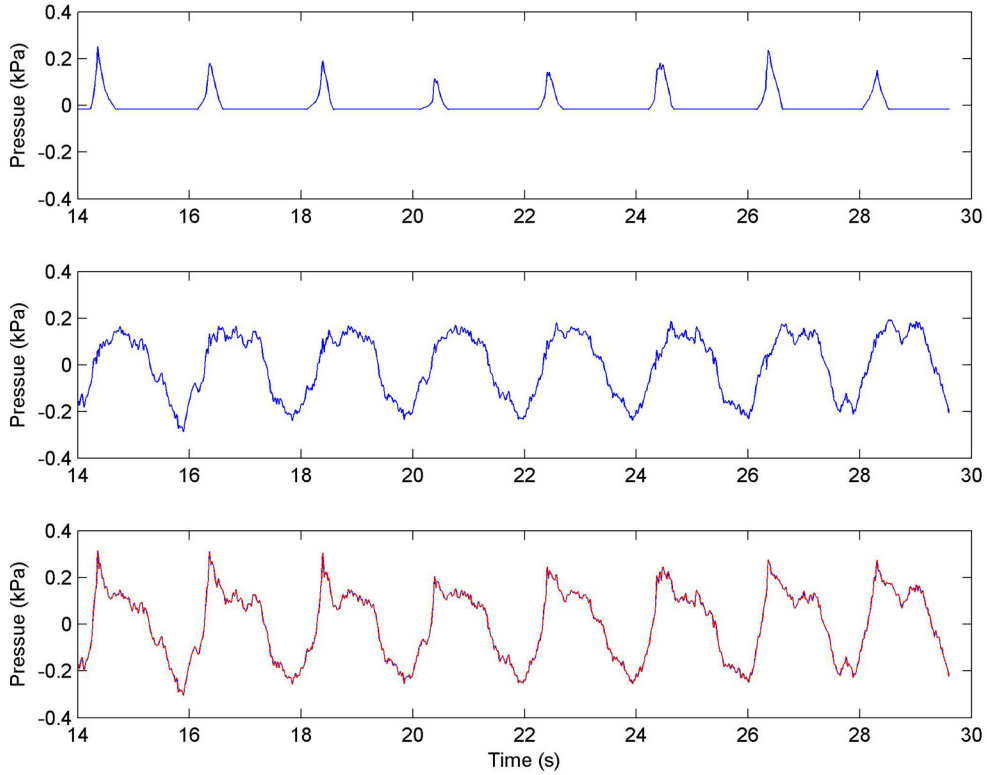


*Figure 4.8:* Top panel: Impulsive pressure responses; Middle panel: Pseudo-sinusoidal pressure response ; Bottom panel: Blue solid line(—): original pressure response, red dashed line(- - -): recombined pressure response.

The top panel displays the pressure response reproduced after application of the ICWTFT approach to the impulse coefficients. These appear to provide a series of sharp pressure responses similar to the idealised pressure response suggested earlier (Figure 4.2). The middle panel is the pressure response reproduced after application of the ICWTFT approach to the remaining coefficients, after removal of the impulse coefficients. This appears to provide a pseudo-sinusoidal signal, indicative of pressure responses generated by water elevation fluctuation. The final panel shows the pressure response resulting from recombination of the two components.

This method appears reasonable for separating impulsive pressure spikes from the pressure oscillations generated by the change in water elevation above the transducers. After successful separation it is possible to deal with the attenuation of the two components separately.

#### 4.2.4.2 Impulsive attenuation review

The attenuation of pressure waves propagating through various materials has been previously studied. The published research incorporates a wide range of material types as well as a variety of frequency ranges, along with consideration of other parameters.

Both solid rock (Ahrens and Duvall 1966; Berryman 1986) and granular material of different sizes (Bardet and Sayed 1993; Chotiros 1995) have been investigated. This research was often conducted to consider the seismic behaviours of materials by seismologists, or by geophysicists and geologists in connection with offshore oil and gas exploration.

Again the basis for the work in this area stems from Biot (1956*a*,*b*) and has generated numerous models (e.g. Stoll and Kan (1981), Yamamoto (1983), and Stern et al. (1985)). The original work indicated that there are multiple waves that pass through a sediment matrix, propagating at different speeds and experiencing different attenuations.

The theory predicts the presence of two co-existing compressional wave modes propagating through materials. The first compressional wave, the fast wave, is observed when fluid and sediment particle motion is in-phase, while the second compressional wave, or slow wave, is observed when fluid and particle motion is out of phase. The two compressional waves were confirmed by Plona (1980), however the slow wave in saturated

and almost-saturated conditions is very difficult to observe (Oelze et al. 2002) due to rapid attenuation.

Figure 4.9 presents the theoretical attenuation of a range of numerical models as a function of frequency, indicating that the attenuation of the slow wave is significantly higher that the attenuation of the fast wave.

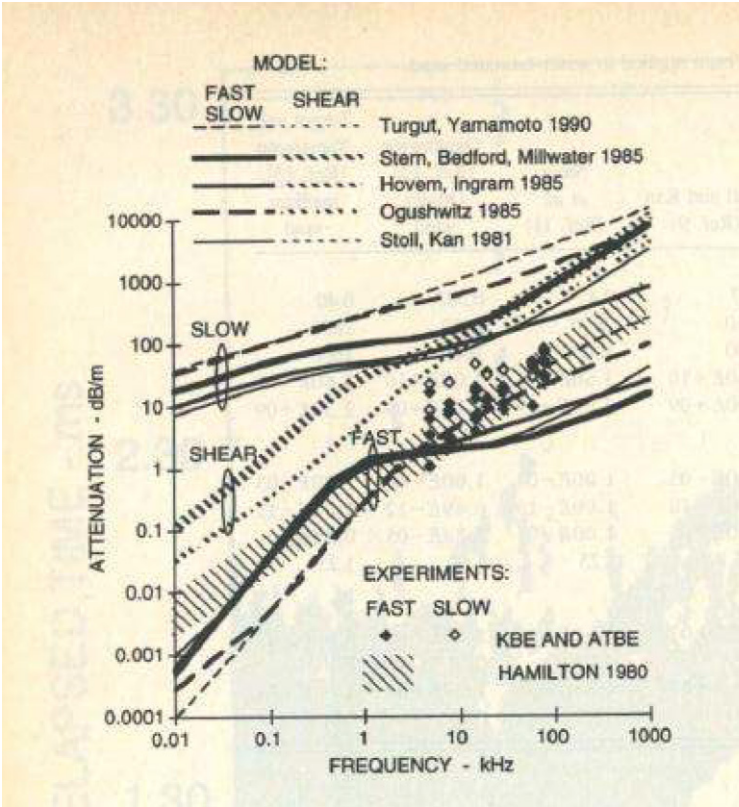


*Figure 4.9:* Wave attenuation of fast and slow waves as a function of frequency (Chotiros 1995).

Chotiros (1995) also reviewed the performance of a number of numerical models and concluded that prediction of slow wave attenuation by Stoll and Kan (1981), Yamamoto (1983), and Stern et al. (1985) was poor compared with experimental data.

Considering the predominant areas of research interest concerning wave attenuation in

porous materials, the large distances involved allows disregard of the slow wave due to the very high attenuation, and most efforts have therefore concerned the fast wave.

The extension of the original Biot work to include two immiscible pore fluids by generalisation of the original single fluid theory was made many decades ago by Brutsaert (1964). In this work the structure put forward by Biot was retained, however the pore spaces were occupied by two fluids with the introduction of effective fluid density and bulk modulus as suitable volume-weighted averages of the density and bulk modulus of each pore fluid. While the pressure within the two fluids remains spatially uniform this approach retains good accuracy (Pride et al. 1992), however this is not the case with an unsaturated beach. The compressibility of the air component causes absorption of some of the energy during propagation, increasing the attenuation compared with a fully saturated condition. Many researchers have recognised this role of sediment saturation level on the degree of attenuation exhibited by propagating waves (e.g. White (1975) and Velea et al. (2000)).

Clukey et al. (1985) investigated liquefaction of sediment particles and discovered that coarse particles are less susceptible to liquefaction as the coarse sediment more effectively dissipates the pore-pressure increase. Unfortunately the effect of sediment grain size on the degree of pressure dissipation was not parametrised.

Bardet and Sayed (1993) described the impact of varying sediment saturation on the compressional wave velocity and attenuation of previously recorded experimental data. An initially small departure from fully saturated sediment resulted in a rapid increase in attenuation, with more steady increase as the saturation continues to decrease below 0.985.

### 4.2.5 Impulse attenuation summary

It has been argued that the method applied by Pedrozo-Acuña et al. (2008) for the attenuation of pressure responses including impact events was inappropriate, and provided inaccurate estimates of the surface pressure. It appears that separation of recorded pressure signals into impulsive and pseudo-sinusoidal components is possible, with handling of the attenuation of each component achieved separately.

Multiple researchers have investigated attenuation of compressional waves propagating through porous materials, highlighting the importance of signal frequency, saturation level, and characteristic sediment parameters. There is no existing numerical model that relates attenuation to all of these variables. There is specifically a sparsity of any models that have been validated against experimental data at the low frequency range involved in this work (less than 100Hz indicated through analysis of preliminary tests), with a lack of studies investigating signals at frequencies below 1kHz.

Most research has been concerned with the attenuation of the fast wave, and neglects consideration of the slow compressional wave due to rapid attenuation. A lack of understanding of how a plunging impact pressure wave is translated through the sediment matrix, and whether both slow and fast waves are involved complicates the handling of attenuation through application of an existing relationship.

Appropriate handling of the attenuation experienced by pressure signals propagating between the bed surface and pressure transducers therefore requires development of a new approach.

### 4.2.6 Attenuation correction of separated signal components

A pragmatic method of estimating the degree of attenuation experienced by different frequencies is presented in this section, to assess the reproduction of a shallow pressure record from greater depth of burial. This utilises the change in coefficient amplitude at each scale of the CWT spectra of co-located pressure transducers.

Firstly the attenuation of the pseudo-sinusoidal component is considered. Although the CWT spectrum of this signal does include more than one frequency, these additional components describe both the departure from non-sinusoidal water elevation fluctuation, and noise within the recorded signal. If each of these frequencies are provided with a frequency-dependent correction, the pressure response will become distorted by greater attenuation-correction of the higher frequencies. The resultant signal would therefore become distorted and dominated by higher frequencies. Therefore the entire signal is corrected by a single attenuation correction determined by the wave frequency. The attenuation-correction is determined through comparison of the amplitude of CWT coefficients of pressure records at different depths.

The attenuation correction of the impulse component is handled through the application of a frequency-dependent correction to each frequency element. The concerns over boosting signal noise is avoided during isolation of the impulsive events as noise occurs at the highest frequencies and can be excluded. The CWT spectrum of the impulse signal of each pressure transducer is compared, and the ratio of the CWT coefficients at each scale provides an estimate of the attenuation experienced.

If a consistent noise level were recorded at a lower frequency in the pressure signal, it could be handled by comparing the amplitude of the fluctuation within the impulse component to the amplitude in the pseudo-sinusoidal component. The difference between the two will correspond to the contribution to the impulse component at that

frequency. This case was not encountered during analysis, so was not utilised.

Validation of the approach of separating a pressure signal into two components, before handling attenuation correction, is conducted through consideration of a section of data recorded at GWK during full-scale testing (López de San Román-Blanco et al. 2006). This data is adopted as the wave impact events occur above co-located pressure transducers, providing clean records with low noise. The pressure recorded at a shallow depth of burial (henceforth PTa) provides a baseline pressure response, while the more deeply buried pressure transducer (henceforth PTb) provides a second record, allowing the attenuation between the transducers to be determined. The recorded pressure responses were separated into impulsive and pseudo-sinusoidal components as described above (Section 4.2.4).

The attenuation correction of the pseudo-sinusoidal component was calculated through comparison of the CWT spectra of these two pressure records. The relative intensity of the CWT coefficients at scales consistent with the wave frequency allows estimation of the attenuation of this component, and a suitable correction can be derived.

The attenuation of the impulsive component is estimated in the same manner, however the attenuation of each frequency is determined, and a related attenuation correction is established. The application of these attenuation corrections to the impulsive component of PTb CWT coefficients. The two components are recombined and an ICWTFT is conducted to reproduce PTa pressure response. The upper panel of Figure 4.10 indicates the original pressure responses of PTa and PTb, while the bottom panel indicates the original pressure response of PTa, and its reproduced response from the attenuation-corrected response of PTb. Similar analysis is conducted for isolated pseudo-sinusoidal (Figure 4.11) and impulse components (Figure 4.12) are also provided.

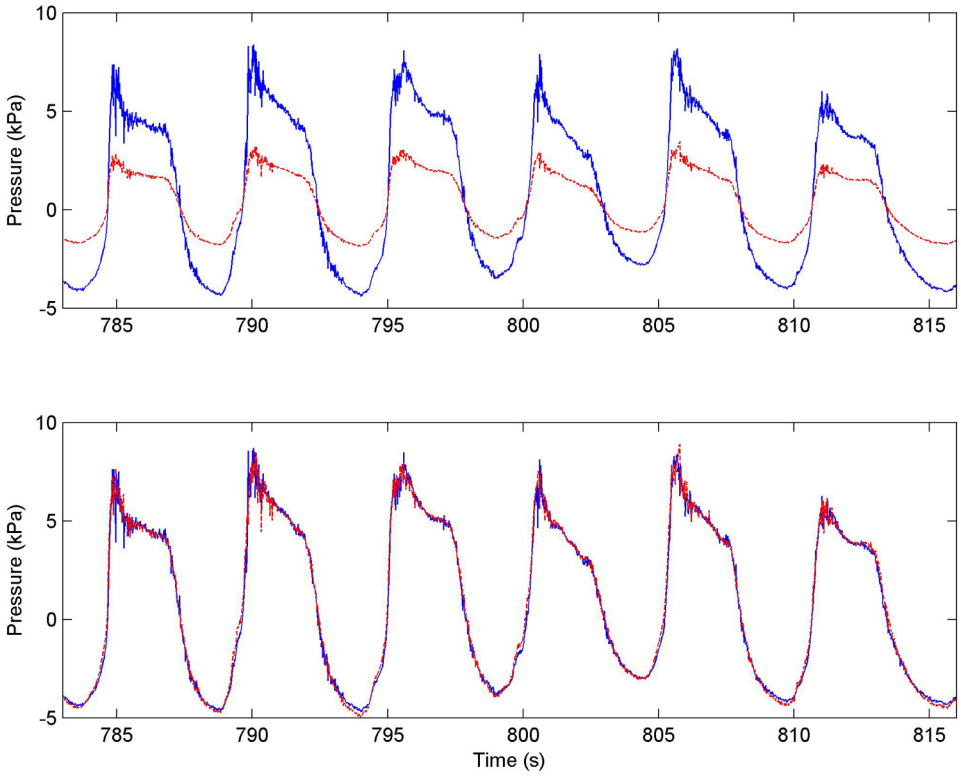


*Figure 4.10:* Top panel: Blue solid line(—): original pressure response at PTa, Red dashed line(- -): original pressure response at PTb. Bottom panel: Blue solid line(—): original pressure response at PTa, Red dashed line(- -): attenuation corrected-pressure response using PTb

The reproduced attenuation-corrected pressure response appears to provide a good representation of the recorded pressure at a location closer to the bed surface for both individual components, and the recombined total signal. This seems to indicate that separation of the signal, and subsequent account for attenuation of the separated components by appropriate frequency-corrections, reproduces a pressure response at a different depth of burial. This is not possible without separation of the pressure signal into impulsive and pseudo-sinusoidal components.

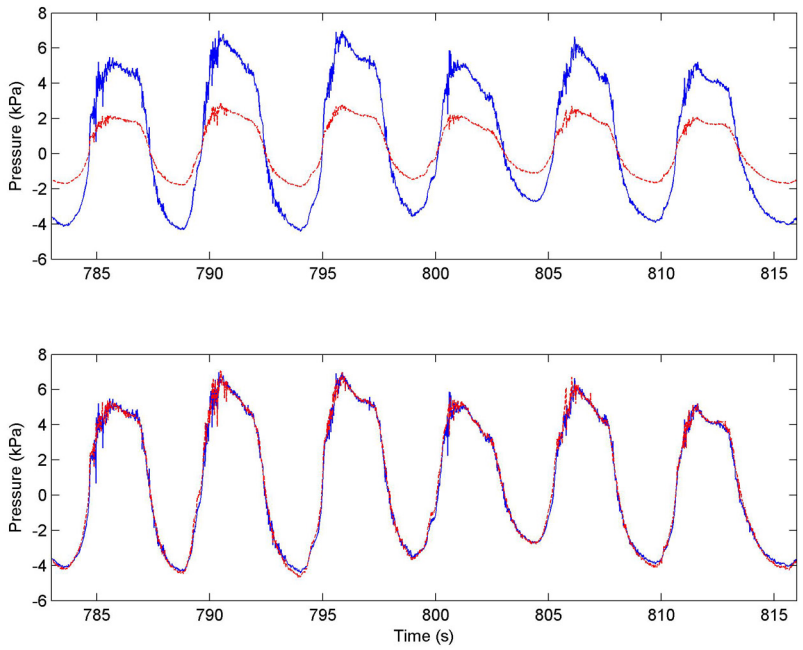


*Figure 4.11:* Application of pseudo-sinusoidal pressure correction approach to GWK data

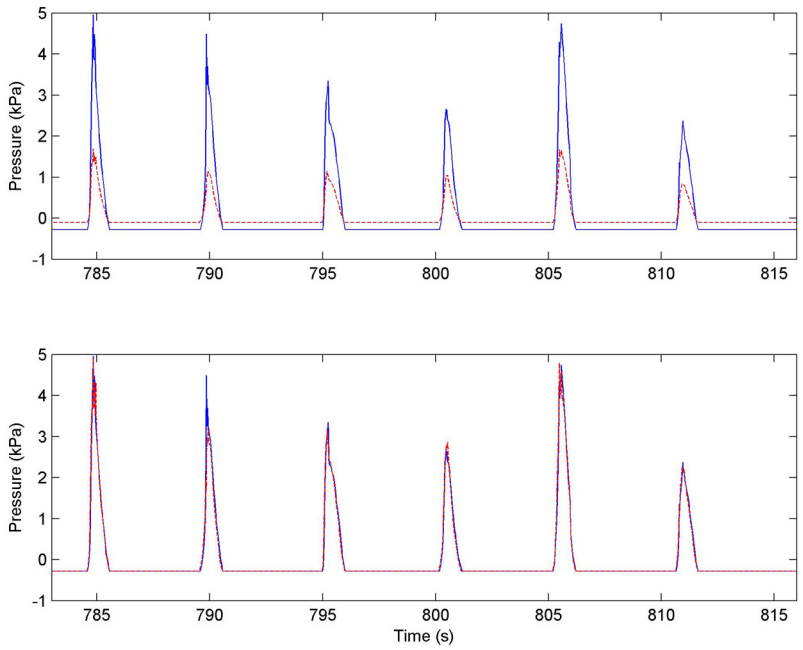


*Figure 4.12:* Application of peak pressure correction approach to GWK data

### 4.2.7 Attenuation correction methodology

The accurate reproduction of the pressure record obtained at GWK was effective, as a direct measure of the attenuation of each frequency between the locations was determined. For further analysis, the pressure response at the bed surface is required, and therefore a direct measurement of the attenuation between the initial and target locations is not possible.

An estimate of the attenuation can however be made if the CWT coefficients of three co-located pressure transducer are utilised. The root mean square (RMS) of the CWT coefficients at each scale provides a measure of the amplitude of signal fluctuation at that scale. Comparison of these values for two locations, provides an indication of the attenuation between the two locations, yet comparison of more than two locations, allows the form of the relationship between CWT coefficient amplitude and depth of burial to be estimated. This permits estimation of the CWT coefficients at the bed surface, and consequently the surface pressure may be estimated.

Monitoring the saturation level within beaches was not conducted in this work. Depth-variation of the degree of saturation of the sediment may have occurred, due to the turbulence introduced by impact events. This would have caused greater aeration closer to the bed surface, thereby increasing attenuation. The attenuation-correction in this work is established using records at depths of burial below the disturbance depth caused by impact events. Any variation in saturation level was therefore unlikely to be recorded. The beach experienced low infiltration at the pressure transducer location as, from inspection of video records, the groundwater exit point remained above the pressure transducer location throughout the swash cycle. This lack of infiltration prevented introduction of additional air content to the sediment matrix, as described by Faybishenko (1995). Lacking further information with regards to the depth variation of the saturation level, it will be assumed that the homogeneous, isotropic nature of the sediment

provided a constant attenuation per unit depth. This seems reasonable due to the good agreement observed between recorded and predicted pressure responses in Figure 4.11. If flux in the saturation level with depth close to the surface did occur, a consequent under-prediction of the surface pressures will be produced.

The relationship between signal attenuation and depth of burial is thus assumed to be of the form:

$$\frac{A_x}{A_0} = e^{-\delta x}, \tag{4.24}$$

where $A_x$ is the magnitude of the CWT coefficient at distance $x$ from a second location, $A_0$ is the magnitude of the CWT coefficient at the second location, and $\delta$ is a function of frequency determining the attenuation. The form of this relationship is consistent with the approach adopted by several researchers, when considering attenuation in different environments (Yamamoto et al. 1978; Oumeraci and Partenscky 1990; Vanneste and Troch 2012).

Rearrangement of Equation (4.24) can be performed as follows:

$$\ln A_x = \ln A_0 - \delta x. \tag{4.25}$$

Linear regression of $\ln A$ vs. $x$ provides a relationship with a gradient of $\delta$. Substituting in Equation (4.24) provides the empirical description of pressure attenuation with depth.

The $\delta$ values for each scale were averaged across analysed tests to provide an average $\delta$ value per scale, and a unit depth was adopted for distance $x$. This was used in Equation (4.24) to produce an estimate of the attenuation-correction per unit depth experienced at each scale. A characteristic relationship was derived between attenuation-correction

and scale by fitting a logarithmic relationship to the data.

It would clearly be preferable to examine additional pressure records, providing additional information, and offering a higher degree of confidence in the established relationships. However, the approach of determining a specific relationship from limited data locations is not uncommon. For example, Massel et al. (2004) use pressure fluxes recorded at four locations to calibrate an attenuation relationship.

One significant complication was encountered during the application of this approach. The comparison of CWT coefficients at all scales between PTs UoP2 and UoP3 indicated a region of apparent amplification in the signal, observable in Figure 4.13. This amplification was not apparent when comparing PTs UoP1 and UoP2. This unexpected observation clearly causes significant difficulties with the application of the approach. Examination of the literature did not provide explanation of this behaviour, therefore the information related to those scales was removed, to prevent undue influence on the derived attenuation relationship. This however involved the removal of approximately one third of the scales analysed, and underlines the preference for including additional measurement locations to establish the attenuation relationship more accurately.

Translating scale to frequency allows an equivalent frequency relationship to be established, derived as:

$$\delta_c = 0.449 \ln(f) + 3.1186, \tag{4.26}$$

where $\delta_c$ is the attenuation correction per m, and f is the frequency of the component. This logarithmic fit provides a relationship consistent with expectations of a constant rate of attenuation within a homogeneous isotropic material, and provides a relationship (Figure 4.14) in line with those presented in the literature.

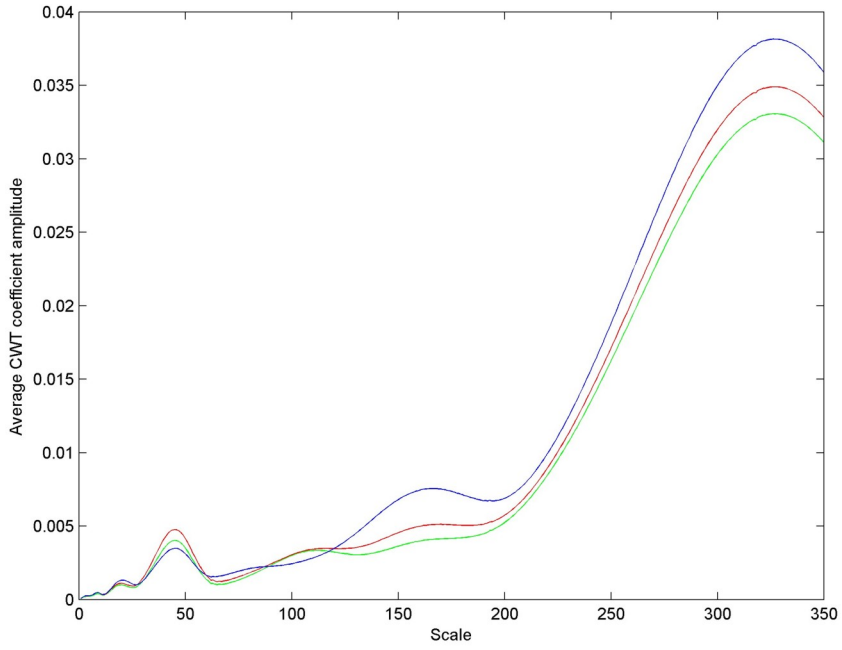


*Figure 4.13:* Example RMS of CWT coefficients for buried pressure transducer array across all scales considered (Test 15 part 1). Solid blue line (—): UoP3, solid red line (—): UoP2, solid green line (—): UoP1.

A reasonably consistent agreement is achieved at low frequencies, with increasing scatter at higher frequency values, which may be due to the small energy level at higher frequencies. Small fluctuations in noise level, may help to explain variation from the predicted relationship.

Thus we have provided a pragmatic approach to deriving the pressure-depth relationship, despite some uncertainty in the response at smaller scales (higher frequencies) in the current data. Nonetheless further work is required to confirm this approach.

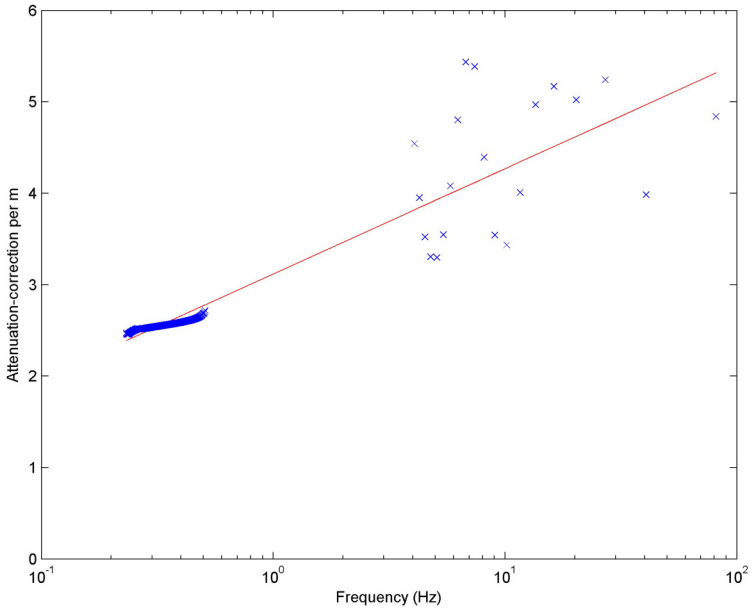


*Figure 4.14:* Frequency vs. attenuation-correction. Blue crosses (x) frequency specific attenuation-correction estimates, solid red line (—) proposed frequency vs. attenuation-correction relationship.

### 4.2.8 Validation of attenuation correction

Validation of this methodology requires pressure responses at a minimum of four locations. This provides measurements at three depths capable of establishing a relationship between amplitude and depth of burial, and a fourth location, where a reproduced signal generated by the proposed relationship can be compared with the actual pressure response recorded at that depth. Unfortunately only three transducers were co-located during the experimental programme, therefore validation requires a known pressure at a known depth of burial.

This can be achieved through consideration of the pseudo-sinusoidal component. The relationship derived between scale and attenuation-correction can be used to estimate the pressure fluctuation of the pseudo-sinusoidal component at the bed surface. If the surface pressure fluctuation is assumed to be generated by variation in the water depth,

an estimate of the hydrostatic surface pressure can be made with use of the video record at the PT location.

Experimental values were investigated for an entire experiment containing well defined pressure fluctuations in the video record (Test 12 part 1). This approach indicated good agreement between the observed hydrostatic surface pressure fluctuation, and the correction of the recorded pressure response at UoP4 corrected to the surface with the proposed relationship. The root mean square error was approximately 0.015kPa, or 2%. This is not unsurprising, as this frequency coincides with the region indicating good agreement with the predicted relationship in Figure 4.14. It is recognised that the validation of this approach is only possible for a narrow region of frequencies, and further confirmation of the assumed relationship, though highly desirable is not possible with the data sources available.

The co-located pressure records used in establishing the attenuation-correction are not used to estimate the bed surface pressure response. The actual transducer record adopted for correction (UoP4) was laterally displaced from the vertical PT array, and the saturation level within the beach may vary between these two locations. However, due to the reasonably close proximity of all the pressure transducers it is unlikely significant fluctuation was experienced.

Fluctuation in embedded depth occurs throughout each test as cross-shore profile change occurs. Profile measurements were made at intervals between wave action, thus allowing calculation of the pressure transducer embedded depth at these times. Due to an absence of real-time embedded depth measurements, it is necessary to make an assumption on the embedded depth throughout each test segment.

As the importance of the large impact pressures generated by plunging impacts are

being investigated, it is important to avoid artificial inflation of the pressure responses. As such, the final depth of burial at each stage will be adopted. This will cause an underestimation of the attenuation that occurred for most pressure responses. For example, for a particular event where attenuation occurred through 100mm, account will only be provided for attenuation through 80mm.

While a linear interpolation may provide a more accurate average prediction for a test segment, morphological response does not occur in linear manner, but with rapid initial change followed by lower rate as an equilibrium profile is approached. Assuming a linear change in embedded depth risks overestimation of the peak pressure in the early phase of each test segment.

Attenuation within a porous media is an active area of research, with specific attention being paid to the development of pressure attenuation at more onshore locations. Przyborska (2010) discusses formulation of a mathematical model for the attenuation of pore pressure when wave breaking is present, capable of dealing with phase-resolving component (induced by surface wave oscillations) and phase-averaged component (induced by wave set-up).

Barrière et al. (2010) recognised the discrepancy in predicted attenuation of elastic waves within partially saturated porous media. Specific attention was paid to the low frequency range (1Hz to 10kHz) where the propagation of P-waves (the primary elastic wave produced by earthquakes) will be investigated and, the attenuation related to the water content and wave frequency in a homogeneous sand.

It is likely that the continued development of theory in this area will provide a more robust method for dealing with the combination of surface wave oscillations and impulsive impacts in the coming years. The complication involved with fluctuation in the aeration

level will remain, with monitoring the change in saturation necessary to provide a more accurate estimate of attenuation.

## 4.3 Beach profile calibration

The coarse-grained sediment beaches recorded at UNAM displayed negligible alongshore profile variation. One profile close to the centre-line of the channel was therefore deemed to be sufficiently representative of the entire beach width. A cross-shore profile was taken after each wave train ceased and the water within the flume returned to a calm state. The profiles were measured with a Leica TCR series total station, utilising a reflecting prism staff.

The specific positioning of each profile measurement for the same cross-shore location varied between experiments, due to human error in staff positioning. To account for this variation in the x- and y-coordinates, it is useful to translate the profile to a consistent base profile line, achievable by correcting any offset from the base profile position by shifting the elevation in an alongshore direction. The consequences of this approach is demonstrated in Figure 4.15.

Each member of the experimental team exhibited a different technique when positioning the staff at the bed surface during profile measurements. This resulted in a discrepancy in the elevation of regions exhibiting no change, however where the entire region of morphological change is contained within the profile measurement, each profile can be de-meaned to provide a consistent datum. Where this was not the case, the mean was unrepresentative and would result in significant error in the sediment transport calculations. In such circumstances, regions where no profile change was experienced throughout the test were adjusted to coincide. A datum in the cross-shore chainage was also established with selection of a location where no morphological change was registered during any of the tests.

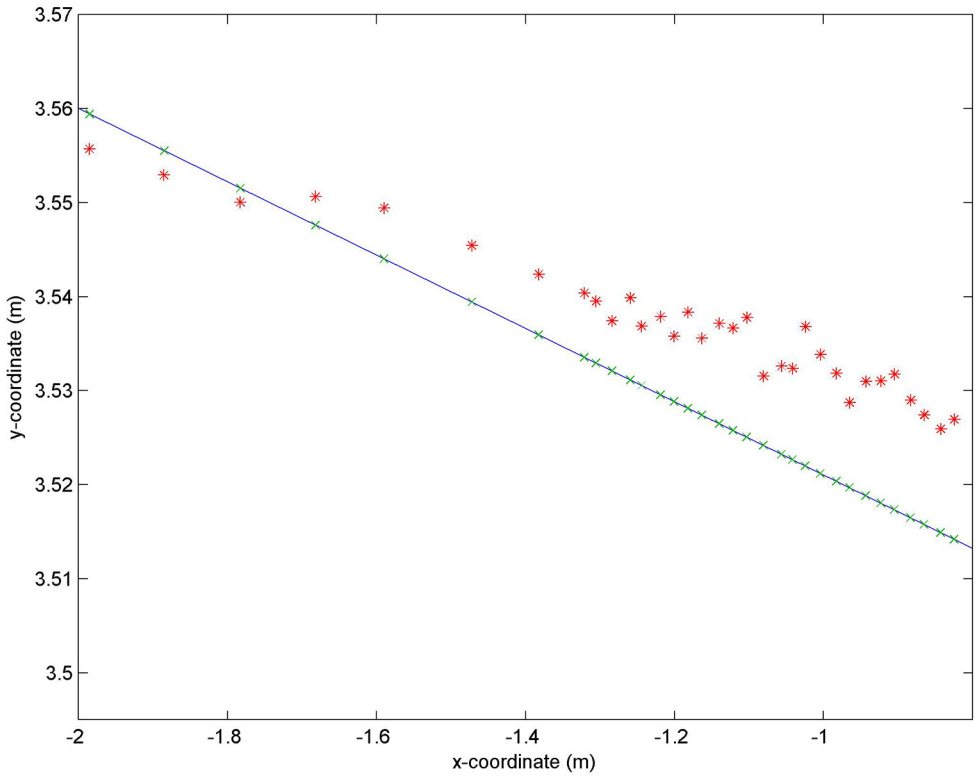


*Figure 4.15:* Co-ordinate adjustment for correcting measurement offset from base profile location (Solid blue line (—): Base profile line, Red stars (*): original profile coordinates, Green crosses (x): corrected profile coordinates

If an obvious elevation error existed, or there was significant discrepancy compared with the additional profile photographs, the profile was discarded.

Due to the variation in measurement location between tests it is not immediately possible to monitor sediment volume flux, therefore the measurements were linearly interpolated onto the same grid for comparison.

The accuracy of measurements can be estimated through inspection of profile elevation measurements in areas where no morphological change occurred. Through inspection of

the upper beach crest where no change was experienced during the entire experimental programme, the standard error of the profile measurements is less than 1mm.

## 4.4 Summary

In order to obtain forcing conditions, translation of the water elevation data to incident wave conditions was achieved through the application of the SIRW method outlined by Friigard and Brorsen (1995). Consideration of the incident and reflected waves provides supporting evidence of the expected behaviour as beach profiles steepen, supporting appropriate handling of the wave separation.

A new approach for analysing a pressure record is presented, that enables isolation of the wave impact and hydrostatic pressure components through use of a continuous wavelet transform. These components can then be handled individually to address the differing attenuation experienced by each.

Attenuation is highly frequency-dependent, therefore an individual attenuation-correction is derived for each frequency contained within the separated impulse pressure response. The pseudo-sinusoidal pressure response, related to water level fluctuation at incident wave frequency, is corrected with a single value based on the wave period. Recombination of the two components provides estimation of the pressure at the bed surface for use in further analysis.

Adjustment of the profile elevation data involved elimination of the offset experienced when positioning the reflecting prism staff, and establishment of a chainage baseline to allow sediment transport calculations.

Preparation of these various data types, allows the investigation into the importance of

breaker type, and associated impact intensity, on the morphological response, and net sediment transport rate of gravel beaches.

# Chapter 5

# Observations of coarse beach dynamics

This chapter presents a summary of the experiments conducted, and provides a selection of the beach profile results, along with subsequent morphological analysis conducted on the data. This analysis and interpretation of the laboratory measurements of profile change on steep beaches will be used to help establish the importance of breaker type in altering the profile response on gravel beaches.

## 5.1 Introduction

This section provides a typical sample of the profile data recorded during the test regime. Fuller details of all the results can be found in Appendix B, along with details of the testing schedule, providing the test codes used for the pressure and wave records, beach profiles, and the associated wave height and wave periods. A summary of the test is presented in Table 5.1. Test 7 appears before test 6 as this retains an ascending wave height with order of presentation, necessitated by a minor discrepancy in test order during the experimental programme.

Figures 5.1 and 5.2 provide a visual description of typical wave breaking that occurred during the experimental programme for plunging breakers and collapsing/surging breakers respectively. The video recorded a limited cross-section of the beach, therefore the entire wave breaking process was not captured. This concentration on the impact location meant that not all morphological features were within the field of view, particularly more seaward features such as the beach step.

| Test number | Wave height at breaking $H_b$ (m) | Wave period $T$ (s) | Wavelength (m) | Iribarren number, $\xi_b$ |
|---|---|---|---|---|
| 7 | 0.109 | 2.01 | 3.727 | 1.52 |
| 6 | 0.124 | 2.01 | 3.724 | 1.42 |
| 8 | 0.133 | 2.01 | 3.726 | 1.38 |
| 9 | 0.149 | 2.01 | 3.720 | 1.30 |
| 10 | 0.172 | 2.00 | 3.698 | 1.20 |
| 11 | 0.087 | 3.04 | 5.843 | 2.58 |
| 12 | 0.093 | 3.04 | 5.848 | 2.48 |
| 13 | 0.105 | 3.04 | 5.842 | 2.34 |
| 14 | 0.119 | 3.04 | 5.853 | 2.21 |
| 15 | 0.118 | 4.03 | 7.860 | 2.94 |
| 16 | 0.134 | 4.06 | 7.904 | 2.77 |
| 17 | 0.145 | 4.04 | 7.883 | 2.65 |

*Table 5.1:* Test conditions estimated after separation of incident and reflected waves.

Figure 5.1 provides a series of six images from the video record, describing an entire wave period for a plunging impact. Panel a) indicates the end of the previous backwash event, prior to the high flow rate of the uprush of an incoming wave, shown in Panel b). Panels c) and d) provide a description of the wave overturning and plunging impact on the beach sediment matrix, and continued uprush. Panel e) indicates the point of maximum run-up limit after deceleration of the uprush flow, consistent with the berm crest elevation. Finally, Panel f) indicates a stage of the backwash with flow accelerating in a seaward direction, prior to interaction with the subsequent incoming swash event.

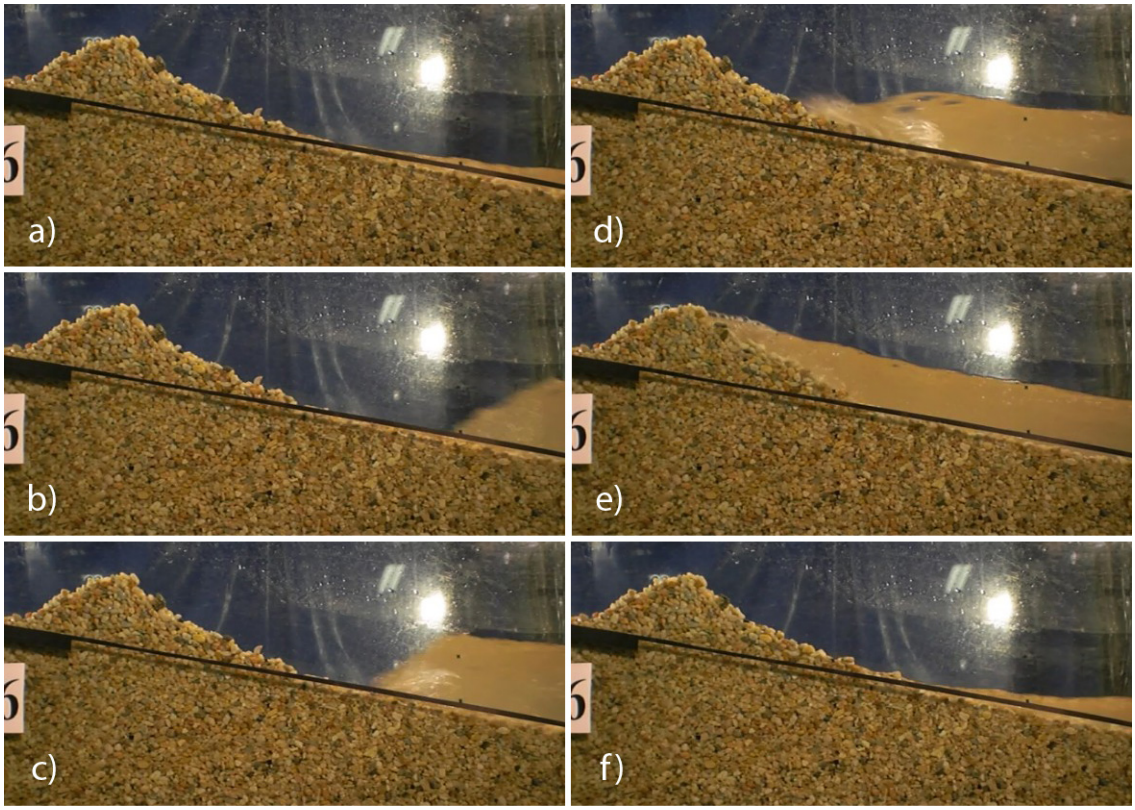


*Figure 5.1:* Sequence of six video frame captures describing a single swash event of a plunging breaker-type for test 20080617T110846.

Figure 5.2 also provides six images from a video record, however a description of a collapsing/surging event is described. Panel a) indicates the rapid flow of the uprush for an incoming wave event. Panel b) includes a small degree of turbulence at the uprush front generated by bore collapse, while Panel c) highlights the continued uprush of the incident swash event. Panel d) indicates the point of maximum run-up limit after deceleration of the uprush flow, consistent with the berm crest elevation. Panel e) displays a drop in the water level as backwash phase progresses, accelerating in a seaward direction. Panel f) indicates the continuation of accelerating flow in the backwash phase of the swash event, prior to the beginning of the subsequent event.

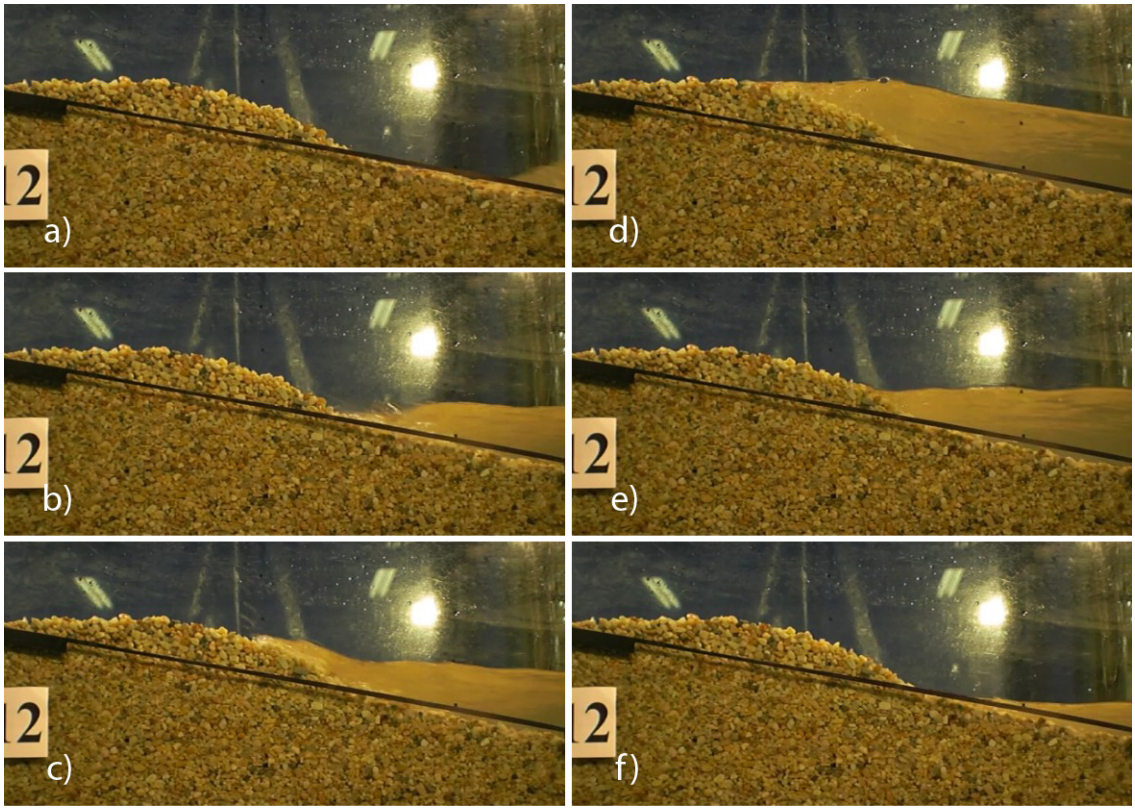


*Figure 5.2:* Sequence of six video frame captures describing a single swash event of a collapsing/surging breaker-type for test 20080703T135742.

## 5.2 Morphological change results

Morphological evolution of the beach under wave conditions is presented in Figure 5.3, with specific reference to Test 9 as the change is sufficiently large to provide a good graphical description of the evolution of the beach profile under wave action. Details of the profile change of the other tests can be found in Appendix B. Net onshore transport of sediment is observable from below the SWL and results in the creation of a berm above the SWL. This pattern of erosion and accretion results in the steepening of the localised beach slope throughout the test. These features are all observed in natural gravel beach environments and are also consistent with the full-scale tests reported by López de San Román Blanco (2003).

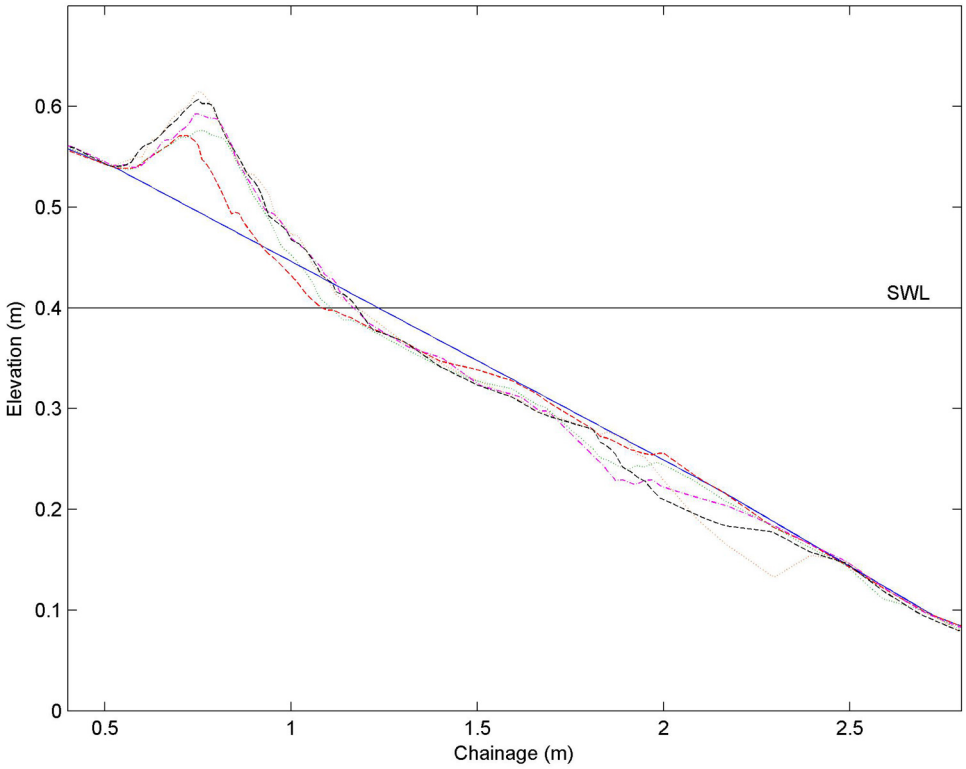


*Figure 5.3:* Cross-shore profile evolution for test 9. Solid blue line (—): initial profile; red dashed line (- - -): profile after 1 min; green dotted line (...): profile after 3 total mins; magenta dotted line (-.-): profile after 7 total mins; black dashed line (- - -): profile after 14 total mins; and orange dotted line (...): profile after 24 total mins.

To further appraise the morphological change, the specific variation in profile elevations between subsequent measurements is considered, with the profiles and fluctuations presented at each phase of testing.

The top panel of Figure 5.4 presents the initial beach profile and the profile recorded after one minute of wave action. The bottom panel indicates the morphological change experienced during the time interval between the two profile measurements. For this comparison, morphological change is largely restricted to a 1.0m region between chainage 0.5m and 1.5m. Accretion of a large volume of material is observable above the SWL, while

erosion occurs over a more extensive area. With consideration of the initial profile being far from equilibrium conditions, and the short duration, a very high sediment transport rate is likely. Fluctuation outside this main region still occurred to a minor extent, however only minimal characteristic feature development can be discerned. This may be a consequence of the under-developed profile hampering swash-swash interaction, or the smaller berm size, and consequent shallower slope, preventing the development of large backwash velocities.

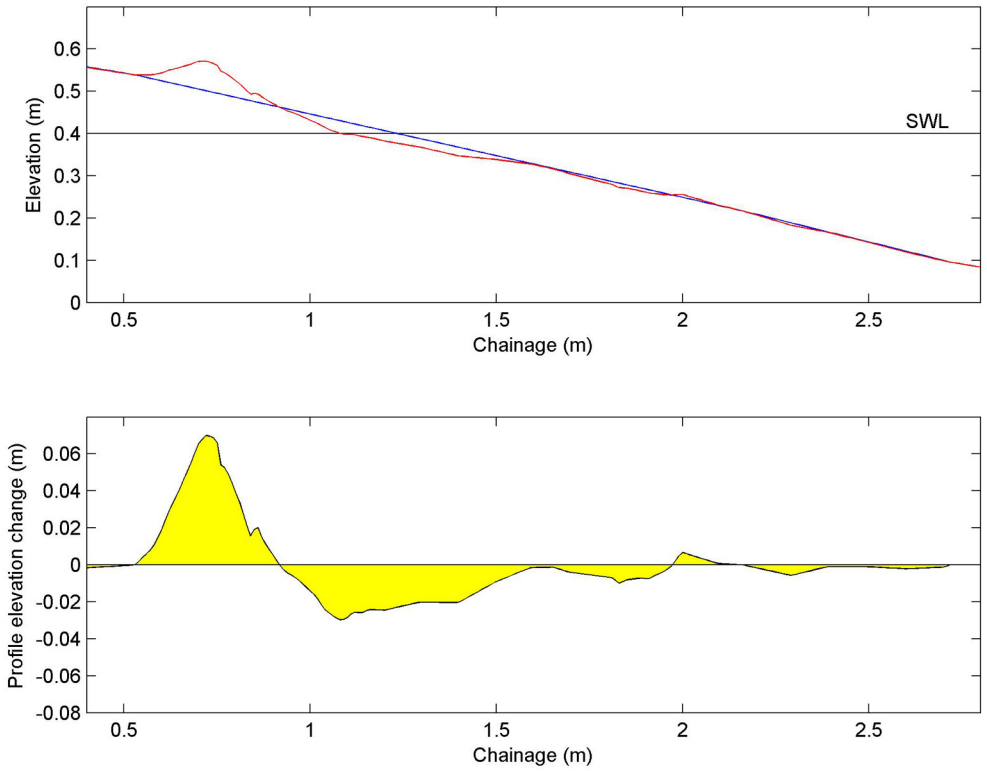


*Figure 5.4:* Cross-shore profile comparison and morphological change between Test 9 Initial conditions and part 1. Top panel: Solid blue line — initial profile, red dashed line - - - profile after 1 min. Bottom Panel: profile change observed between the two profile measurements.

Figure 5.5 presents the profiles after one minute, and three total minutes of wave action, combined with the morphological change observed between the two profiles. The net onshore transport is maintained during the time interval between the two profiles, with

morphological change occurring across a wider region.

Accretion is maintained above the SWL producing increased berm growth with the majority occurring at the seaward face of the berm. Additional excavation below the SWL results in a continued transition to the equilibrium profile, and development of a beach step appears to be forming at approximately chainage 1.9m. Increased berm slope due to the strong uprush, may be permitting larger backwash velocities to develop, generating strong swash-swash interactions and reinforcing beach step development.

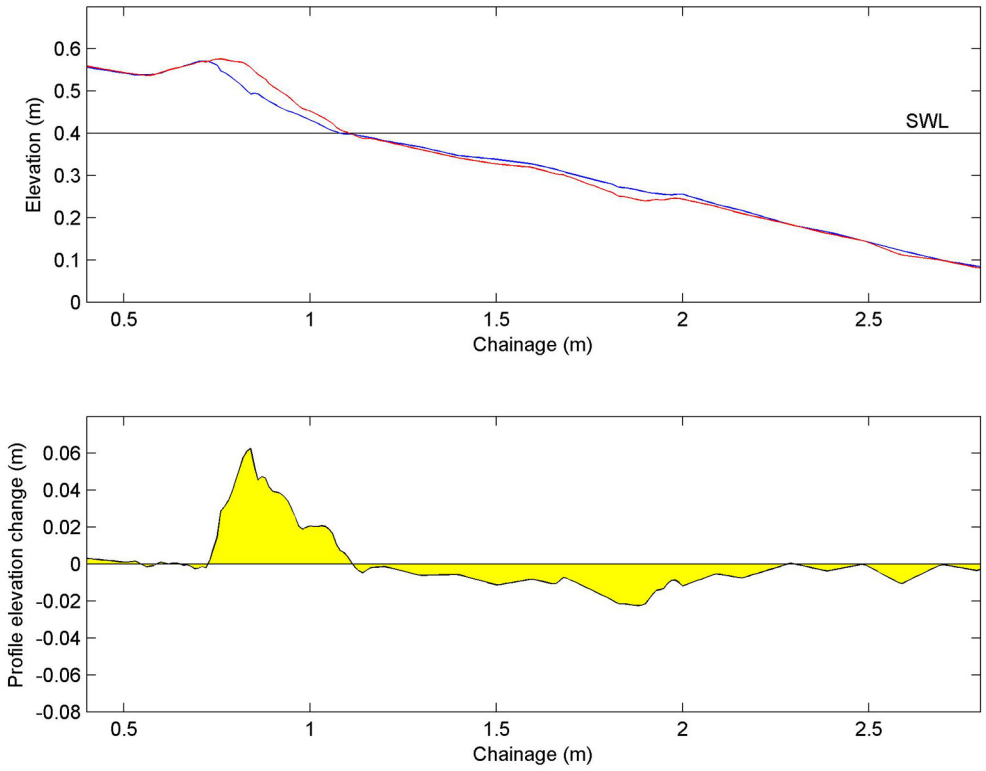


*Figure 5.5:* Cross-shore profile comparison and morphological change between Test 9 part 1 and part 2. Top panel: Solid blue line — profile after 1 min, red dashed line - - - profile after total 3 mins. Bottom Panel: profile change observed between the two profile measurements.

Figure 5.6 presents the profiles after three total minutes, and seven total minutes of wave action, combined with the morphological change observed between the two pro-

files. Net onshore transport is maintained during the time interval between the profiles, and morphological change occurring across an approximately 2.0m region. Peak total profile evolution change is reduced when compared with Figure 5.5

The berm crest height increased, with significant accretion again occurring on the seaward face of the berm, due to onshore transport of material from further offshore. Continued erosion below the SWL is observed with further development of the beach step.

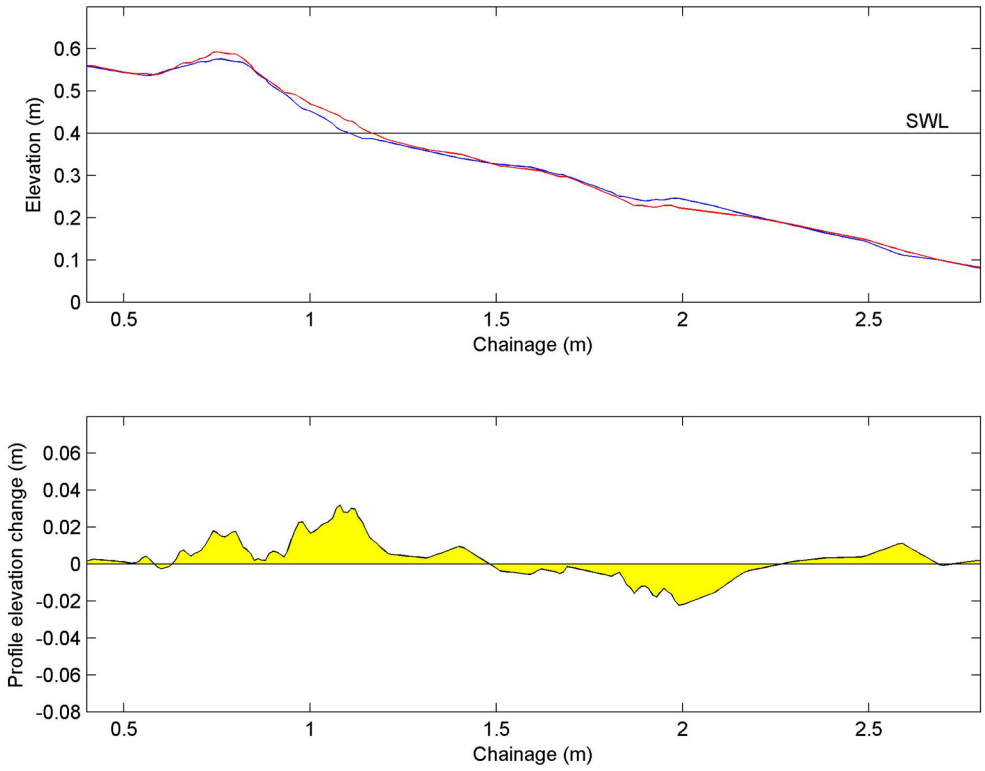


*Figure 5.6:* Cross-shore profile comparison and morphological change between Test 9 part 2 and part 3. Top panel: Solid blue line — profile after total 3 mins, red dashed line - - - profile after total 7 mins. Bottom Panel: profile change observed between the two profile measurements.

Figure 5.7 presents the profiles after seven total minutes, and fourteen total minutes of wave action, combined with the morphological change observed between the two pro-

files. Net onshore transport is maintained during the time interval between the profiles, and morphological change occurring across almost the entire beach. Total profile elevation fluctuation appears markedly reduced from previous measurements indicating an approach toward an equilibrium profile.

The berm crest height further increased, with the majority of accretion occurring on the landward slope, possibly due to increased wave run-up caused by fluctuation in wave height or change in breaker shape. The slope may also have exceeded the critical angle of repose at a localised position. The beach step experiences evolution propagating offshore as it transitions towards an equilibrium location.

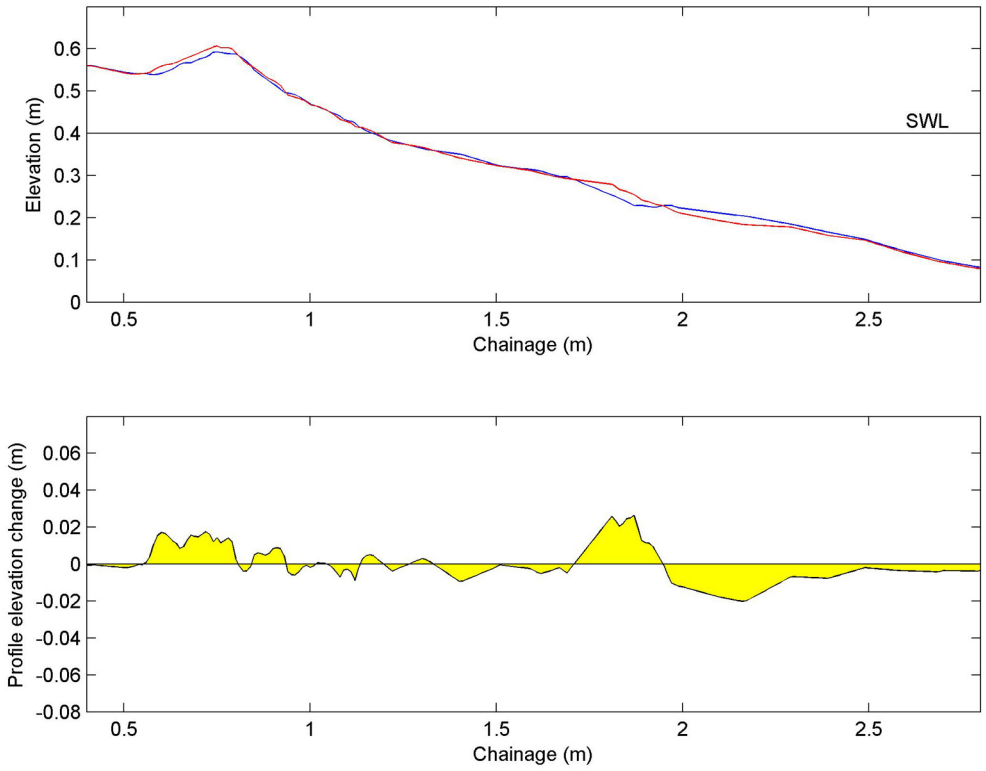


*Figure 5.7:* Cross-shore profile comparison and morphological change between Test 9 part 3 and part 4. Top panel: Solid blue line — profile after total 7 mins, red dashed line - - - profile after total 14 mins. Bottom Panel: profile change observed between the two profile measurements.

Figure 5.8 presents the profiles after fourteen total minutes and twenty-four total minutes of wave action, combined with the morphological change observed between the two profiles. The minor fluctuations in berm size and shape appears to suggest this region is close to equilibrium, with an offshore propagation of the beach step likely causing breaking further offshore. Net onshore transport is still reported during the time interval between the profiles, however morphological change is largely restricted to a small approximately 0.6m region below the SWL. This more developed profile will likely offer increased undertow velocities, with a consequent increase in turbulent energy during swash-swash interaction. If this is the case, additional sediment mobilisation is likely, with net onshore transport by the uprush event following swash-swash interaction.

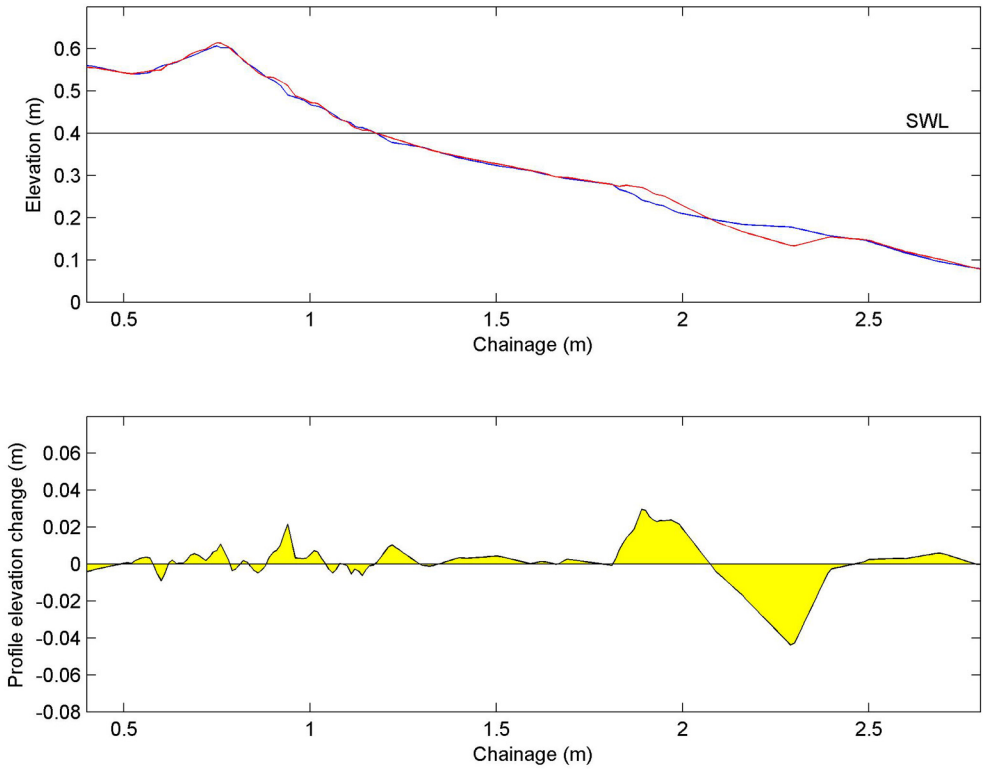


*Figure 5.8:* Cross-shore profile comparison and morphological change between Test 9 part 4 and part 5. Top panel: Solid blue line — profile after total 14 mins, red dashed line - - - profile after total 24 mins. Bottom Panel: profile change observed between the two profile measurements.

The berm experiences minor alteration in the profile, while the beach step propagates further offshore, with significant deepening.

Under consistent wave action, and in the absence of tidal fluctuations, a beach will be expected to reach an equilibrium profile when the processes affecting sediment transport become balanced. Though regions of morphological change were still occurring during the final period of wave action, the reasonably consistent berm size and shape, suggests equilibrium was being approached, therefore additional testing was not conducted.

Table 5.2 presents the details of the evolution of the berm above SWL for test 9. The total berm volume was assessed as the additional accreted volume of material above the initial profile at each interval.

| Test | Berm crest chainage (m) | Berm crest elevation (m) | Berm volume ($m^3/m$) |
|---|---|---|---|
| Part 1 | 0.72 | 0.571 | 0.0126 |
| Part 2 | 0.75 | 0.576 | 0.0219 |
| Part 3 | 0.76 | 0.593 | 0.0272 |
| Part 4 | 0.75 | 0.607 | 0.0303 |
| Part 5 | 0.75 | 0.615 | 0.0317 |

*Table 5.2:* Berm morphological change for test 9.

The berm location remained fairly constant throughout the test, with only slight seaward propagation of the peak. The berm crest elevation and total volume both rapidly increased, with most development occurring over the first three minutes of wave action ($0.0219m^3/m$ of the final $0.0317m^3/m$ berm volume). Most deposition occurred on the seaward face of the initial berm, with the minor deposition on the landward face towards the end of the test, possibly due to local exceedance of the critical angle of repose, or slight variation in the wave height resulting in a small degree of over-wash.

Details of the berm elevation, cross shore position, and total volume evolution for each test can be found in Appendix B. The details of these results are summarised in Figures 5.9, 5.10 and 5.11.

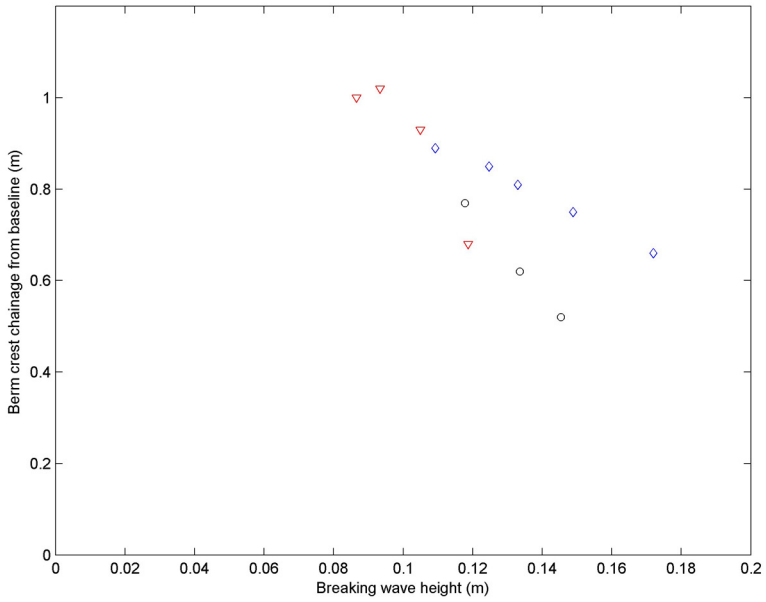


*Figure 5.9:* Final berm crest chainage from baseline vs average wave height at breaking. Blue diamonds (◇) 2-second wave tests, red triangles (∇) 3-second wave tests, black circles (o) 4-second wave tests.

As wave height increases with constant period, the chainage of the berm crest moves further shoreward (smaller chainage). This is consistent with expectations, as larger wave conditions will involve a transport across a wider cross-shore region, due to the larger uprush and backwash limits. The relationship between incident wave height and the final berm crest elevation presented in Figure 5.10 shows increasing crest elevation with increasing wave height. Again this is in line with expectation, as larger waves offer more energetic hydrodynamic conditions within the swash zone, causing a consequent increase in crest elevation, as well as total transport.

Figure 5.11 presents the relationship between the average wave height at breaking and

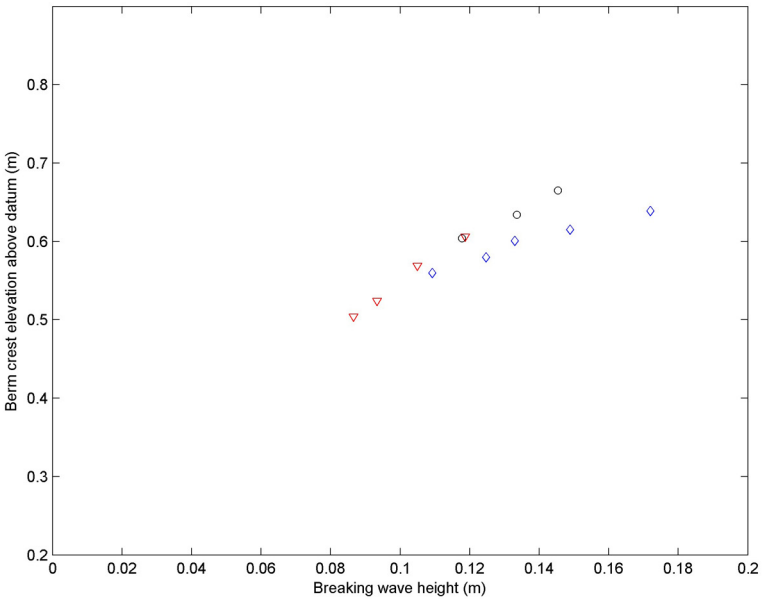


*Figure 5.10:* Final berm crest elevation above datum vs average wave height at breaking. Blue diamonds (◇) 2-second wave tests, red triangles (▽) 3-second wave tests, black circles (o) 4-second wave tests.

the final berm volume, exhibiting a general increase in berm size with increasing wave height. This assessment can be adopted as a proxy for the total sediment transport, and therefore conforms to expectations as discussed previously.

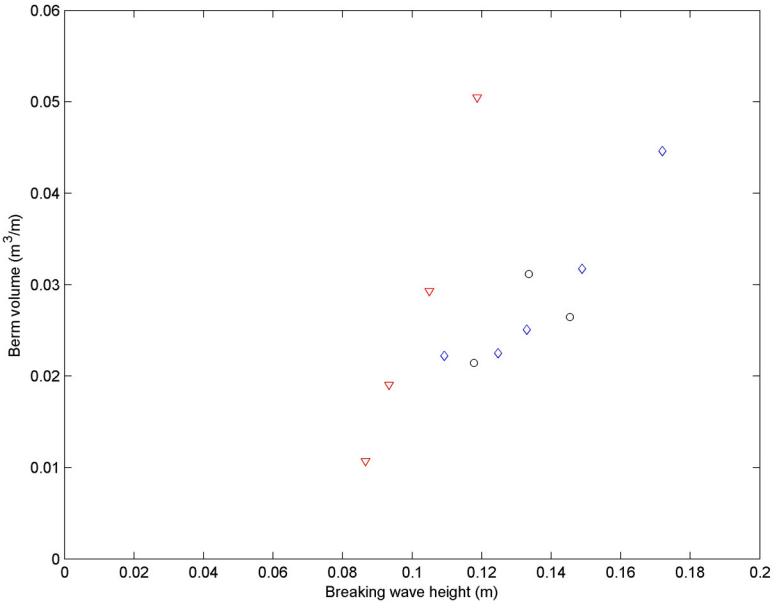


*Figure 5.11:* Final berm volume vs average wave height at breaking. Blue diamonds (◇) 2-second wave tests, red triangles (▽) 3-second wave tests, black circles (o) 4-second wave tests.

## 5.3 Sediment transport analysis

Examining the differences in subsequent profiles allows the determination of net time-averaged cross-shore transport rates as well as berm crest evolution.

The individual profiles provide little information with respect to transport rates without further analysis. The conservation law was applied to the sediment volume with a known boundary condition (Q(x) = 0 at landward and seaward boundaries). The cross-shore transport rate, Q(x), is given as follows (Manoonvoravong 2009):

$$Q(x_n) = Q(x_{n-1}) - \int_{x_{n-1}}^{x_n} M \frac{\Delta z_b}{\Delta t} \, \mathrm{d}x \tag{5.1}$$

where $Q(x_n)$ is the integral volume of sediment per period of time at the position $n$ ($\mathrm{m}^2/\mathrm{s}$), $\Delta z_b$ is the difference in surface bottom between measurements (m), $\Delta t$ is the

time step, and $M$ is the solid fraction of the sediment (1-$n$).

As no total over-wash of the beach occurred during any of the tests, there exists a landward position in each case where the transport of sediment is equal to zero. This provides the landward boundary for Equation (5.1). Sediment transport occurs across a varying length of the beach slope, however in each test there was a seaward boundary point demarking the end of sediment transport. The calculations begin at a landward boundary of zero net transport and translates cross-shore to the seaward boundary of zero net transport.

Figure 5.12 presents the integral-corrected net sediment transport rates for Test 9, consistent with the test analysed above. Similar figures for the other test are available in Appendix B, while a summary of the peak transport rates for the first part of each test are provided in Table 5.3. The increase in net sediment transport are generated in regions of accretion, while a reduction in net sediment transport occurs in regions of erosion.

Transport rates are not provided for test 17 as the seaward closure of the integral-correction (Q=0 at seaward location) is not possible.

The results outlined in Table 5.3 indicate a general decrease in transport rate as each test continues, which can be attributed to the transition towards an equilibrium position. There is a general tendency for the peak transport rate to propagate further offshore throughout each experiment, due to the early development of a stable berm, and the dynamic nature of the excavated region below the SWL.

Figure 5.13 presents the relationship between the peak transport observed during part 1 of each test, and the wave height at breaking for that experiment.

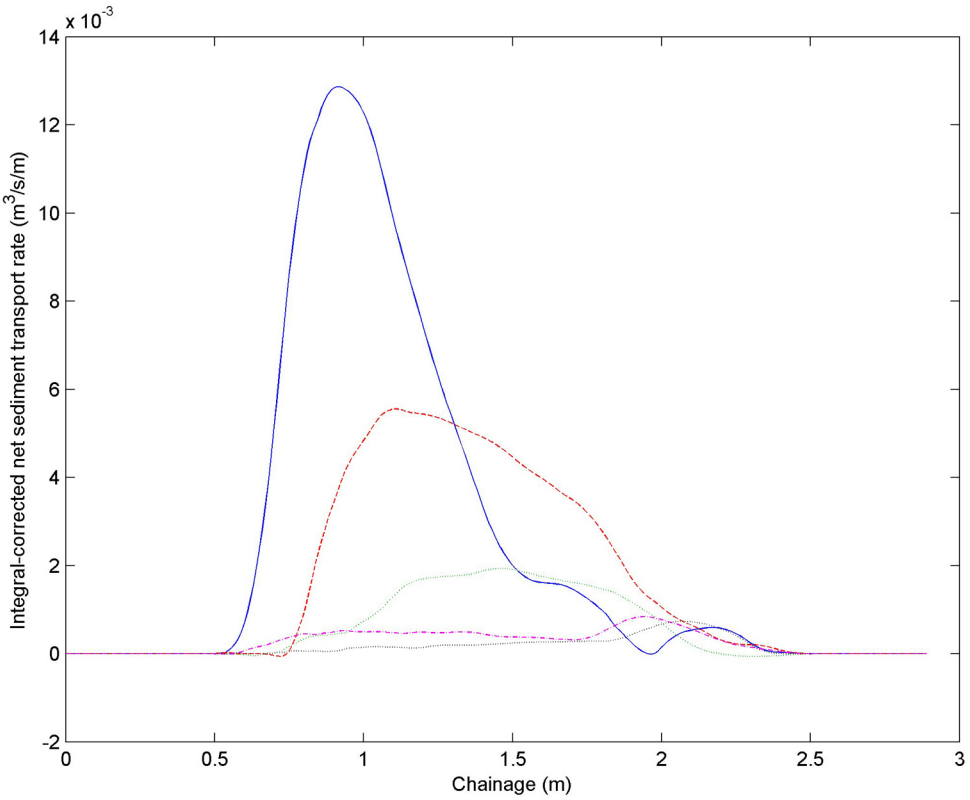


*Figure 5.12:* Integral-corrected sediment transport rates (assuming Q(x)=0 at landward and seaward boundaries) for Test 9. Solid blue line (—) 0-1min, red dashed line (- - -) 1-3min, green dashed line (...) 3-7min, magenta dashed-dotted line (- . -) 7-14min, black dotted line (...) 14-24min

Increasing wave height appears to provide an increase in peak net transport rate. This is as expected, with larger waves offering increased swash energy level and increased flow velocities in the backwash, therefore producing higher turbulence and and sediment transport in the swash zone.

As the peak sediment transport rate appears to be heavily dependent on the breaking wave height, it is not possible to quantitatively assess the relationship between breaker-type and peak transport with the data presented in this work. However, it is possible to assess the role of breaker type in a qualitative manner through inspection of beach

| Test number | Part 1 peak transport | Part 2 peak transport | Part 3 peak transport | Part 4 peak transport | Part 5 peak transport |
|---|---|---|---|---|---|
| 7 | 0.00398 | 0.00293 | 0.00198 | 0.00077 | 0.00009 |
| 6 | 0.00543 | 0.00321 | 0.00130 | 0.00074 | 0.00044 |
| 8 | 0.01082 | 0.00483 | 0.00086 | 0.00066 | 0.00039 |
| 9 | 0.01287 | 0.00556 | 0.00193 | 0.00084 | 0.00073 |
| 10 | 0.01739 | 0.00489 | 0.00162 | 0.00116 | 0.00165 |
| 11 | 0.00228 | 0.00113 | 0.00074 | 0.00024 | 0.00024 |
| 12 | 0.00695 | 0.00261 | 0.00124 | 0.00042 | 0.00027 |
| 13 | 0.01459 | 0.00471 | 0.00124 | 0.00050 | 0.00018 |
| 14 | 0.01198 | 0.00650 | 0.00250 | 0.00191 | 0.00123 |
| 15 | 0.00509 | 0.00233 | 0.00159 | 0.00085 | 0.00049 |
| 16 | 0.00915 | 0.00310 | 0.00123 | 0.00124 | 0.00071 |
| 17 | - | - | - | - | |

*Table 5.3:* Peak integral-corrected net sediment transport rates (all values are in $m^3/s/m$).

profiles under different breaker types.

Figures 5.14 and 5.15 provide the details of the profile evolution for two tests of similar wave height, exhibiting breaking through different mechanisms.

The berm development observed in Figure 5.14 is characteristic of beach development experienced under plunging breakers. Berm development results in a steep sloped structure on both seaward and shoreward faces, while the excavated region below the SWL produced a pronounced step. Figure 5.15, characteristic of collapsing waves, indicates the berm is wider with a more gradual slope on the seaward and shoreward faces. The excavated region below the SWL extends further offshore, while the development of the beach step is less pronounced.

The discrepancy is similar to the differences noted between observed profiles, and predicted profiles from numerical models, indicated in Figure 5.16 (Jamal 2011). The modelled profiles appear to under-predict the berm crest elevation, with a more rounded

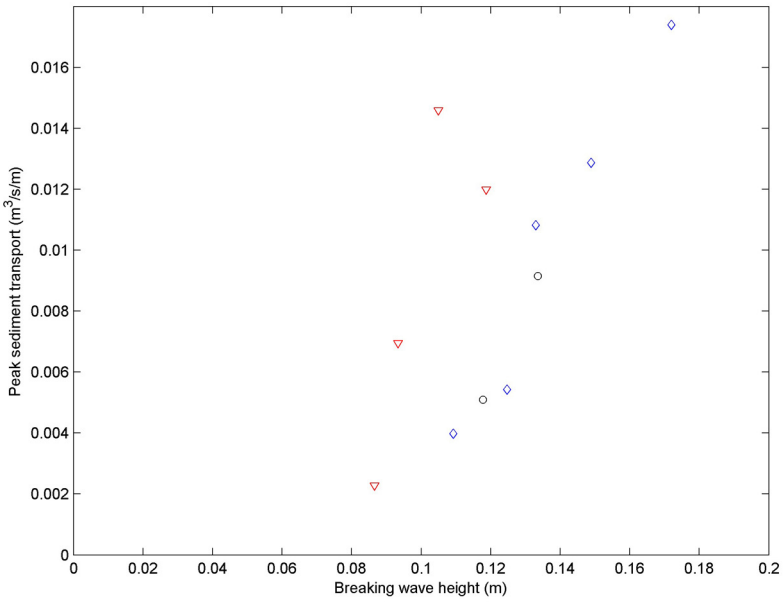


*Figure 5.13:* Peak sediment transport rate for part 1 of each test vs average wave height at breaking. Blue diamonds (◇) 2-second wave tests, red triangles (▽) 3-second wave tests, black circles (o) 4-second wave tests.

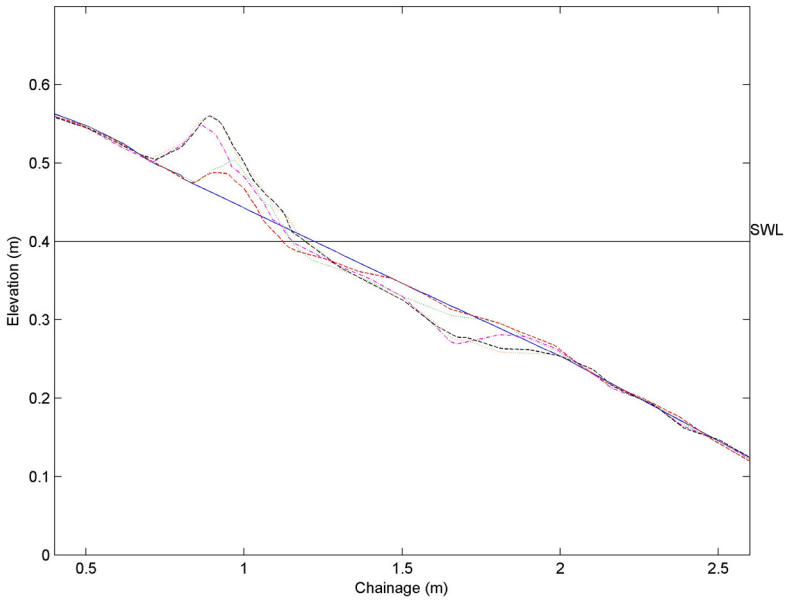


*Figure 5.14:* Beach profile evolution for Test 7 (Plunging breakers), $H_i = 0.109m$ $T = 2.01s$ $\xi_b = 1.52$. (—) initial profile,(- - -) 1 min, (...) 3 mins, (-.-) 7 mins, (- - -) 14 mins, (...) 24 mins.

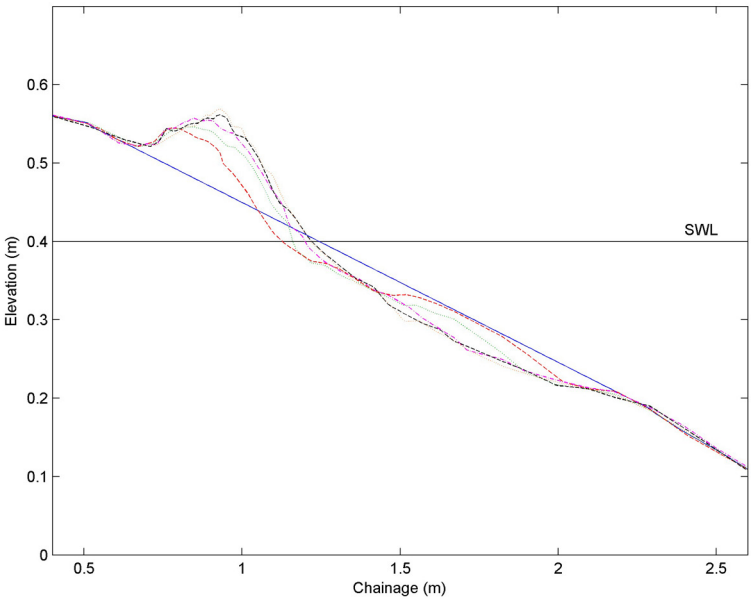


*Figure 5.15:* Beach profile evolution for Test 13 (Collapsing breakers), $H_i = 0.105m$ $T = 3.04s$ $\xi_b = 2.34$. (—) initial profile,(- - -) 1 min, (...) 3 mins, (-.-) 7 mins, (- - -) 14 mins, (...) 24 mins.

appearance compared to the experimental beach profile. The berm profiles observed under plunging breakers within this work, appear to be more consistent with the experimentally observed profile in Figure 5.16. The berm profile observed under collapsing breakers is more consistent with the modelled profiles, exhibiting a more rounded appearance, with shallower beach slopes. Finally the predicted profile by Jamal (2011) does not offer a well defined beach step, which is more apparent in the experimental profile.

The comparison between between cross-shore profiles generated by different breaker types presented in this work appears to provide partial evidence in support of the influence of breaker type on beach response. The characteristic shape of modelled profiles is similar to that recorded by collapsing wave conditions, further suggesting processes taking place under plunging waves, currently unaccounted for numerically, may be significant. More complete analysis may be provided through additional experimentation,

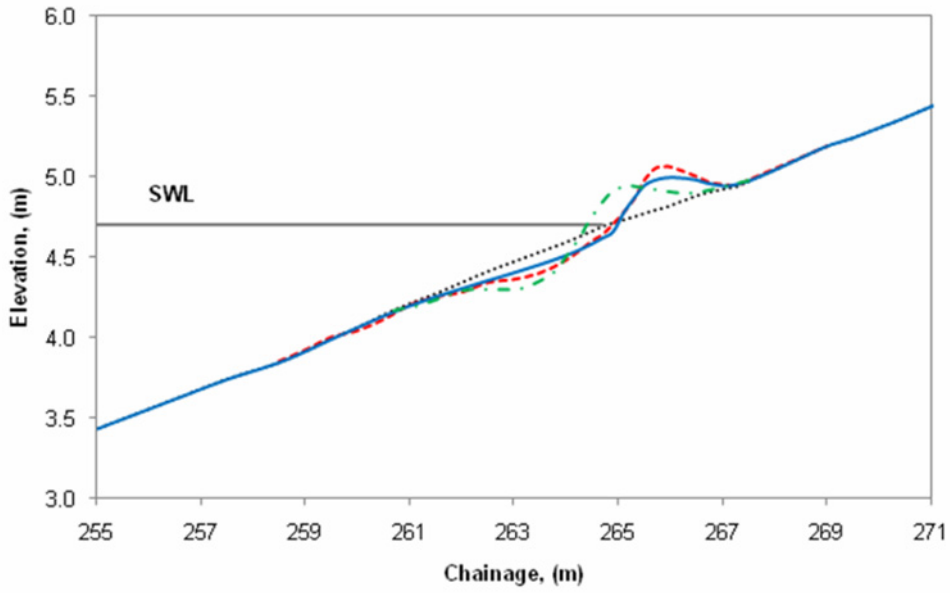


*Figure 5.16:* Experimentally observed and numerically predicted profile evolution for tests conducted at GWK (López de San Román Blanco 2003). (...) initial profiles, (- - -) experimental profile, (- . -) model prediction by Pedrozo-Acuña (2005), (—) model prediction by Jamal (2011).

with constant wave height and varying wave steepness, to adjust breaker type. This will eliminate the dominant control of sediment transport by wave height, and allow relation between breaker type and sediment transport rate.

# Chapter 6

# Impact pressure investigation

The work conducted by Pedrozo-Acuña et al. (2008) investigated the pressure response of plunging waves, and indicated a maximum in the non-dimensional impact pressure at lower Iribarren values, consistent with plunging breakers. The data analysed in that work occupied a fairly narrow region of the Iribarren parameter ($0.5 < \xi_b < 1.0$) and well represented the reduction in impact pressure as the breaker type moves towards the collapsing and surging regime. There is however a lack of data indicating an expected increase in impact pressure as the breaker type moves from spilling to plunging breakers ($\xi_b < 0.4$), and also fails to describe the relationship for higher Iribarren values, as the breaking changes from plunging to collapsing types ($\xi_b > 2.0$).

## 6.1 Impact event identification

For each pressure record, impact events were identified, quantified, and quality rated. The quality rating involved the assignment of a rating between five (best) and one (worst) according to the following criteria:

- 5. Sharp distinct initial peak. Clear minimum pressure. Small noise fluctuations.
- 4. Distinct initial peak. Clear minimum pressure. Small level of noise may be present in signal.
- 3. Initial pressure peak identifiable but less distinct. Less well defined response. Some noise present.
- 2. Indistinct maximum and/or minimum impact pressure. Wide ambiguous initial

pressure peak. Significant noise.

- 1. Indistinct maximum and/or minimum impact pressure. Significant noise in the record.

Figure 6.1 shows example impact pressure responses for the various rating values (1-rated event not included as the signal is largely indistinct, with no identifiable impact).

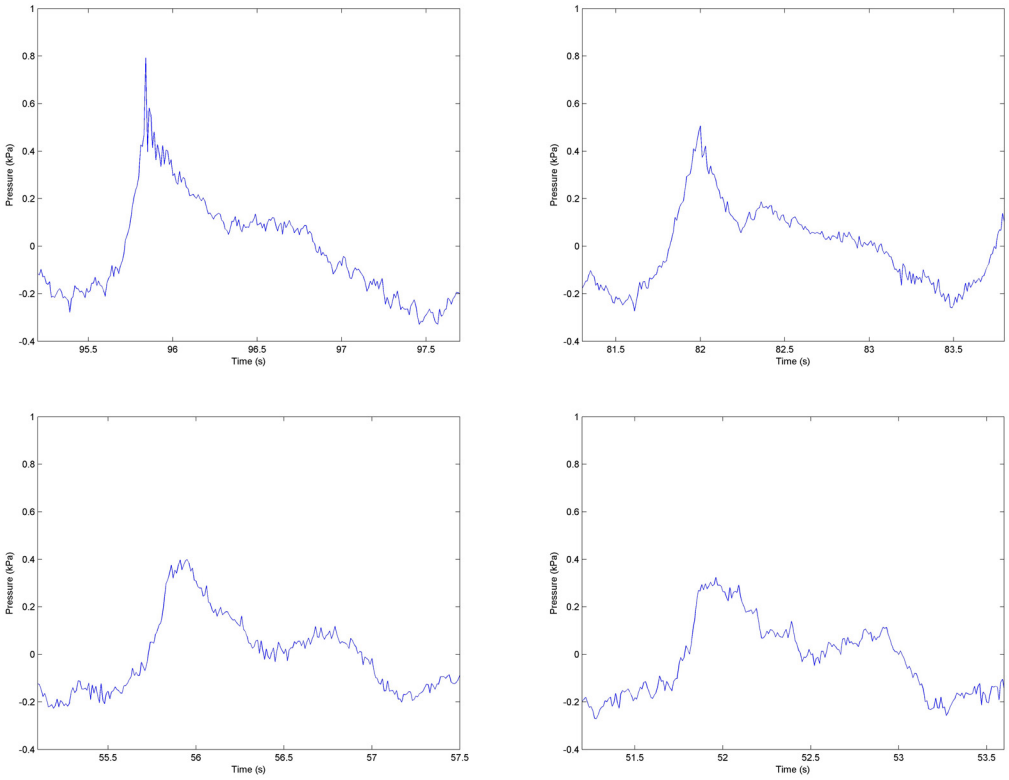


*Figure 6.1:* Example pressure response ratings, rated five (top left panel); rated four (top right panel); rated three (bottom left left panel); rated two (bottom right panel). Response rated as one are not shown.

After each event was assessed, the results were filtered to include only impacts events rated as four or five. These events were included due to the clear, easily determined, pressure increase relating to the initial breaking impact, with these events assumed to relate to wave impacts impinging on the beach close to the pressure transducer. Cross-referencing with the video record at the pressure transducer location, confirms

the events rated as four or five tend to relate to clearly impacting events above the pressure transducers.

For plunging impacts, the rapid increase in pressure associated with an impact event is often clear in the pressure-time plot and in the wavelet output. However, for collapsing and surging events the impact event is less well defined in the pressure-time plot, as previously discussed in Chapter 4. It was shown in Figure 4.6 that although an impact event is harder to identify in the pressure-time plot, inspection of the related CWT spectrum allows for a more detailed examination of the pressure signal components, and identification of an impact event.

The CWT spectrum of each event of each test was examined and assessed. Where a clear unbranching and well-defined impulse component was present, the event was carried forward for further analysis. If the CWT spectrum for an impact showed branching, or a loss of clarity, it was discarded due to the uncertainty of the magnitude of the impact pressure.

A plunging impact occurs in a more localised position and through a more definitive process than a collapsing/surging event. The may help explain the additional branching, and loss of overall clarity present in the CWT spectrum at low scales for the collapsing/surging breaker type, compared with that seen for plunging breakers. These features of the CWT spectrum for collapsing and surging breakers resulted in a reduction in the total number of suitable events carried forward for further analysis. This resulted in fewer data points present in the subsequent analysis for 3-second and 4-second waves, compared with plunging impacts characteristic of the 2-second waves.

## 6.2 Previous parametrisations

For comparison of relative impacting intensity across a variety of wave conditions, it is useful to normalise the impact pressure. Pedrozo-Acuña et al. (2008) determined the impact intensity (non-dimensional pressure) as $Pi/\rho g H_s$. This was different from that adopted in Bullock et al. (2007), where the incident wave height was used for normalisation ($P_i/\rho g H_i$). It is possible that the motivation for this change was driven by the shift from regular to irregular wave conditions.

The relationships investigated by Pedrozo-Acuña et al. (2008) include: dimensionless impact pressure ($P_i/\rho g H_s$) vs. dimensionless wave height ($H_i/H_s$), $P_i/\rho g H_s$ vs. dimensionless maximum vertical displacement ($\eta_{max}/H_s$), $P_i/\rho g H_s$ vs. Iribarren number ($\tan\beta/(H_i/L_0)^{0.5}$), and $P_i/\rho g H_s$ vs. wave steepness ($H_i/L_0$). These relationships are discussed in the sections below.

### 6.2.1 Impact pressure vs. wave height relationship

Figure 6.2 indicates monotonic relationships between the dimensionless impact pressure and dimensionless wave height, and dimensionless impact pressure and dimensionless maximum vertical displacement.

For the relationship $P_i/\rho g H_s$ vs. $H_i/H_s$, and consideration of a range of wave incident wave heights and Iribarren numbers, a simple monotonic relationship will be encouraged. While larger incident wave heights will generally be expected to generate larger impact pressures, the normalisation of the impact pressure with a constant value, $\rho g H_s$, introduces a bias towards the observed relationship.

If a small wave breaks on a beach through a strong plunging action, the relative impact pressure would be high, however the absolute pressure increase may still be small due to

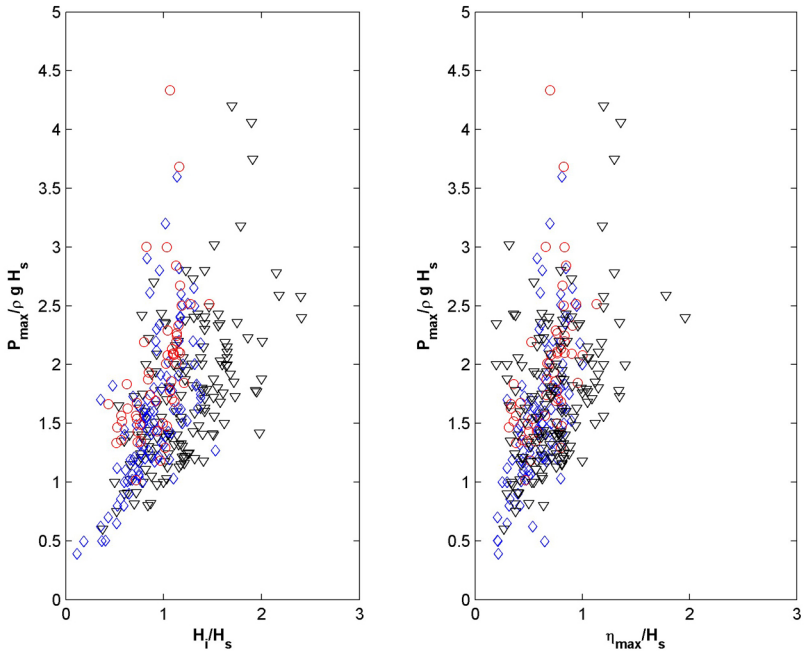


*Figure 6.2:* Non-dimensional impact pressures vs the non-dimensional local wave height (left panel) and Non-dimensional impact pressures vs non-dimensional maximum vertical displacement (right panel) (For three alternative wave cases). Pedrozo-Acuña et al. (2008).

the small initial wave height. If a second, much larger wave, breaks on a beach through a collapsing breaker, the pressure response will be substantially different. The relative intensity of the impact may be expected to be much less than the plunging impact, however the actual pressure increase may still be large due to the larger initial wave height.

With consideration of these two waves, and by normalising the impact pressure through the approach taken by Pedrozo-Acuña et al. (2008), the more intense impact event would receive a smaller impact pressure than the less intense event, aiding the establishment of the relationship observed in Figure 6.2. It is worth noting that the narrow Iribarren range of the events studied by the authors would limit the potential discrepancy in impacting intensity for different breaker types, but, as will be seen in the following

section, a relationship between impact pressure and Iribarren number was proposed.

### 6.2.2 Impact pressure vs. Iribarren number

Figure 6.3 presents the relationship between dimensionless impact pressure and Iribarren number from Pedrozo-Acuña et al. (2008). The range of Iribarren values investigated relates to violently plunging breaker types and seems to indicate a decrease in impact intensity as the breaker type transitions through the plunging breaker region towards the collapsing breaker type.

Considering several waves of equal incident wave height but varying Iribarren value, it would be expected to observe a range of impact intensities. This will result in a range of $P_i/\rho g H_s$ for a single $H_i/H_s$ value, and therefore helps explains the scatter observed in Figure 6.2.

For this relationship, the impact pressure is again normalised with a single value $\rho g H_s$, while the Iribarren number is described as $\tan\beta/(H_i/L_0)^{0.5}$ and is therefore a measure for each individual wave. Increasing wave steepness produces smaller $\xi_b$ values. If this is achieved through an increase in wave height, events with larger wave heights may be expected to produce smaller $\xi_b$ values. As discussed in the previous section, with the adopted normalisation of impact pressure, large waves may artificially generate large impact pressures. If large waves also generate smaller Iribarren number, an inherent relationship may be expected between these two parameters, irrespective of the actual relative intensity of the event.

The intention of the normalisation is to compare the intensity of the impact pressures in different regions of $\xi_b$, irrespective of the incident wave conditions generating the individual impacts. The dependence of the variables, introduced by the adopted normalisation for impact pressure, makes this difficult to determine.

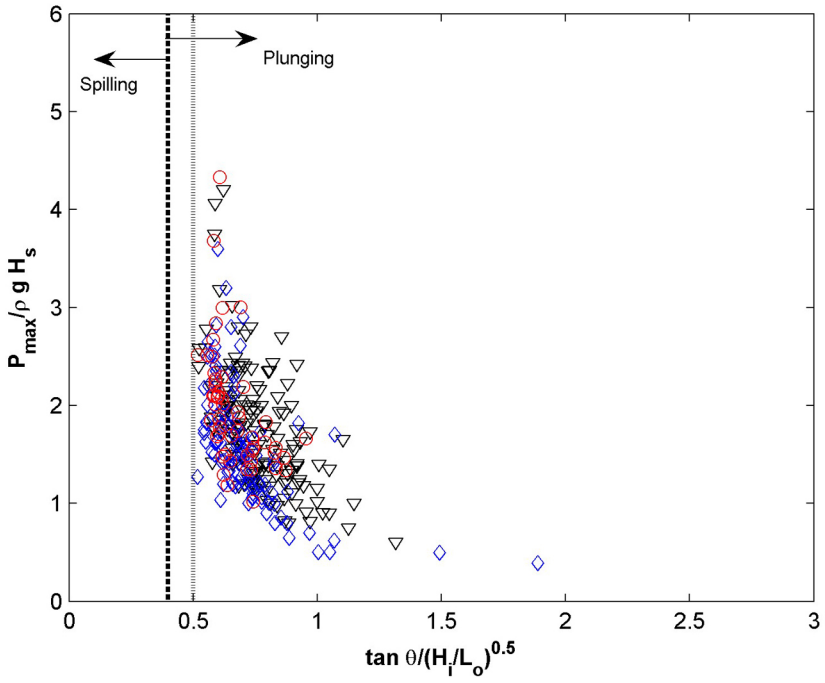


*Figure 6.3:* Non-dimensional impact pressures vs. Iribarren (For three alternative wave cases). Pedrozo-Acuña et al. (2008).

### 6.2.3 Impact pressure vs. wave steepness

Figure 6.4 presents the relationship between non-dimensional impact pressure and wave steepness by Pedrozo-Acuña et al. (2008). Again the same normalisation of the impact pressure is conducted as in the previous analysis, while the steepness is presented as $H_i/L_0$.

This was provided to establish a relationship between the intensity of the impact events through increasing wave steepness, a measure of increasing wave non-linearity. It should not be overlooked that the wave steepness is incorporated into the calculation of the Iribarren number. As the beach slope value remains constant for each test, the variation in the $\xi_b$ values is determined by variation in $1/\sqrt{H_i/L_0}$. Considering the observed relationship in Figure 6.3, a monotonic relationship between non-dimensional impact

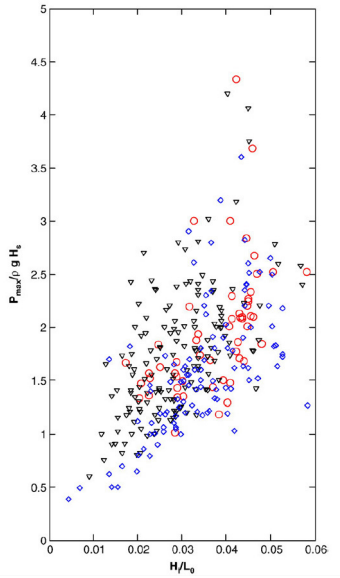


*Figure 6.4:* Non-dimensional impact pressures vs. individual wave steepness (For three alternative wave cases). Pedrozo-Acuña et al. (2008)

pressure and wave steepness would be expected.

### 6.2.4 Description of new peak pressure normalisation

An appropriate handling of the difficulties described in the previous analysis by Pedrozo-Acuña et al. (2008) would be to provide a more robust method of determining the dimensionless impact pressure.

Use of the significant wave height is considered inappropriate in the previous work, as it affects the relationships by generally allowing large non-dimensional impact pressures from large wave events. Consideration of the individual incident/breaking wave height associated with each recorded pressure, as adopted by Bullock et al. (2007), will provide a more reasonable alternative. Calculating the non-dimensional impact pressure as $P_i/\rho g H_b$ provides a measure of the recorded impact against the hydrostatic pressure for a water depth equivalent to the wave height at breaking. This is a measure of the impact pressure referenced to the wave height that caused the impact, and will provide a better

measure of how intense the individual impact events were. This will avoid a built in dependence of the impact pressure on the wave height, and therefore allow insight into whether plunging breakers generate larger impact pressures than other breaker types.

## 6.3 Impact pressure to wave height for UNAM data

Figure 6.5 presents the relationship between the non-dimensional impact pressure against the breaking wave height associated with generating each impact event, for data collected at UNAM.

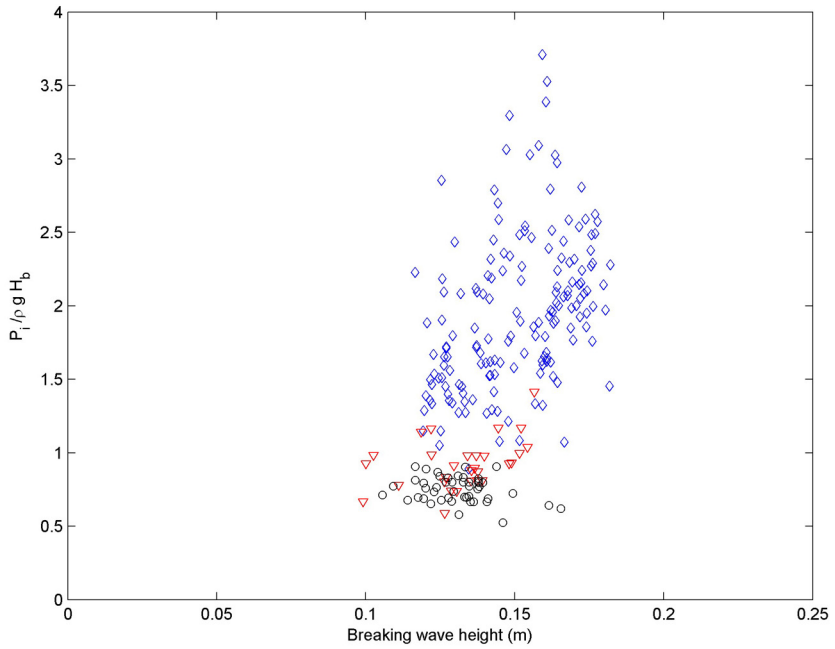


*Figure 6.5:* Non-dimensional impact pressures vs. breaking wave height. Blue diamonds (◇) 2-second wave tests, red triangles (▽) 3-second wave tests, black circles (o) 4-second wave tests.

The non-dimensional impact pressure varies between 0.5 and greater than 3.5. The observation of large impacting events is consistent with the observations of Bullock et al. (2007) on impermeable slopes, and Pedrozo-Acuña et al. (2008) for gravel beaches,

despite the disagreement over the validity of the the normalisation procedure. The magnitude of the impacts reported here, is significantly lower than than those on impermeable slopes, which may be attributed to the different hydrodynamics introduced by the impermeable slope.

There is significant scatter across the entire range of wave heights when considering all of the data, with no apparent relationship. Individually each data set displays significant scatter, however the impacts generated by 2-second tests generates the largest impacts, while 4-second test produces the smallest impacts. There does not appear to be a clear relationship between the parameters when considering each individual data set.

The lack of a relationship between the non-dimensional impact pressure and wave height was discussed previously. Although a larger wave would be expected to generate a larger impact than a similar smaller wave, this parametrisation does not account for the differences in wave shape and breaker type that likely play a significant role in determining the intensity of a wave impact.

## 6.4 Impact pressure to breaker type for UNAM data

The Iribarren number for this stage of analysis is calculated with consideration of the wave height at breaking. Spilling breakers tend to occur at $\xi_b$<0.4, plunging breakers occur at $0.4 < \xi_b < 2.0$, while collapsing and surging breakers occur at $2.0 < \xi_b$.

Figure 6.6 presents the relationship between the non-dimensional impact pressure against the associated Iribarren number.

The data presented clearly covers a wider range of Iribarren values than the previous

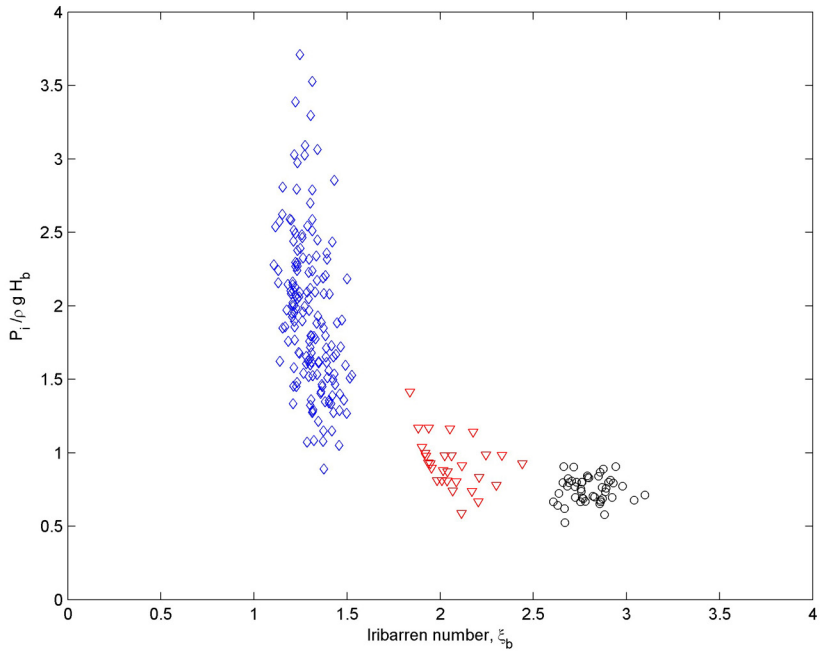


*Figure 6.6:* Non-dimensional impact pressures vs. Iribarren number. Blue diamonds (◇) 2-second wave tests, red triangles (▽) 3-second wave tests, black circles (o) 4-second wave tests.

study on gravel beaches, and therefore covers a wider variation in the breaker type. The range in Iribarren values is approximately $1 < \xi_b < 3$, providing inclusion of a large section of the plunging breaker region and significant extension into the collapsing and surging breaker region.

The largest impacts were registered during the 2-second tests, although significant variation in impact pressure was present throughout. The range of Iribarren values included $1.1 < \xi_b < 1.6$, and therefore falls entirely within the plunging breaker region, with impact pressures across a wide range of values. 3-second tests are restricted to a range of $1.8 < \xi_b < 2.5$, and therefore corresponds to the transition between plunging breakers and collapsing breakers. The impact pressure are concentrated around 1, however substantial variation occurs in the pressure values. 4-second tests are restricted to a range of $2.6 < \xi_b < 3.2$, corresponding to collapsing and surging breaker types. The pressure

values remain below 1, again with large variation in the values.

It is clear that there are a large number of reported impacts for the 2-second data set, while fewer events are reported for both 3-second and 4-second data sets. This is attributable to the dominant wave breaking type present in each data set. Plunging events provide an easily analysed pressure response, with an often clear initial impact pressure followed by a quasi-hydrostatic pressure. As wave breaking changes, the magnitude of the initial peak relative to the quasi-hydrostatic pressure is reduced, and may become obscured by the larger component.

Overall an inverse relationship appears to exist between Iribarren number and non-dimensional pressure. Large impact pressures are reported within the plunging breaker region, while transition to the collapsing and surging breaker types at higher Iribarren numbers results in a decrease in the impact pressure.

Variation in the impact pressure for events with similar Iribarren number is perhaps expected. Different events with the same $\xi_b$ value may exhibit dissimilar bore collapse, entraining different quantities of air, or interacting differently with previous swash events. This will result in variation of the non-dimensional impact pressure. Impact events may also not impinge on the beach at the same location each time, causing a discrepancy in the recorded response.

Unfortunately with lack of data for Iribarren values less than 1.0, the transition between spilling and plunging breakers is not described. However, the large impact pressures associated with plunging breaker events provides supporting evidence for the concept that plunging breakers are more violent than other breaker types. This larger impact pressure may be responsible for mobilising additional sediment for cross-shore transport.

## 6.5 Impact pressure to wave steepness for UNAM data

Figure 6.7 presents the relationship between the non-dimensional impact pressure against the wave steepness. This relationship provides an estimate of increasing wave non-linearity and this relationship is presented for completeness of comparison with the original work by Pedrozo-Acuña et al. (2008).

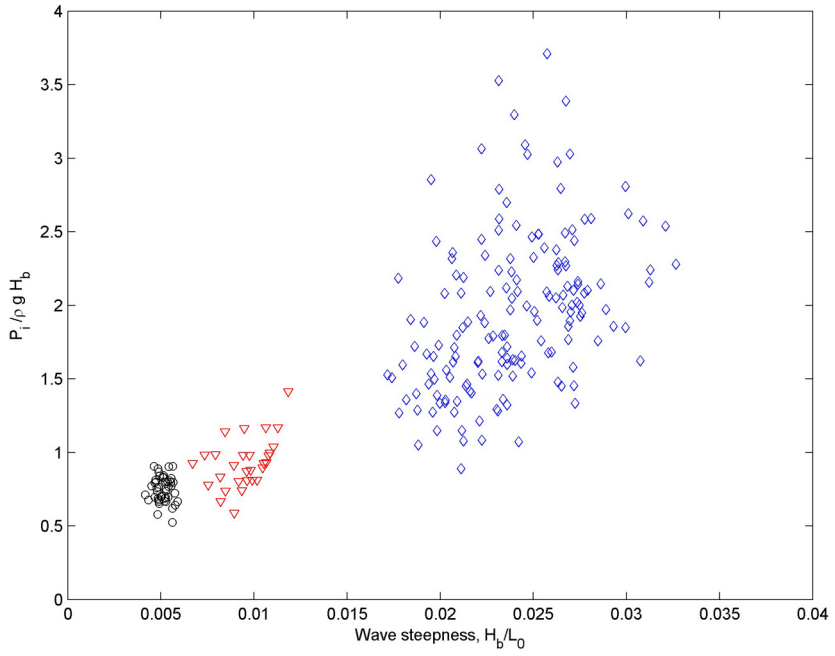


*Figure 6.7:* Non-dimensional impact pressures vs. wave steepness. Blue diamonds (◇) 2-second wave tests, red triangles (▽) 3-second wave tests, black circles (o) 4-second wave tests.

It appears a monotonic relationship may exist between the two parameters, with large scatter on the data, particularly for the 2-second test data. In general the steeper the wave, the larger the impact pressure associated with that event. It is likely that this relationship exists largely because the data does not include spilling breaker events. As the wave steepness extends beyond the range recorded here, events will exhibit spilling breaker types. The nature of the spilling breaker event is less dynamic and introduces less turbulence, resulting in a lower non-dimensional impact pressure.

# Chapter 7

# Discussions and conclusions

Pedrozo-Acuña et al. (2007, 2008) suggested that when modelling the morphological response of gravel beaches, it may be necessary to consider the large impact pressures generated by plunging impact events, and the subsequent entrainment and transport of additional sediment.

Pedrozo-Acuña et al. (2008) examined the variation of Iribarren number on the non-dimensional impact pressure, for a narrow region of $\xi_b$. Large impact pressures were identified within the plunging breaker region of the Iribarren parameter. It was hypothesised by Pedrozo-Acuña et al. (2008), that plunging impact events may cause localised bed fluidisation, and subsequent increased onshore transport. A plunging impact event causes a sudden increase in the pore pressure, resulting in a decrease in the effective stresses between sediment particles. If the increase in pore pressure exceeds a threshold, the effective stresses are reduced to zero, along with the shear stress of the gravel (as effective stress is proportional to shear stress). Under this condition the gravel becomes fluidised, with individual particles supported by the pore fluid. The fluidised sediment is subsequently transported onshore by the incoming uprush event.

The particular deficiency of morphological response prediction in present numerical modelling is seen during comparison of the observed and predicted berm crest elevation and location (Pedrozo-Acuña 2005; Jamal 2011; Williams et al. 2012b). The effect of breaker type, and associated wave impact, is unaccounted for in these existing modelling

approaches, and therefore there was a need for further investigation into impacting pressures, and consequences for sediment transport.

The narrow region of $\xi_b$ investigated by Pedrozo-Acuña et al. (2008) did not offer a detailed understanding of how impact pressure and breaker type were related. Further, the adoption of a potentially unsuitable normalisation of the impact pressure, resulted in difficulty in interpreting the results in a meaningful way.

The handling of the signal attenuation experienced during the testing at GWK, was also questioned. Adoption of a single attenuation-correction value appears to introduce a vast simplification of the attenuation experienced by the complicated pressure response of impacting events, composed of multiple frequencies.

Due to these difficulties, additional research was necessary to investigate the significance of the impact pressures of plunging breakers, and possible consequences for sediment transport. This research included an experimental programme conducted at UNAM, investigating the interaction between a steep gravel beach and various wave conditions. The conditions investigated offered a wider range of Iribarren numbers, extending to the upper limit of plunging breakers ($\xi_b = 2.0$), and beyond into plunging and surging breaker types.

Rapid profile response was observed, with continuation of wave action until quasi-equilibrium conditions were achieved during each test. The largest impact pressures were registered under plunging breaker impacts, with a decline in the impact pressure as the breaker type transitioned from plunging to collapsing and surging.

Monochromatic waves were adopted for each test, to permit measurement of the cross-shore profile, at initially very short intervals. The short one-minute duration of the

first experimental section of each test, could experience unrepresentative morphological response from individual waves when exposed to random wave conditions. Monochromatic waves are very uncommon in the natural environment, where lower frequency swash oscillations are observed Mase (1988), driven by a more random incident wave field.

It is recognised that on natural beaches swash transport is driven by both these low-frequency infragravity waves, and higher-frequency turbulence from bore collapse. The uprush phase, dominated by the turbulent bore collapse, is balanced by the lower frequency, infragravity-frequency dominated, backwash. Morphological response is determined by the difference between these opposing transports (Butt and Russell 2000; Masselink et al. 2005). It has however been demonstrated that, for steeper slopes the sediment transport becomes dominated by the higher incident wave frequency (Masselink and Russell 2006; Miles et al. 2006). The beach considered throughout this work was steep ($\tan\beta = 0.2$), and sediment transport would therefore be dominated by incident wave conditions even if exposed to random wave climates (thereby introducing infragravity energy).

Although these experiments were conducted in a laboratory flume, the experiments should not be considered a scale model representation of a real world location, but instead as small wave conditions on a natural beach. Comparison of the recorded impact pressure response with larger data will require consideration of scale effects present in mobile bed models. Researchers have discussed methods for accounting for the difficulties involved in comparing scale model tests to larger conditions, with a good discussion provided by Hughes (1983).

Ultimately these tests provide an interesting alternative to the data collected at close to full-scale at the GWK (López de San Román Blanco 2003). Significant similarities are

observable between the two experimental data sets, with large impulse events detected under plunging impact events. The morphological response of the beaches involved in the experimental programme of this thesis reflects similar features observed in both large scale facility tests and the natural environment.

## 7.1 Discussion of analysis conducted

The data collected during the experimental programme was broadly separated into two sections. The cross-shore profile measurements were used to monitor morphological change throughout each experiment, assist in observation of the development of characteristic profile features, and to provide an estimate of the net sediment transport. The pressure and wave records were used to investigate the pressure response associated with varying wave conditions and breaker types.

### 7.1.1 Discussion and conclusion of morphological analysis

With increasing wave height, the morphological change occurs over a broadly wider cross-shore region, which can be attributed to the increased run-up and run-down limits of larger waves, resulting in higher flow rates in the swash. These higher flow rates, combined with a broader swash zone, will result in exceedance of the local critical Shields parameter, permitting mobilisation of sediment for longer durations, and across a wider area.

The berm crest position indicated a general shoreward retreat, and increasing crest elevation, under larger wave conditions. The change in hydrodynamic conditions produces higher run-up limits, allowing transport of material to higher elevations, and consequently the berm crest occupies a more shoreward profile location. The final total berm volume, and peak net sediment transport, both indicate a strong dependence on wave height. Larger wave heights mobilise additional sediment, and increase onshore trans-

port of material. As the wave run-up of these larger waves reaches a more shoreward position, with higher elevation, infiltration of the swash lens into the unsaturated region of the beach becomes significant. This will reduce the strength of the backwash at higher regions of the beach, and helps account for the larger accretion and total berm volume recorded under increased wave height.

With the measurements included in this work, it is not possible to quantify a relationship between breaker type, assessed through $\xi_b$, and net sediment transport rate. Variation in $\xi_b$ is largely achieved through fluctuation in wave height, however as net transport rate appears to be strongly related to wave height, this masks any relationship that may exist between $\xi_b$ and net sediment transport rate. To assess this relationship, it would be necessary to examine numerous wave conditions with a consistent wave height, and variation in wave steepness to provide fluctuation in $\xi_b$. Under this scenario, and with consideration of the $\xi_b$ range examined in this work, an inverse relationship is hypothesised. More intense impact events associated with plunging breakers will likely generate higher sediment transport through bed fluidisation, as discussed by Pedrozo-Acuña et al. (2008). As $\xi_b$ increases, and breaking transitions to collapsing and surging, the sediment transport rate is expected to decline, as a consequence of reduced sediment mobilisation through bed fluidisation under breaking impact.

A qualitative assessment of the impact of breaker type can be made to a limited extent, through consideration of the profile shape typical of different breaker types. Profiles formed by plunging breaker events are characterised by a steep sloped berm above the SWL, and a well defined beach step below the SWL. Profiles formed by collapsing breakers are characterised by a more gently sloping berm, with a less well defined beach step below the SWL. The discrepancy in profile response beneath the SWL may be attributable to the larger swash-swash interaction of the higher frequency tests adopted in plunging breakers. Under plunging breaker conditions in the work, the incident wave

frequency is higher, offering greater interaction with the backwash of one event and the incoming uprush of the next swash event. Under collapsing breaker types, the wave period is longer, allowing completion of the backwash event, before the subsequent incident event propagates into swash zone. This reduced swash-swash interaction generates less turbulence and reduced morphological change at the beach step.

The longer wave period observed for collapsing wave conditions may also encourage additional infiltration in the upper beach. This will result in a reduced volume during the backwash, and has an influence on the effective weight of particles (Turner and Masselink 1998). This will further adjust the profile response observed between the profile generated through different breaker types in this work.

It appears the numerical model representations by Pedrozo-Acuña et al. (2006) and Jamal (2011) are more consistent with the profile details observed under collapsing breaker types, with a lower, more gently-sloping berm, and a less well defined beach step. This suggests that processes dictating specific profile response under plunging breakers are not contained within existing numerical simulations.

### 7.1.2 Discussion and conclusion of pressure response analysis

The nature of the pressure response under impact events was discussed in Sections 4.2.2 and 4.2.3. The signal was considered to be composed of responses dictated by two separate processes. A large, temporally-consistent, hydrostatic component was generated by fluctuation in the water elevation above the pressure transducer location. A second, more dynamic pressure component associated with wave impact events also contributes to the recorded response.

Each of these components is composed of different frequencies, and can therefore be expected to experience different attenuation as they propagate through the porous beach

from the bed surface, to the recording location. It is therefore inappropriate to handle attenuation with a single value, as adopted by Pedrozo-Acuña (2005), but instead each process must be corrected separately.

This was achieved through wavelet analysis to assess the frequencies present in each impact event. The impulse component was then separated from the pseudo-sinusoidal, hydrostatic component, allowing attenuation-correction of each section separately. This approach was adopted for analysis of data containing plunging impacts, recorded at GWK (López de San Román Blanco 2003). The attenuation of each frequency between two locations was assessed, and this was used to correct the separated components of the more deeply buried record. Recombination of the two components offered a good representation of the pressure response recorded at the shallower depth.

This approach offers a capability not possible without separation of the pressure response to two components. Without separation, the higher frequencies present in the pseudo-sinusoidal component will also be corrected by a frequency-dependent value. This will lead to a significant increase in the amplitude of the background noise, and would not provide a good representation of the target signal.

This correction was made with assessment of the measured attenuation between two recorded locations. For assessment of the impact pressures under breaking waves, the bed surface pressure response is required. This attenuation-correction will therefore be between the bed surface and depth of burial of the assessed record. The measured attenuation between these two locations is unknown, therefore a new pragmatic approach was presented for assessing this attenuation rate, allowing the pressure at the bed surface to be established.

The sediment matrix is assumed to be homogeneous and isotropic, therefore offering

a constant rate of attenuation with depth. Comparison of the amplitude of each frequency component from three co-located pressure transducer allows an assessment of the relative attenuation at each frequency. An exponential relationship was adopted, consistent with previous handling of attenuation in porous media (Yamamoto et al. 1978; Oumeraci and Partenscky 1990; Vanneste and Troch 2012).

An attenuation rate was derived for each frequency analysed in the work, and these values were used to establish a relationship between attenuation and frequency. A significant portion of the analysed frequencies were discarded due to an apparent amplification with depth between two measurement locations. This made any relationship derived at these frequencies suspect, and inclusion in the derivation of the attenuation-frequency relationship would have adversely affected the derived relationship.

The poor fit between attenuation coefficients generated from observed measurements and the proposed attenuation relationship at higher frequencies, may be partially attributable to the low energy level present at such frequencies. Small discrepancies in the recorded amplitude between transducers at low energy levels could have consequences on the apparent attenuation. Much less scatter is observed at lower frequencies, where energy of the signal tends to be higher. A dedicated investigation of signal attenuation and the influence of depth of burial is required to understand the complex relationship at the frequency range considered.

The relationship presented was developed with consideration of the unseparated pressure records, and is therefore influenced by the inclusion of two processes within the signal. The pressure transducer array was further onshore than the impact location, introducing significant turbulence during bore collapse and swash uprush between the impact location and pressure transducer array. This will have consequences for the recorded signal, and makes isolation of a single impact event at this more onshore loca-

tion difficult, and somewhat subjective. Despite this, preliminary examination indicates a reduction in data spread at high frequencies might be achieved with consideration of separated impulse components, however large fluctuations are still recorded.

The pressure transducer location remained below the groundwater exit point of the beach in each test. It is therefore assumed the beach does not experience significant infiltration, and associated decrease in saturation level as described by Faybishenko (1995). Due to isotropic nature of sediment, and lack of additional monitoring of the saturation level within the beach, it is assumed the level remains constant throughout both the short (wave cycle) and long-term (experiment duration).

It is possible that in practice plunging impact events will introduce additional air content to the sediment matrix, affecting the attenuation experienced by pressure wave propagating through the beach. However, it was demonstrated that the hydrostatic (pseudo-sinusoidal) component of a pressure record can be accurately predicted using the pressure response from a co-located pressure transducer, through adoption of a single correction value. Significant variation in saturation level would create differential attenuation throughout the wave cycle, and would be apparent in the comparison of recorded and predicted pressure signals.

There are also additional considerations involved in implementation of the attenuation-correction during each experiment. These have been touched on in the previous chapters, but are discussed in detail here.

The depth of burial of the pressure transducer fluctuates throughout each experiment as morphological change of the beach occurs. This change in depth of burial, alters the distance through which pressure waves propagate, and therefore alters the attenuation experienced throughout the duration of each experiment. As a real-time measurement

of the depth of burial was not recorded, a simplification of the scenario was required. To avoid overestimation of the impulse pressure under impacting events, where excavation was registered the depth of burial at the end of each experiment was adopted, while during times of accretion the depth of burial at the start of each experiment was adopted.

If bed fluidisation occurs as hypothesised by Pedrozo-Acuña et al. (2008), it is likely that the adjustment in the nature of the sediment matrix will alter the process of signal transmission occurring in this region. The attenuation will consequently be altered, however to the author's knowledge, no studies have investigated this effect, therefore the consequences remain undefined.

Despite the limitations of the approach discussed here, the methodology still accurately predicts the attenuation experienced at wave frequencies. This is the only frequency region at which four locations of known pressures can be used to confirm prediction, and provide an initial validation of the proposed technique.

This discussion of the separation of the pressure signal components, and separate handling of the attenuation of each component, has significant implications for previous research. The consequent surface pressure derived by Pedrozo-Acuña et al. (2008) were carried forward to validate the accuracy of a Reynolds-averaged Navier-Stokes (RANS) numerical model representation of plunging impacts on almost full-scale laboratory conditions (Pedrozo-Acuña et al. 2010). It is likely that the peak pressure is underestimated, although the degree of underestimation is difficult to establish, without reanalysis of the original pressure response. As such it is difficult to comment on the impact of changing the analytical approach on the conclusions drawn in those works.

However, the varying attenuation experienced by different frequencies of impulse components, may help to explain the apparent differential attenuation of subsequent wave

events observed in some tests, for example Figure 4.1 (example pressure responses at different depths of burial from GWK tests).

The frequency content of a particular event may be controlled in part by the breaker type or wave impact angle. As such random wave conditions would be more likely to provide greater fluctuation in the observed attenuation rate of subsequent impulse events. Stable wave conditions within a monochromatic wave field should provide similar breaking processes on a wave-by-wave basis. Consequently the frequency content of each event recorded at UNAM should be similar for all waves in each individual test.

The analysis conducted on the calculated bed surface pressures responses for the UNAM data reproduces the analytical approach of Pedrozo-Acuña et al. (2008), providing detail of a wider $\xi_b$ range. One key difference between the two approaches is adopted in the handling of the normalisation of the impact pressure.

Bullock et al. (2007) provided estimation of the non-dimensional impact pressure as $P_i/(\rho g H_i)$, where the pressure impulse was associated with the relevant wave height that generated the impulse. This was adjusted in Pedrozo-Acuña et al. (2008) to $P_i/(\rho g H_s)$, which has significant implications for the subsequent relationships expected when using this parameter. The adoption of an average wave height in place of an event specific value, introduces an inherent preference for large individual wave events generating large impact pressures. In this work, the link between impulse pressure and associated individual wave height is re-established, through adoption of non-dimensional impact pressure as $P_i/(\rho g H_b)$.

Overall, the magnitude of the impact intensity is less than that reported by Bullock et al. (2007) for plunging events on impermeable beach slopes. It is not possible to assess whether the difference in magnitude is related to a deficiency in the attenuation-

correction approach, or a manifestation of the variation in the hydrodynamic conditions caused by alteration of the bed to a porous medium. Despite this, the magnitude of the impact pressure registered through plunging impacts may still be highly relevant for consideration within sediment mobilisation.

The comparison of non-dimensional impact pressure and wave height does not appear to provide a defined relationship. The large scatter presented in the plot is likely due to a variation in the breaker type, which is not accounted for in the parameters. Small waves of intense breaking will create larger non-dimensional impact pressures than large waves of gentle impacting, creating significant scatter.

#### 7.1.2.1 Speculation for untested data region

Potentially the most significant relationship examined in this work, is between non-dimensional impact pressure, and Iribarren number. Although a wide range of Iribarren values were considered in this work, the experimental data does not extend to $\xi_b < 1.0$. Values below this limit include both waves exhibiting breaking through spilling and plunging, with the spilling breakers transitioning to plunging breakers as $\xi_b$ increases above 0.4. It is useful to consider the nature of wave impacts in this range, to offer a hypothesis of the expected relationship in this untested region.

Spilling breakers are highly likely to generate smaller bed surface pressure fluctuations than a comparative plunging impact(Ting and Kirby 1996). This is due to the less dynamic breaking process (Chanson and Jaw-Fang 1997), and as such smaller surface pressure fluctuation can be expected, when compared to plunging breakers. It is therefore hypothesised that spilling breakers, will create characteristically small non-dimensional impact pressures. A general increase in this parameter will therefore be expected in the untested Iribarren region ($0.4 < \xi_b < 1.0$), as breaker type transitions from spilling to plunging. If this relationship holds, a peak in the breaker intensity may be identifiable

within the region associated with plunging breakers.

Figure 7.1 presents the non-dimensional impact pressures vs.Iribarren number data collected at UNAM (shown earlier in Figure 6.6), with an indicative relationship provided for the observed data, and an example hypothesised relationship in the untested region for lower Iribarren values.

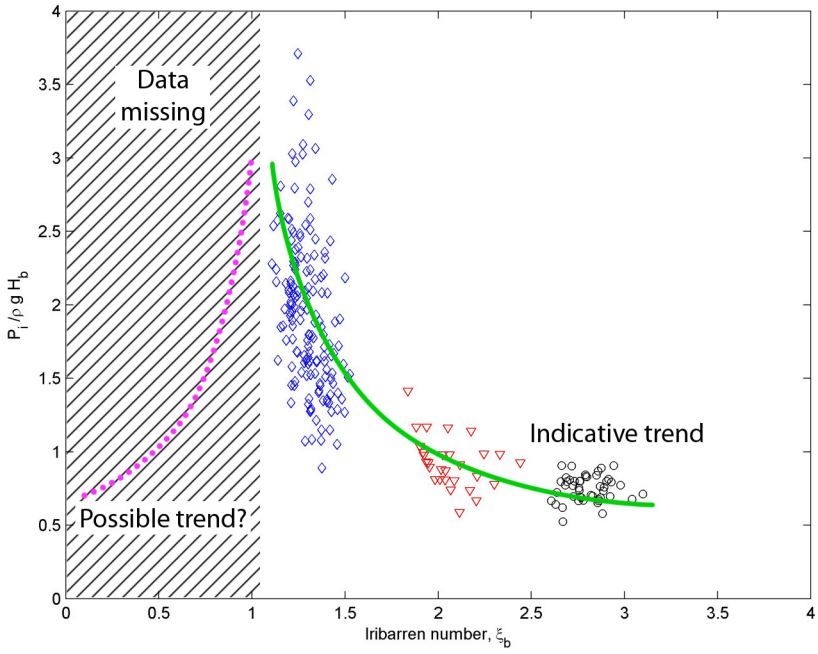


*Figure 7.1:* Recorded non-dimensional impact pressure vs. Iribarren number, as presented in Chapter 6, with; green line (—) indicative trend of existing data, and magenta line (...) example hypothesised trend in untested region.

The exact position and shape of the relationships indicated in Figure 7.1 can only be confirmed with additional testing at lower Iribarren numbers. This will also established the validity of a hypothesised peak generated at the interface between these two relationships.

#### 7.1.2.2 Discussion within tested data region

Within the range of Iribarren numbers considered, a non-linear inverse relationship appears to exist, with a decline in the non-dimensional impact pressure observed with increasing $\xi_b$. The relationship provided in Figure 7.1 reflects this, indicating that the localised bed surface pressure under plunging events is significantly larger than that experienced during different breaker types. It has previously been discussed that this may be significant for sediment transport, with a hypothesised account for the process by which this may occur (Pedrozo-Acuña et al. 2008).

The bore collapse of plunging breakers is often described as a jet event, causing a significant increase in localised pressure. This is capable of propagating through the water column to the bed (Ting and Kirby 1995), and therefore can provide significant contribution to the mobilisation of sediment. Impulses characterised through alternative breaker types do not offer such a direct pressure increase, therefore offering smaller non-dimensional impact pressures.

The specific relationship included in Figure 7.1 for the data range $1 < \xi_b < 3$ is an indicative relationship, rather than a fit based on regression analysis. This was a concious decision based on the expected change in relationship at lower Iribarren numbers discussed in Section 7.1.2.1. It is possible that a hypothesised peak in impact pressure may occur at Iribarren values within the tested region, and thus a peak may be partially described by the recorded experimental data. The uncertainty over whether a significant change in the nature of the relationship indicated by the experimental data discouraged adoption of regression analysis, and promotes the suitability of an indicative relationship.

The analysis of the cross-shore profiles provides limited evidence that the nature of characteristic profile features appears to vary depending on the type of breaking experienced.

Typical profile response under plunging waves recorded at UNAM is consistent with the typical response observed at GWK. The berm and eroded morphology predicted by existing numerical models, replicating plunging conditions, appears to produce closer agreement with the typical profile produced by collapsing breakers at UNAM. This typically results in a lower shallower slopes berm, with a less well defined beach step.

Clearly the modelling approach is still lacking additional parametrisation that might otherwise improve prediction capabilities. The inclusion of the indicative relationship between non-dimensional impact and Iribarren number, and the consequences for sediment transport may help improve accuracy of berm and beach step representation.

## 7.2 Discussion of error

The following section summarises the potential sources of error that may have been introduced during the experimental and analytical phases of this work, and the consequences these errors have on the results.

The first source of error discussed is the experimental error introduced due to limitations in the measurement capability of the equipment adopted. For the pressure transducers the full-scale accuracy ($\pm 0.1\%$) translated to the experimental pressure measurement range, combined with the stated long-term stability ($\pm 0.1\% pa$), provides a measurement error of approximately $\pm 1\%$.

Human error was potentially introduced in the cross-shore beach profile measurement with incorrect placement of the measurement equipment, particularly the reflecting staff. The error was previously discussed in Section 4.3, and after analysis of the recorded elevations at landward locations where morphological change did not occur, the standard random error was calculated at less than 1mm.

The application of an empirical relationship for the estimation of the wave shoaling during onshore propagation of incident waves will have also introduced a degree of error. The exact magnitude of this error is difficult to establish, however the work by Tsai et al. (2005), indicated the performance of the equations adopted performed well for the steep slope utilised in this work. An alternative to the empirical approach would have been to adopt a hydrodynamic model capable of handling the wave transformation to the breaking location. Although this approach may have generated a small increase in accuracy, depending on the numerical approach adopted, the additional computational requirement needed to process these calculations was considered inefficient, particularly considering the high performance of the empirical approach (Tsai et al. 2005). Further, the dynamic evolution of the beach morphology would require simplification in the numerical model during an experiment, similar to that adopted during the empirical approach.

In the attenuation-correction procedure it was not possible to monitor the depth-varying saturation level of the sediment matrix, without also influencing the morphological development of the beach due to equipment positioning. Therefore, it is not possible to make a accurate estimate of the error that depth-varying fluctuation in the sediment saturation may have had. A detailed discussion of the validity and potential sources of error was provided in Section 7.1.2.

In conclusion, multiple sources of experimental error may have been introduced to the calculations at different stages of data recording and analysis. The spread of the data observed in Figure 6.6 may be partially attributed to the error discussed here; however the variability of wave impacts may also explain some of the spread. Although care was taken to select impacts located above the transducer location, variation in the precise location will adjust the distance over which attenuation occurred and will likely result

in under-prediction of bed surface pressure response in some cases. Variation in the nature of the bore collapse may also produce some spread in the data. Fluctuation of the impact angle, created by swash-swash interaction, or effects due to interaction between the swash lens above the beach and the collapsing bore may produce different pressure responses and frequency components for two waves of equal breaking wave height. These differences would lead to varied predictions for surface pressure responses, with variation likely to be more pronounced for plunging breakers, than collapsing and surging breakers. This may explain the reduction in data spread as the Iribarren number increases, with maximum deviation of data points from the indicative relationship changing from approximately 35% for plunging breakers, to approximately 20% for surging breakers.

## 7.3 Consequences of speculative relationship for numerical modelling

The adoption of different coefficients in the uprush and backwash phases of some numerical models is included to improve model performance. While this helps increase prediction accuracy of cross-shore profile evolution, it lacks the detail offered by correctly modelling the unaccounted underlying processes. Inclusion of the influence of varying breaker types on sediment mobilisation and transport can be introduced to existing numerical models, therefore reducing the necessity for varying coefficients in different swash phases.

For gravel beach scenarios, numerical models predominantly adopt a Shields based bedload transport module, with the suspended sediment load assumed as negligible due to the large fall velocity of the sediment. As discussed in Chapter 2, the entrainment of sediment is determined by the exceedance of a critical Shields parameter, based on the local shear stress exceeding a critical value, due to large flow velocities close to the bed.

There are multiple limitations with this approach. Derivation of this relationship was conducted for unidirectional flow of fine gravel in a uniform channel. The application

to oscillating flow may introduce inertial effects (Baldock and Holmes 1997), which would alter the point of sediment mobilisation. Also, the gravel is characterised by a single $d_{50}$ value, and therefore may be unrepresentative for beaches with non-uniformly graded material. Despite these limitations, Shields-based models have been effectively employed by many researchers to accurately represent bedload transport in various environments.

The existing data presented in Figure 6.6 (non-dimensional impact pressure vs. Iribarren number) is not sufficient to derive a relationship across the entire region of interest. As discussed, further testing is necessary to describe the relationship at low $\xi_b$ during transition between spilling and plunging, however the likely relationship has been discussed. With greater understanding of the complete relationship, it would be possible to introduce the effect of breaker-type on sediment mobilisation to modelling approaches.

Such a relationship could be introduced with modification of existing terms, or inclusion of additional terms. The event-specific Iribarren number can be assessed from the hydrodynamic module of existing numerical models. This can be used to determine if a specific wave event falls within the region where additional sediment mobilisation is expected, and if this is the case, the modified or additional term is activated.

An initial visualisation of this change could involve modification of the shear stress in a Shields-based bedload model. Pedrozo-Acuña et al. (2008) hypothesised how impact events may result in reduction of the sediment shear stress, making sediment mobilisation more likely. This can be introduced through adjustment in the critical shear stress dependent on the Iribarren number.

The specifics of the adjustment may be achieved in numerous ways, however the application of a trigonometric function is discussed as an example. The adoption of a

trigonometric function would allow fluctuation of the influence of the additional sediment mobilisation, in line with the suggested relationship between non-dimensional pressure and Iribarren number. Within the region of additional mobilisation, the bed shear stress may be reformulated to provide a breaker-type-adjusted critical instantaneous bed shear stress, $\tau'_{cr}$, as follows:

$$\tau'_{cr} = \tau_{cr} - \tau_{cr}.\sin\left[\pi\frac{(\xi_{bi} - \xi_{min})}{(\xi_{max} - \xi_{min})}\right], \tag{7.1}$$

where $\tau_{cr}$ is the critical instantaneous bed shear stress, $\xi_{bi}$ is the event specific value of $\xi_b$, $\xi_{max}$ and $\xi_{min}$ are the upper and lower limits of $\xi_b$ where wave breaker type causes an increase in impact pressure intensity. The consequence of this approach would result in a reduction of the bed shear stress as the breaker type transitions from spilling to intense plunging. A maximum will be reached where bed shear stress is equal to zero, consistent with bed fluidisation, before an increase in bed shear stress is registered as the breaker type transitions from intense plunging, to collapsing and surging.

An alternative process for increased sediment transport under intense impact events, may occur through entrainment of particles to suspended load. Most models consider the presence of suspended sediment within the swash zone of gravel beaches to be negligible. Advection of pre-suspended sediment from further offshore, and the large turbulence levels created during swash-swash interactions, may introduce suspended sediment to the swash zone. However, the high settling velocities common to gravel is often assumed to cause these particles to rapidly settle to the bed as waves propagate onshore. While this approach has been adopted in numerical models that provide reasonable profile predictions, if sediment is introduced into suspension at a more shoreward location, the distance these individual grains travel may be underestimated.

Fundamentally this process may occur through the same entrainment mechanism de-

scribed by Pedrozo-Acuña et al. (2008) for bed fluidisation, however in that scenario, transport of the mobilised material was assumed to occur as bedload during subsequent uprush. Intense impact events, and plunging bore collapse may result in large vertical flow velocities, as well as onshore swash flow, permitting the suspension of material for significant durations. It is likely that this form of transport will influence morphology at lower regions of the beach, as decelerating flow and dissipation of turbulence during uprush will allow settling of suspended sediment. This potential process may however assist is explaining the discrepancies between predicted and observed profile response below the SWL.

Inclusion of suspended sediment transport to existing models, would require the significant adjustment. Determination of suspended sediment concentration may be achieved through examination of event-specific Iriabrren number, and local flow rates in a hydrodynamics model capable of handling turbulent flow. With suspension established, the particle position within the water column may be determined with comparison of fall velocity to local flow rate and direction.

## 7.4 Additional process consideration

The improvement in modelling by Jamal (2011) was achieved through introduction of a pragmatic implementation of infiltration of water into the unsaturated beach region, similar to the approach by Dodd et al. (2008). While this encompasses some of the processes involved with infiltration, particularly the reduction of backwash flow volume and associated transport, this approach is somewhat limited. The beach is assumed to be unsaturated at elevations above the SWL; groundwater effects are ignored; and exfiltration is not included.

Horn and Li (2006) specifically discussed the relevance of the inclusion of infiltration/exfiltration effects for accurate berm prediction. The simplification of infiltration,

and absence of exfiltration, fails to include a range of effects that are significant to sediment mobilisation and morphological change. Infiltration and exfiltration modify the effective weight of surface particles, while the adjustment of the boundary layer has an effect on bed shear stresses (Turner and Masselink 1998). These can clearly play a significant role in mobilisation and transport of sediment, particularly on gravel beaches where infiltration and exfiltration are more prevalent.

## 7.5 Review of research programme objectives

The main objectives of this work, described in Chapter 2, are discussed here with an assessment of whether they were achieved.

The first objective was the creation of a data set providing beach profiles at the wave impact location, and this was achieved through completion of an experimental programme at the Wave Laboratory at UNAM in Mexico City. A total of 12 full tests, each divided into five sections, were conducted to investigate various wave conditions, producing 60 total experimental records. The experimental programme comprised variation in both wave height (between 0.08m and 0.16m) and wave period (between 1s and 4s).

The second objective was the assessment of the profile evolution, with estimation of the sediment transport rate under different wave conditions and breaker types. This was achieved with the measurement of cross-shore beach profile at intervals throughout each experiment. The spatial interval spacing between cross-shore profile measurement locations was reduced close to the SWL and across the impact region, to improve cross-shore resolution in the region of highest morphological evolution. The recorded beach profiles were then used to calculate the integral-corrected sediment transport rates, in accordance with the method outlined by Manoonvoravong (2009).

Finally, the third objective was the investigation of the pressure response under wave impact events, and assessing whether this may contribute to the discrepancy in numerical prediction of beach profiles. After the adoption of wavelet analysis to identify the individual processes contributing to the pressure response, and addressing the signal attenuation experienced by the pressure signal as it passes through the beach, the pressure records were able to be analysed. The results of this analysis indicate that the breaker type, assessed through the Iribarren number, is important in determining the specific pressure at the bed surface. This large and rapid fluctuation in surface pressure may contribute to the discrepancies noted in present numerical modelling approaches.

The key objectives set forth at the outset of this work have been completed, with both adoption of previous research methodologies, and development of new analytical techniques, such as the adoption of wavelet analysis for the separation of impact pressure responses. The achievement of these objectives will feed into improved understanding of these important processes and techniques for sediment transport research, although more work is still necessary for the accurate modelling of the cross-shore profile of gravel beaches.

# Chapter 8

# Future Work

This thesis helps to extend the knowledge base in several ways, however further work is still necessary to confirm and extend the approaches and relationship presented herein. In this chapter, suggestions for additional study are provided.

Examining the specific profile response under various Iribarren values would provide valuable information on how net sediment transport, and specific profile features are affected. The apparent link between net sediment transport and wave height will dictate retention of a stable wave height across a large range of Iribarren numbers, to prevent masking of any relationship between sediment transport and breaker type.

The presented approach of examining the CWT coefficients of co-located transducers appears to provide an accurate account of the attenuation experienced between the bed and recorded locations, at specific frequencies. It is essential to further validate this approach, with particular attention paid to assessment of a wide frequency range. A dedicated set of tests may be adopted, with pressure recording at multiple depths of burial in a porous bed, as well as at the bed surface. This will enable measurement of the actual attenuation, and assessment of the accuracy of the analytical approach.

Research into pressure attenuation has been largely limited to fine sediments, and has avoided the complexities introduced through wave breaking. Consideration of only fine sediments is understandable, as the validity of assuming Darcian flow becomes less sta-

ble as the sediment size increases. However the prevalence and importance of gravel as a sea defence, or coastal protection, strengthens the need for a robust approach for handling attenuation in coarse grained beaches.

The extension of wave conditions to include the untested plunging breaker and spilling breakers regions ($\xi_0 < 1.0$) will provide significant additional information. The transition between plunging breakers and collapsing and surging breakers is well described with the data presented here, however the transition between spilling and plunging breakers is not covered. This additional information will allow a relationship between the two parameters to be established.

A brief discussion has been provided on how it may be possible to incorporate the additional sediment mobilisation into a numerical representations. This procedure would prove valuable in determining how inclusion of this process affects the accuracy of morphological prediction. If morphological prediction is improved, a subsequent sensitivity analysis will allow determination of whether inclusion of this process is sufficient to account for the differences in experimental observed and numerically predicted profiles.

# Appendix A

# Sediment characteristics

| Sieve size (mm) | Weight retained (g) | Retained (%) | Cumulative retained (%) | Percentage passing (%) |
|---|---|---|---|---|
| 11.2 | 7.5 | 0.37 | 0.37 | 99.63 |
| 8 | 399.9 | 19.99 | 20.37 | 79.63 |
| 6.35 | 455.8 | 22.79 | 43.16 | 56.84 |
| 4.76 | 856.2 | 42.81 | 85.97 | 14.03 |
| Base | 280.7 | 14.03 | 100 | 0 |

*Table A.1:* Sediment sieve analysis details.

| Test | Total volume (ml) | Water volume (ml) | Porosity |
|---|---|---|---|
| 1 | 1000 | 380 | 0.38 |
| 2 | 1000 | 400 | 0.40 |
| 3 | 1000 | 400 | 0.40 |
| 4 | 1000 | 400 | 0.40 |
| 5 | 1000 | 420 | 0.42 |
| 6 | 1000 | 420 | 0.42 |
| 7 | 1000 | 400 | 0.40 |

*Table A.2:* Porosity test details.

| Test | Time (s) | Volume (ml) | Discharge ($cm^3$) | Pressure head (cm) | Permeability (m/s) | Hydraulic gradient | Hydraulic conductivity (m/day) |
|---|---|---|---|---|---|---|---|
| 1 | 19.00 | 320 | 16.84 | 4.0 | 0.0097 | 0.392 | 839.89 |
| 2 | 21.17 | 240 | 11.90 | 2.5 | 0.0105 | 0.245 | 904.56 |
| 3 | 21.33 | 560 | 26.25 | 6.5 | 0.0093 | 0.637 | 805.70 |
| 4 | 19.55 | 380 | 19.44 | 4.5 | 0.0100 | 0.441 | 861.61 |
| 5 | 26.50 | 520 | 19.62 | 4.5 | 0.0101 | 0.441 | 869.83 |
| 6 | 18.22 | 480 | 26.34 | 6.5 | 0.0094 | 0.637 | 808.48 |
| 7 | 17.11 | 540 | 31.56 | 8.5 | 0.0086 | 0.833 | 740.65 |
| 8 | 21.33 | 600 | 28.13 | 7.0 | 0.0093 | 0.686 | 801.59 |
| 9 | 29.39 | 520 | 16.80 | 4.0 | 0.0102 | 0.392 | 882.33 |
| 10 | 35.65 | 480 | 13.46 | 3.0 | 0.0104 | 0.294 | 895.26 |

*Table A.3:* Permeability tests, with associated hydraulic gradient and hydraulic conductivity values

# Appendix B

# Results in full

The following section presents the details of each test undertaken in the experimental regime.

| Test number | Test code | Profile code | Wave height at breaking $H_b$ (m) | Wave period $T$ (s) | Active wave action (s) |
|---|---|---|---|---|---|
| | 20080617T163700 | PLY31 | 0.096 | 2.01 | 60 |
| | 20080617T170531 | PLY32 | 0.103 | 2.01 | 120 |
| 7 | 20080618T084646 | PLY33 | 0.109 | 2.00 | 240 |
| | 20080618T112843 | PLY34 | 0.111 | 2.02 | 420 |
| | 20080618T120934 | PLY35 | 0.111 | 2.02 | 600 |
| | 20080617T093946 | PLY25 | 0.124 | 2.01 | 60 |
| | 20080617T103104 | PLY26 | 0.117 | 2.01 | 120 |
| 6 | 20080617T110846 | PLY27 | 0.125 | 2.01 | 240 |
| | 20080617T114013 | PLY28 | 0.127 | 2.01 | 420 |
| | 20080617T122441 | PLY29 | 0.125 | 2.02 | 600 |
| | 20080624T124725 | PLY36 | 0.129 | 2.01 | 60 |
| | 20080624T161348 | PLY37 | 0.126 | 2.01 | 120 |
| 8 | 20080624T164058 | PLY38 | 0.134 | 2.01 | 240 |
| | 20080624T170953 | PLY39 | 0.135 | 2.02 | 420 |
| | 20080624T175442 | PLY40 | 0.133 | 2.01 | 600 |
| | 20080625T093240 | PLY41 | 0.149 | 2.01 | 60 |
| | 20080625T153048 | PLY42 | 0.142 | 2.01 | 120 |
| 9 | 20080625T160020 | PLY43 | 0.150 | 2.01 | 240 |
| | 20080625T164945 | PLY44 | 0.151 | 2.01 | 420 |
| | 20080625T172843 | PLY45 | 0.149 | 2.02 | 600 |
| | 20080701T121805 | PLY46 | 0.162 | 2.01 | 60 |
| | 20080701T125100 | PLY47 | 0.169 | 2.01 | 120 |
| 10 | 20080701T150437 | PLY48 | 0.175 | 2.01 | 240 |
| | 20080701T160016 | PLY49 | 0.171 | 2.01 | 420 |
| | 20080701T163555 | PLY50 | 0.173 | 1.98 | 600 |

*Table B.1:* 2-second wave test details.

| Test number | Test code | Profile code | Wave height $H_m$ (m) | Wave period $T_m$ (s) | Active wave action (s) |
|---|---|---|---|---|---|
| | 20080703T091902 | PLY51 | 0.098 | 3.04 | 60 |
| | 20080703T095743 | PLY52 | 0.092 | 3.04 | 120 |
| 11 | 20080703T103247 | PLY53 | 0.088 | 3.04 | 240 |
| | 20080703T110312 | PLY54 | 0.087 | 3.04 | 420 |
| | 20080703T113954 | PLY55 | 0.084 | 3.04 | 600 |
| | 20080703T131045 | PLY56 | 0.113 | 3.04 | 60 |
| | 20080703T133554 | PLY57 | 0.106 | 3.03 | 120 |
| 12 | 20080703T135742 | PLY58 | 0.097 | 3.04 | 240 |
| | 20080703T143522 | PLY59 | 0.091 | 3.04 | 420 |
| | 20080703T151126 | PLY60 | 0.089 | 3.04 | 600 |
| | 20080703T164446 | PLY61 | 0.133 | 3.01 | 60 |
| | 20080703T172122 | PLY62 | 0.129 | 3.01 | 120 |
| 13 | 20080704T084439 | PLY63 | 0.105 | 3.05 | 240 |
| | 20080704T091345 | PLY64 | 0.101 | 3.04 | 420 |
| | 20080704T094501 | PLY65 | 0.100 | 3.04 | 600 |
| | 20080704T114911 | PLY66 | 0.138 | 3.05 | 60 |
| | 20080704T122103 | PLY67 | 0.123 | 3.05 | 120 |
| 14 | 20080704T162925 | PLY68 | 0.116 | 3.04 | 240 |
| | 20080704T171440 | PLY69 | 0.122 | 3.05 | 420 |
| | 20080704T175600 | PLY70 | 0.115 | 3.04 | 600 |

*Table B.2:* 3-second wave test details.

| Test number | Test code | Profile code | Wave height $H_m$ (m) | Wave period $T_m$ (s) | Active wave action (s) |
|---|---|---|---|---|---|
| | 20080708T094050 | PLY71 | 0.107 | 4.04 | 60 |
| | 20080708T101509 | PLY72 | 0.106 | 4.02 | 120 |
| 15 | 20080708T110001 | PLY73 | 0.109 | 4.02 | 240 |
| | 20080708T113007 | PLY74 | 0.118 | 4.03 | 420 |
| | 20080708T120210 | PLY75 | 0.124 | 4.05 | 600 |
| | 20080708T125453 | PLY76 | 0.122 | 4.03 | 60 |
| | 20080708T154955 | PLY77 | 0.124 | 4.04 | 120 |
| 16 | 20080708T162052 | PLY78 | 0.130 | 4.04 | 240 |
| | 20080708T165203 | PLY79 | 0.135 | 4.05 | 420 |
| | 20080708T172609 | PLY70 | 0.137 | 4.07 | 600 |
| | 20080709T124428 | PLY81 | 0.134 | 4.00 | 60 |
| | 20080709T132751 | PLY82 | 0.134 | 4.02 | 120 |
| 17 | 20080709T165944 | PLY83 | 0.146 | 4.01 | 240 |
| | 20080709T174314 | PLY84 | 0.147 | 4.05 | 420 |
| | 20080709T182332 | PLY85 | 0.147 | 4.06 | 600 |

*Table B.3:* 4-second wave test details.

## B.1 Wave records

| Test | H (m) | T (s) | $K_{R-p1}$ | $K_{R-p2}$ | $K_{R-p3}$ | $R_{R-p4}$ | $R_{R-p5}$ |
|---|---|---|---|---|---|---|---|
| 7 | 0.074 | 2.01 | 0.185 | 0.278 | 0.342 | 0.360 | 0.386 |
| 6 | 0.086 | 2.01 | 0.226 | 0.294 | 0.328 | 0.414 | 0.431 |
| 8 | 0.094 | 2.01 | 0.175 | 0.232 | 0.353 | 0.357 | 0.338 |
| 9 | 0.108 | 2.01 | 0.163 | 0.183 | 0.283 | 0.272 | 0.277 |
| 10 | 0.129 | 2.00 | 0.105 | 0.156 | 0.168 | 0.205 | 0.326 |
| 11 | 0.053 | 3.04 | 0.366 | 0.401 | 0.447 | 0.490 | 0.522 |
| 12 | 0.058 | 3.04 | 0.356 | 0.438 | 0.528 | 0.589 | 0.615 |
| 13 | 0.067 | 3.04 | 0.309 | 0.445 | 0.578 | 0.614 | 0.617 |
| 14 | 0.078 | 3.04 | 0.330 | 0.456 | 0.557 | 0.584 | 0.594 |
| 15 | 0.076 | 4.03 | 0.372 | 0.390 | 0.412 | 0.483 | 0.549 |
| 16 | 0.089 | 4.06 | 0.346 | 0.385 | 0.434 | 0.474 | 0.546 |
| 17 | 0.099 | 4.04 | 0.303 | 0.353 | 0.409 | 0.470 | 0.498 |

*Table B.4:* Calculated reflection coefficients ($K_{R-p1}$: reflection coefficient for part one of the relevant test, $K_{R-p2}$: reflection coefficient for part two of the relevant test etc.) using Friigard and Brorsen (1995).

## B.2 Beach profile results

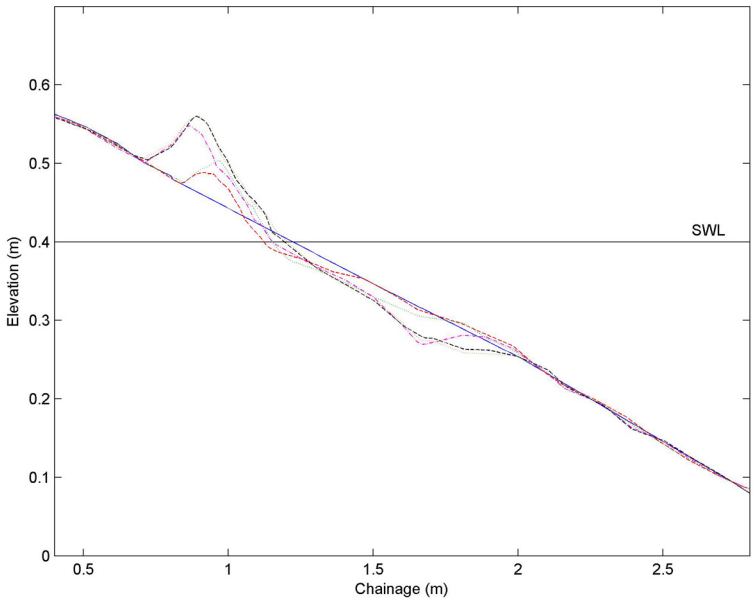


*Figure B.1:* Beach profile evolution for Test 7; $H_b = 0.109m$, $T = 2.01s$, $\xi_b = 1.52$. (—) initial profile, (- - -) 1 min, (...) 3 mins, (-.-) 7 mins, (- - -) 14 mins, (...) 24 mins.

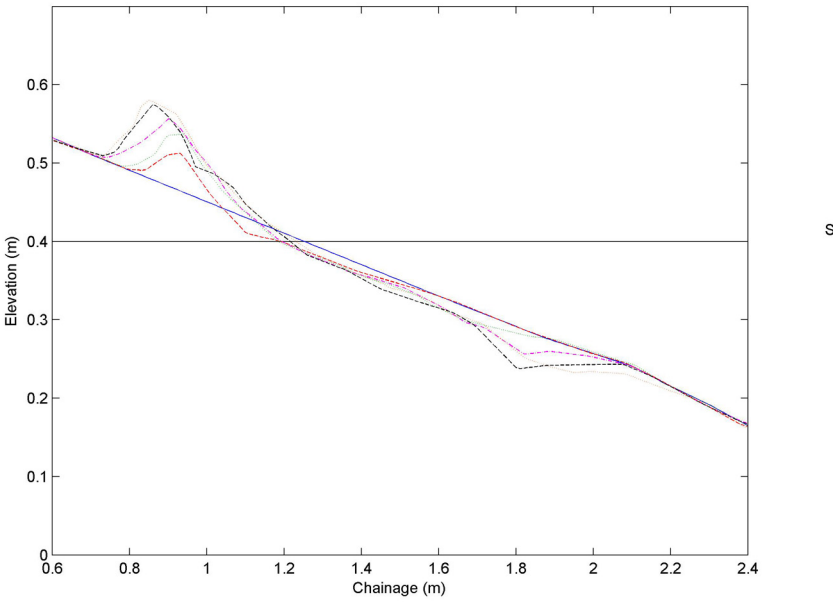


*Figure B.2:* Beach profile evolution for Test 6; $H_b = 0.124m$, $T = 2.01s$, $\xi_b = 1.42$. (—) initial profile,(- - -) 1 min, (...) 3 mins, (-.-) 7 mins, (- - -) 14 mins, (...) 24 mins.

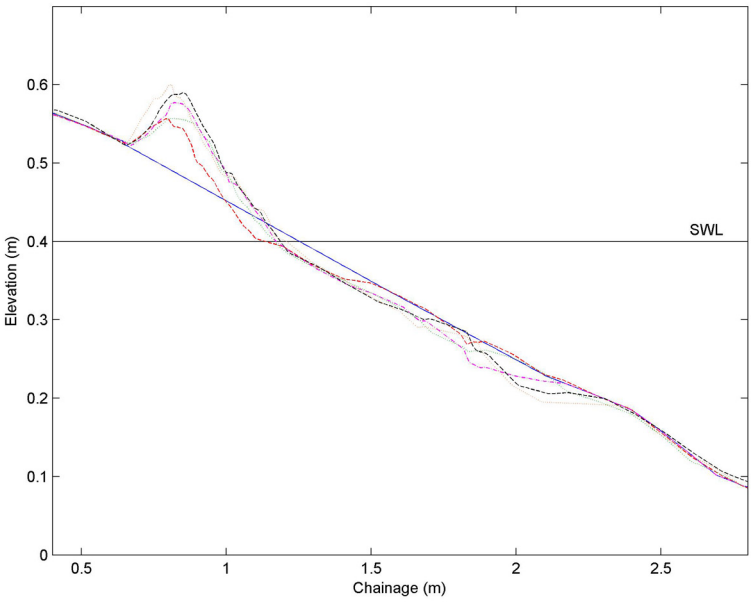


*Figure B.3:* Beach profile evolution for Test 8; $H_b = 0.133m$, $T = 2.01s$, $\xi_b = 1.38$. (—), initial profile, (- - -) 1 min, (...) 3 mins, (-.-) 7 mins, (- - -) 14 mins, (...) 24 mins.

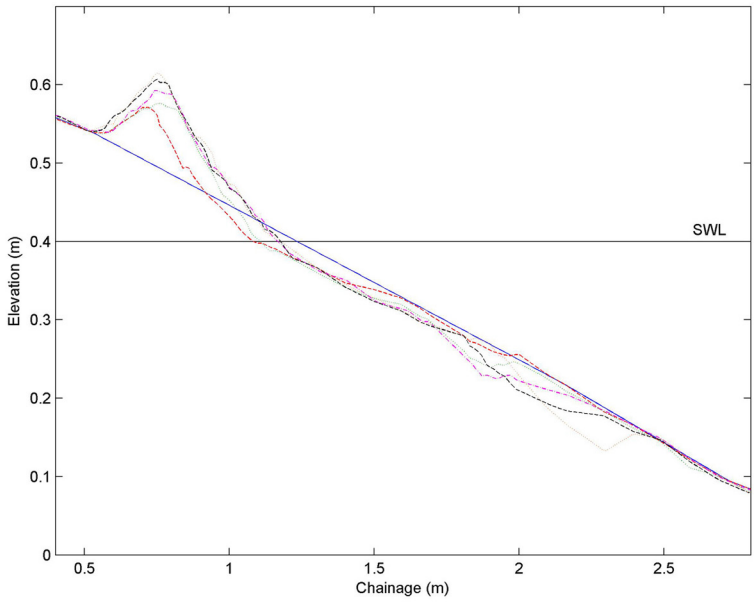


*Figure B.4:* Beach profile evolution for Test 9; $H_b = 0.149m$, $T = 2.01s$, $\xi_b = 1.30$. (—) initial profile, (- - -) 1 min, (...) 3 mins, (-.-) 7 mins, (- - -) 14 mins, (...) 24 mins.

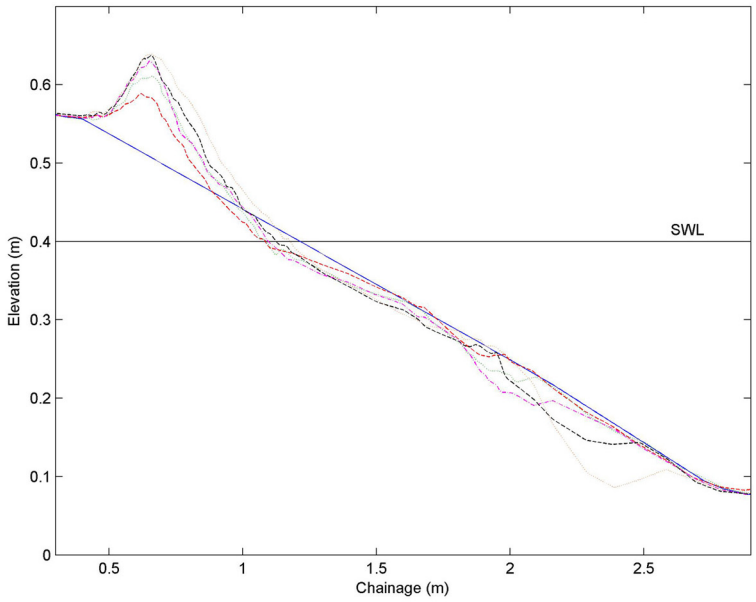


*Figure B.5:* Beach profile evolution for Test 10; $H_b = 0.172m$, $T = 2.00s$, $\xi_b = 1.20$. (—) initial profile, (- - -) 1 min, (...) 3 mins, (-.-) 7 mins, (- - -) 14 mins, (...): 24 mins.

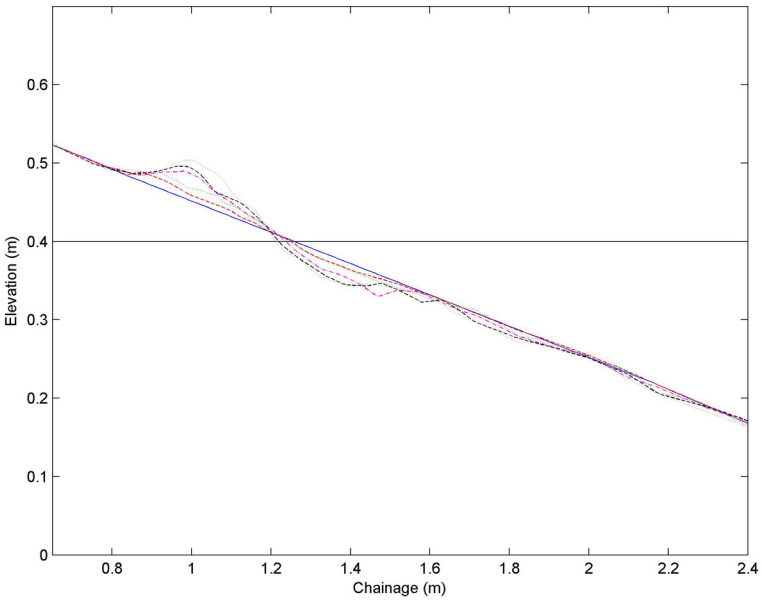


*Figure B.6:* Beach profile evolution for Test 11; $H_b = 0.087m$, $T = 3.04s$, $\xi_b = 2.58$. (—) initial profile, (- - -) 1 min, (...) 3 mins, (-.-) 7 mins, (- - -) 14 mins, (...) 24 mins.

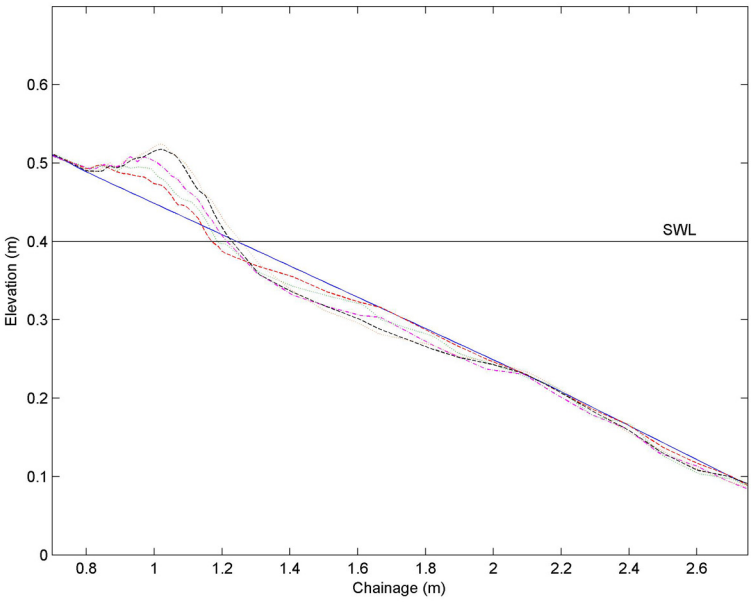


*Figure B.7:* Beach profile evolution for Test 12; $H_b = 0.093m$, $T = 3.04s$, $\xi_b = 2.48$. (—) initial profile, (- - -) 1 min, (...) 3 mins, (-.-) 7 mins, (- - -) 14 mins, (...) 24 mins.

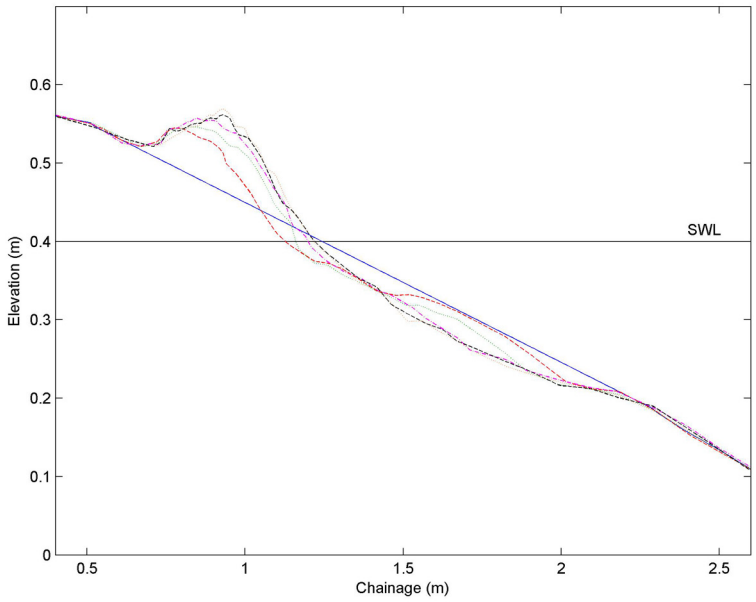


*Figure B.8:* Beach profile evolution for Test 13; $H_b = 0.105m$, $T = 3.04s$, $\xi_b = 2.34$. (—) initial profile, (- - -) 1 min, (...) 3 mins, (-.-) 7 mins, (- - -) 14 mins, (...) 24 mins.

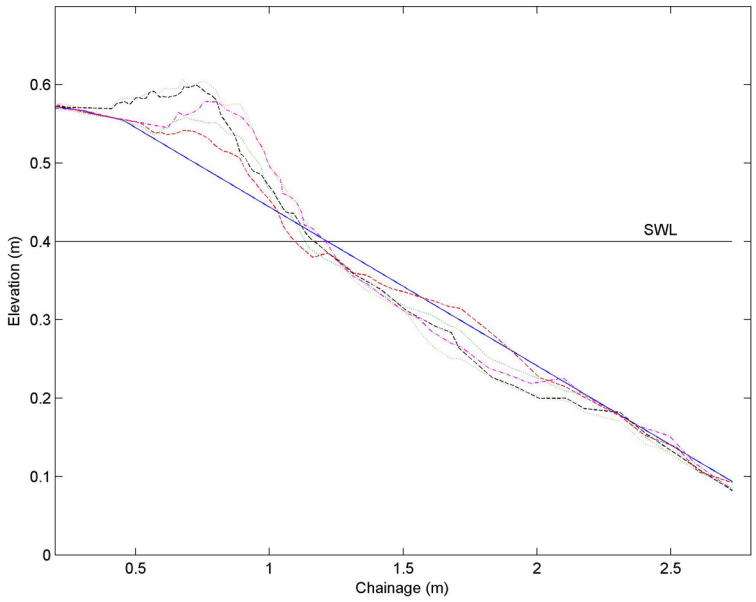


*Figure B.9:* Beach profile evolution for Test 14; $H_b = 0.119m$, $T = 3.04s$, $\xi_b = 2.21$. (—) initial profile, (- - -) 1 min, (...) 3 mins, (-.-) 7 mins, (- - -) 14 mins, (...) 24 mins.

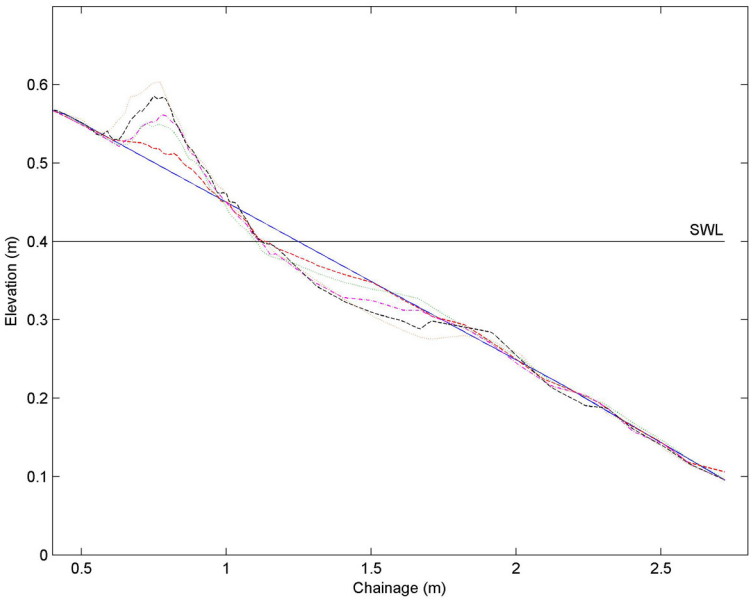


*Figure B.10:* Beach profile evolution for Test 15; $H_b = 0.118m$, $T = 4.03s$, $\xi_b = 2.94$. (—) initial profile, (- - -) 1 min, (...) 3 mins, (-.-) 7 mins, (- - -) 14 mins, (...) 24 mins.

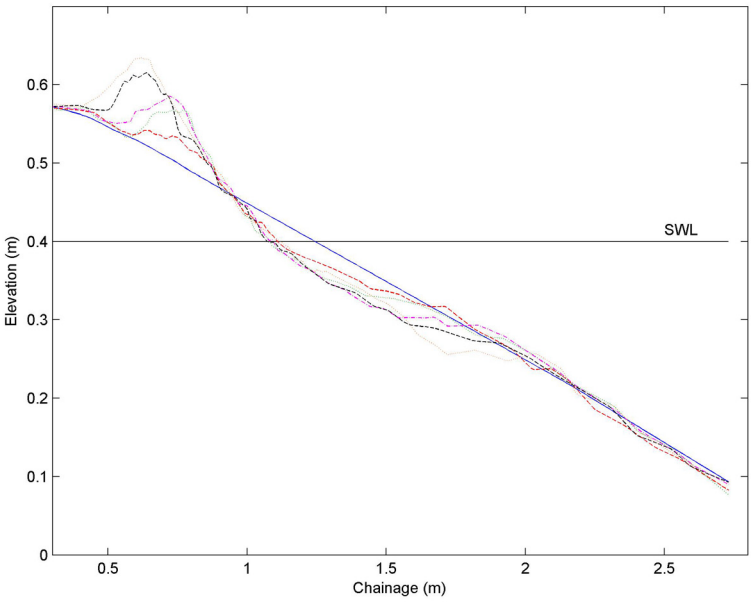


*Figure B.11:* Beach profile evolution for Test 16; $H_b = 0.134m$, $T = 4.06s$, $\xi_b = 2.77$. (—) initial profile, (- - -) 1 min, (...) 3 mins, (-.-) 7 mins, (- - -) 14 mins, (...) 24 mins.

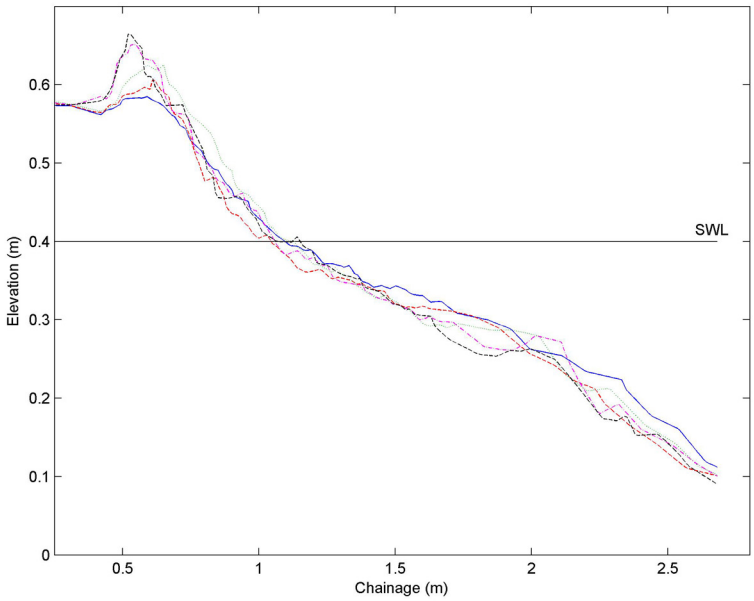


*Figure B.12:* Beach profile evolution for Test 17; $H_b = 0.145m$, $T = 4.04s$, $\xi_b = 2.65$. (—) initial profile, (- - -) 1 min, (...) 3 mins, (-.-) 7 mins, (- - -) 14 mins, (...) 24 mins.

## B.3 Berm morphological change details

| Test | Berm crest chainage (m) | Berm crest elevation (m) | Berm volume ($m^3/m$) |
|---|---|---|---|
| 7 part 1 | 0.92 | 0.488 | 0.00442 |
| 7 part 2 | 0.97 | 0.504 | 0.00826 |
| 7 part 3 | 0.87 | 0.548 | 0.01613 |
| 7 part 4 | 0.89 | 0.560 | 0.02126 |
| 7 part 5 | 0.89 | 0.560 | 0.02222 |
| 6 part 1 | 0.93 | 0.513 | 0.00552 |
| 6 part 2 | 0.94 | 0.537 | 0.01125 |
| 6 part 3 | 0.90 | 0.557 | 0.01613 |
| 6 part 4 | 0.86 | 0.575 | 0.01961 |
| 6 part 5 | 0.85 | 0.580 | 0.02248 |
| 8 part 1 | 0.79 | 0.556 | 0.01175 |
| 8 part 2 | 0.82 | 0.557 | 0.01821 |
| 8 part 3 | 0.82 | 0.577 | 0.02110 |
| 8 part 4 | 0.85 | 0.590 | 0.02478 |
| 8 part 5 | 0.81 | 0.601 | 0.02509 |
| 9 part 1 | 0.72 | 0.571 | 0.01263 |
| 9 part 2 | 0.75 | 0.576 | 0.02193 |
| 9 part 3 | 0.76 | 0.593 | 0.02724 |
| 9 part 4 | 0.75 | 0.607 | 0.03028 |
| 9 part 5 | 0.75 | 0.615 | 0.03173 |
| 10 part 1 | 0.62 | 0.589 | 0.01839 |
| 10 part 2 | 0.66 | 0.611 | 0.02720 |
| 10 part 3 | 0.65 | 0.630 | 0.02992 |
| 10 part 4 | 0.66 | 0.638 | 0.03525 |
| 10 part 5 | 0.66 | 0.639 | 0.04462 |
| 11 part 1 | 0.87 | 0.489 | 0.00274 |
| 11 part 2 | 0.92 | 0.489 | 0.00483 |
| 11 part 3 | 0.98 | 0.490 | 0.00698 |
| 11 part 4 | 0.97 | 0.496 | 0.00813 |
| 11 part 5 | 1.00 | 0.504 | 0.01068 |

*Table B.5:* Berm morphological change for tests 6 to 11.

| Test | Berm crest chainage (m) | Berm crest elevation (m) | Berm volume ($m^3/m$) |
|---|---|---|---|
| 12 part 1 | 0.84 | 0.498 | 0.00628 |
| 12 part 2 | 0.86 | 0.496 | 0.00922 |
| 12 part 3 | 0.93 | 0.508 | 0.01297 |
| 12 part 4 | 1.02 | 0.518 | 0.01670 |
| 12 part 5 | 1.02 | 0.524 | 0.01902 |
| 13 part 1 | 0.78 | 0.545 | 0.01379 |
| 13 part 2 | 0.84 | 0.546 | 0.02117 |
| 13 part 3 | 0.85 | 0.557 | 0.02582 |
| 13 part 4 | 0.93 | 0.562 | 0.02833 |
| 13 part 5 | 0.93 | 0.569 | 0.02929 |
| 14 part 1 | 0.69 | 0.542 | 0.01346 |
| 14 part 2 | 0.69 | 0.559 | 0.02273 |
| 14 part 3 | 0.76 | 0.579 | 0.03518 |
| 14 part 4 | 0.73 | 0.599 | 0.03738 |
| 14 part 5 | 0.68 | 0.606 | 0.05046 |
| 15 part 1 | 0.77 | 0.518 | 0.00463 |
| 15 part 2 | 0.77 | 0.550 | 0.01002 |
| 15 part 3 | 0.78 | 0.561 | 0.01132 |
| 15 part 4 | 0.75 | 0.585 | 0.01627 |
| 15 part 5 | 0.77 | 0.604 | 0.02145 |
| 16 part 1 | 0.73 | 0.533 | 0.00842 |
| 16 part 2 | 0.77 | 0.568 | 0.01475 |
| 16 part 3 | 0.72 | 0.586 | 0.01873 |
| 16 part 4 | 0.64 | 0.616 | 0.02419 |
| 16 part 5 | 0.62 | 0.634 | 0.03116 |
| 17 part 1 | 0.59 | 0.585 | 0.01509 |
| 17 part 2 | 0.61 | 0.606 | 0.01677 |
| 17 part 3 | 0.65 | 0.625 | 0.02902 |
| 17 part 4 | 0.54 | 0.651 | 0.02772 |
| 17 part 5 | 0.52 | 0.665 | 0.02647 |

*Table B.6:* Berm morphological change for tests 12 to 17.

## B.4 Integral-corrected net sediment transport results

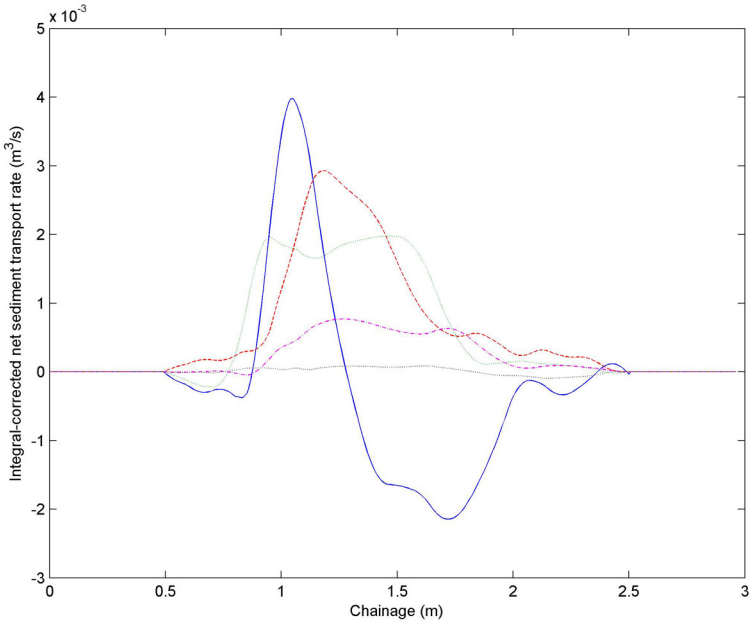


*Figure B.13:* Integral-corrected sediment transport rates for Test 7 $H_b = 0.109m$, $T = 2.01s$, $\xi_b = 1.52$. (—) 0-1min, (- - -) 1-3min, (...) 3-7min, (- . -) 7-14min, (...) 14-24min.

No integral-corrected sediment transport rates are estimated for Test 17 as the seaward boundary where transport ceases was not captured in the profile measurements.

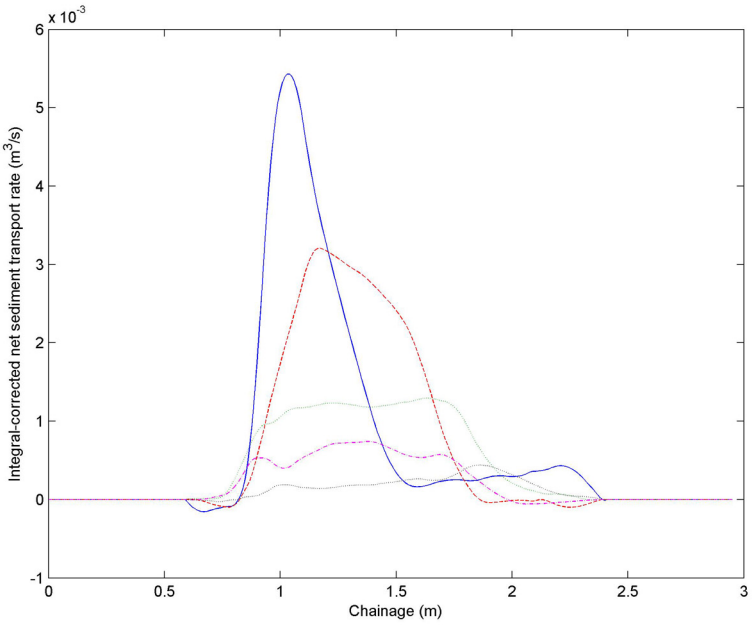


*Figure B.14:* Integral-corrected sediment transport rates for Test 6 $H_b = 0.124m$, $T = 2.01s$, $\xi_b = 1.42$. (—) 0-1min, (- - -) 1-3min, (...) 3-7min, (- . -) 7-14min, (...) 14-24min.

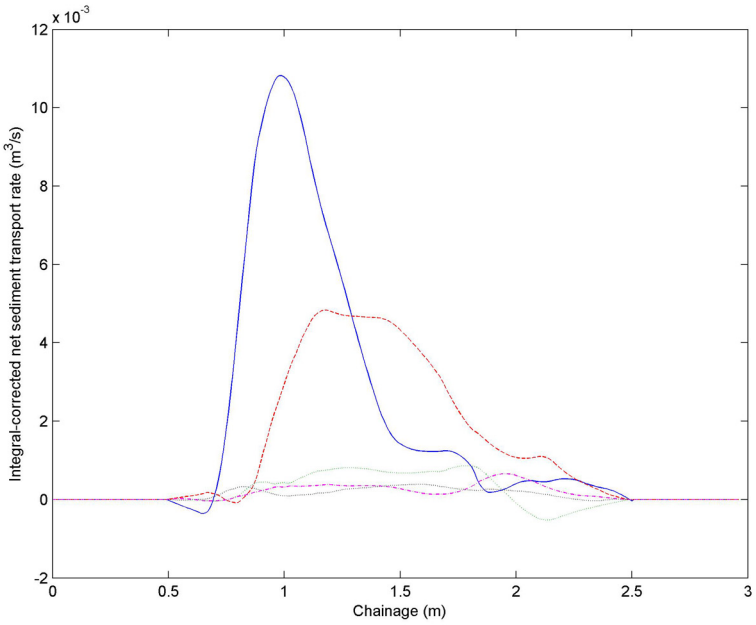


*Figure B.15:* Integral-corrected sediment transport rates for Test 8 $H_b = 0.133m$, $T = 2.01s$, $\xi_b = 1.38$. (—) 0-1min, (- - -) 1-3min, (...) 3-7min, (- . -) 7-14min, (...) 14-24min.

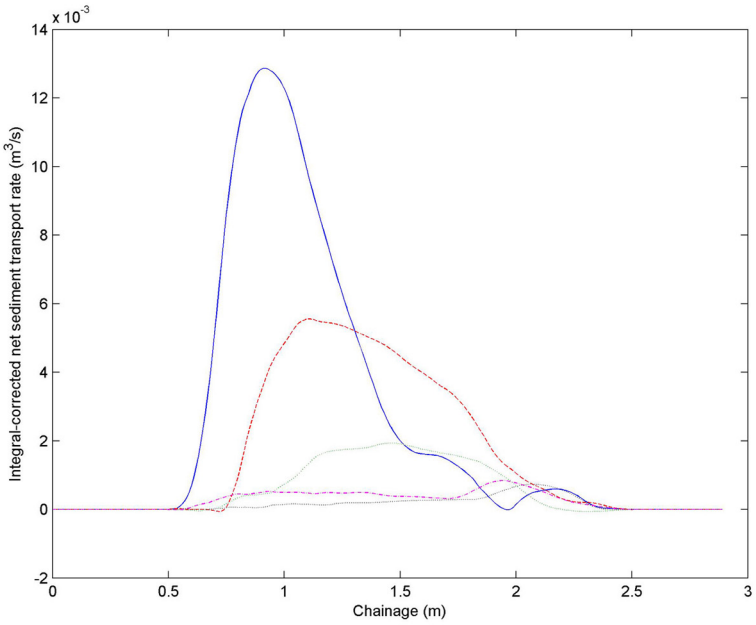


*Figure B.16:* Integral-corrected sediment transport rates for Test 9 $H_b = 0.149m$, $T = 2.01s$, $\xi_b = 1.30$. (—) 0-1min, (- - -) 1-3min, (...) 3-7min, (- . -) 7-14min, (...) 14-24min.

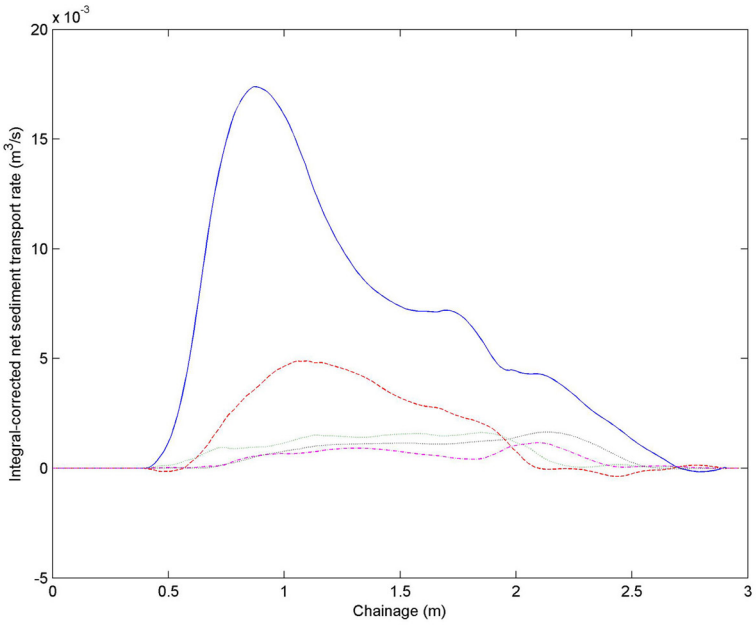


*Figure B.17:* Integral-corrected sediment transport rates for Test 10 $H_b = 0.172m$, $T = 2.00s$, $\xi_b = 1.20$. (—) 0-1min, (- - -) 1-3min, (...) 3-7min, (- . -) 7-14min, (...) 14-24min.

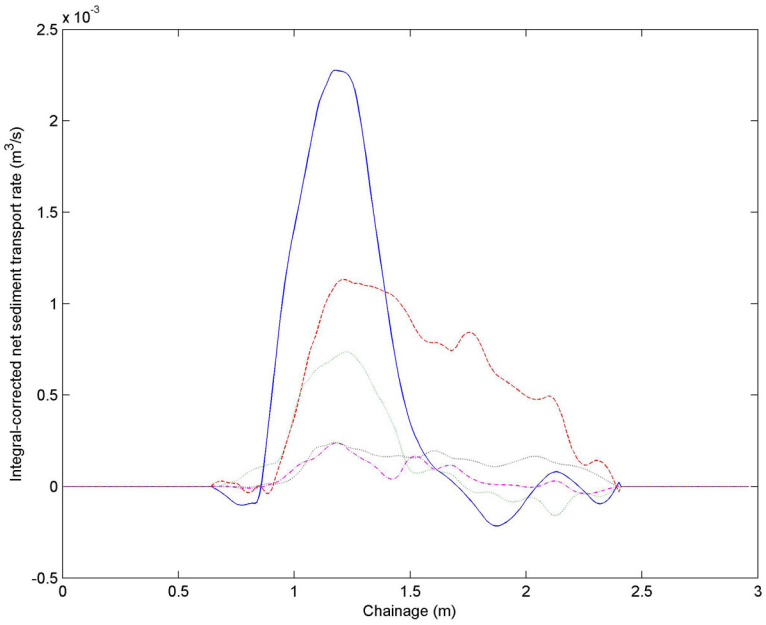


*Figure B.18:* Integral-corrected sediment transport rates for Test 11, $H_b = 0.087m$, $T = 3.04s$, $\xi_b = 2.58$. (—) 0-1min, (- - -) 1-3min, (...) 3-7min, (- . -) 7-14min, (...) 14-24min.

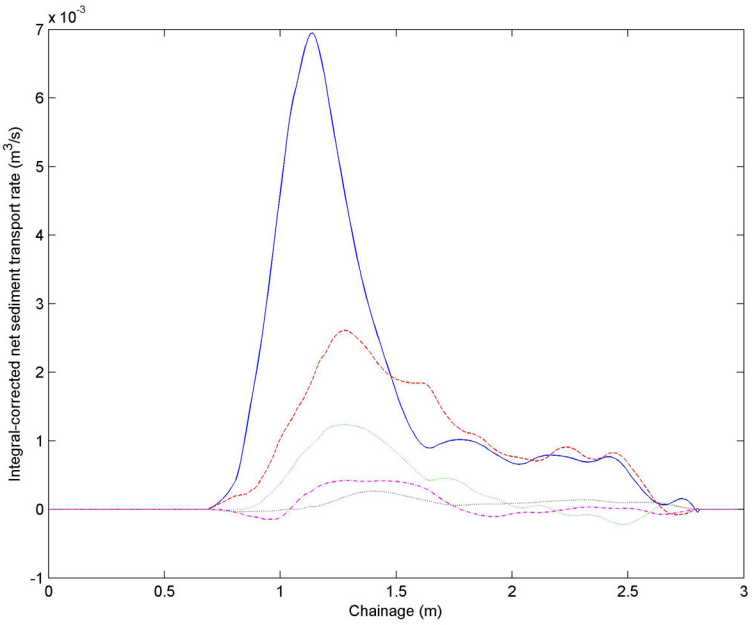


*Figure B.19:* Integral-corrected sediment transport rates for Test 12; $H_b = 0.093m$, $T = 3.04s$, $\xi_b = 2.48$. (—) 0-1min, (- - -) 1-3min, (...) 3-7min, (- . -) 7-14min, (...) 14-24min.

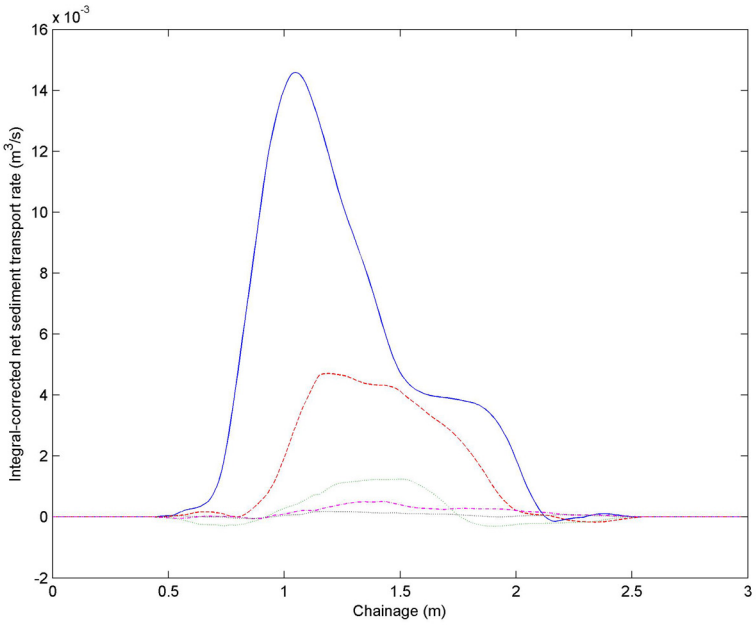


*Figure B.20:* Integral-corrected sediment transport rates for Test 13; $H_b = 0.105m$, $T = 3.04s$, $\xi_b = 2.34$. (—) 0-1min, (- - -) 1-3min, (...) 3-7min, (- . -) 7-14min, (...) 14-24min.

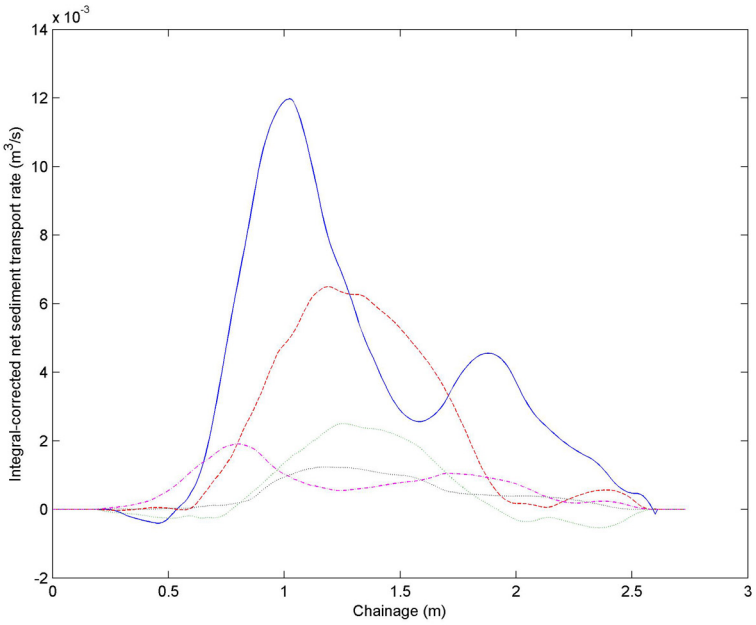


*Figure B.21:* Integral-corrected sediment transport rates for Test 14; $H_b = 0.119m$, $T = 3.04s$, $\xi_b = 2.21$. (—) 0-1min, (- - -) 1-3min, (...) 3-7min, (- . -) 7-14min, (...) 14-24min.

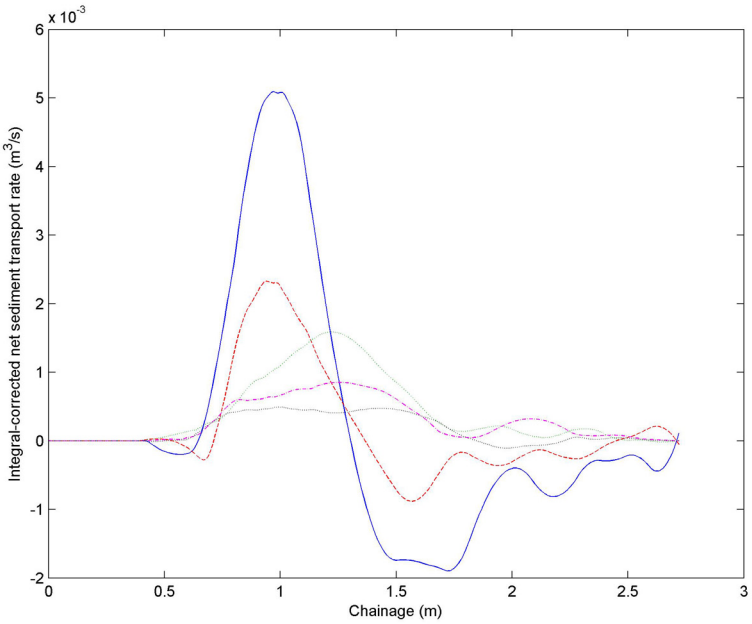


*Figure B.22:* Integral-corrected sediment transport rates for Test 15; $H_b = 0.118m$, $T = 4.03s$, $\xi_b = 2.94$. (—) 0-1min, (- - -) 1-3min, (...) 3-7min, (- . -) 7-14min, (...) 14-24min.

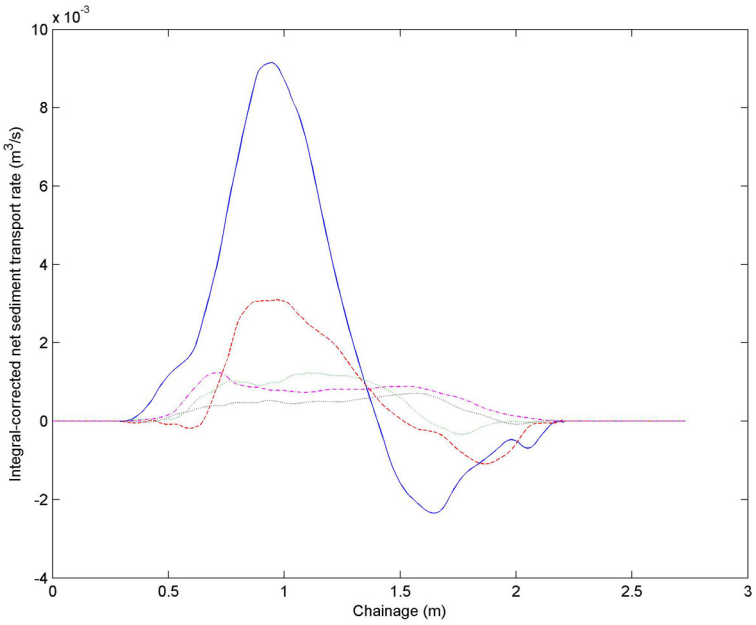


*Figure B.23:* Integral-corrected sediment transport rates for Test 16; $H_b = 0.134m$, $T = 4.06s$, $\xi_b = 2.77$. (—) 0-1min, (- - -) 1-3min, (...) 3-7min, (- . -) 7-14min, (...) 14-24min.

# References


Aagaard, T. and Hughes, M. (2006), 'Sediment suspension and turbulence in the swash zone of dissipative beaches', *Marine Geology* **228**, 117–135.

Ahrens, T. and Duvall, G. (1966), 'Stress relaxation behind elastic shock waves in rocks', *Journal of Geophysical Research* **71**, 4349–4360.

Austin, M. (2005), Swash, groundwater and sediment transport processes on a gravel beach, PhD thesis, Loughborough University.

Austin, M. J. and Masselink, G. (2006*a*), 'Observations of morphological change and sediment transport on a steep gravel beach', *Marine Geology* **229**, 59–77.

Austin, M. J. and Masselink, G. (2006*b*), 'Swash-groundwater interaction on a steep gravel beach', *Continental Shelf Research* **26**, 2503–2519.

Bagnold, R. A. (1940), 'Beach formation by waves: some model experiments in a wave tank', *Journal of the Institute of Civil Engineers* **15**, 27–53.

Baird, A., Horn, D. and Mason, T. (1998), 'Validation of a boussinesq model of beach ground water behaviour', *Marine Geology* **148**, 55–69.

Bakhtyar, R., Barry, D., Li, L., Jeng, D. and Yeganeh-Bakhtiary, A. (2009), 'Modeling sediment transport in the swash zone: A review', *Ocean Engineering* **36**, 767–783.

Baldock, T., Barnes, M. and Hughes, M. (2006), Field observations of instantaneous cross-shore free surface profiles and flow depths in the swash zone, *in* 'Coastal Dynamics 2005'.

Baldock, T. and Holmes, P. (1997), Swash hydrodynamics on a steep beach, *in* 'Coastal Dynamics Conference, Plymouth, UK'.

Baquerizo, A. (1995), Reflexión del oleaje en playas. Métodos de evaluación y predicción, PhD thesis, Universidad de Cantabria.

Bardet, J. and Sayed, H. (1993), 'Velocity and attenuation of compressional waves in nearly saturated soils', *Soil dynamics and earthquake engineering* **12**, 391–401.

Barnes, M. and Baldock, T. (2007), 'Direct bed shear stress measurements in laboratory swash', *Journal of Coastal Research* **50**, 641–645.

Barnes, M., O'Donoghue, T., Alsina, J. and Baldock, T. (2009), 'Direct bed shear stress measurements in bore-driven swash', *Coastal Engineering* **56**, 853–867.

Barrière, J., Sénéchal, P., Bordes, C. and Perroud, H. (2010), 'Relationship between P-wave attenuation and water saturation in an homogeneous unconsolidated and partially saturated porous media : An experimental study', *AGU Fall Meeting Abstracts* p. C1205.

Battjes, J. A. (1974), Computation of set-up, longshore currents, run-up and overtopping due to wind-generated waves, PhD thesis, Delft University of Technology.

Battjes, J. and Janssen, J. (1978), Energy loss and setup due to breaking of random waves, *in* 'Proceedings of the 13th International Conference of Coastal Engineering'.

Berryman, J. (1986), 'Elastic wave attenuation in rocks containing fluids', *Applied Physics Letters* **49**, 552–555.

Biot, M. (1941), 'General theory of three-dimensional consolidation', *Journal of Applied Physics* **12**, 155–164.

Biot, M. (1956*a*), 'Theory of propagation of elastic waves in a fluid-saturated porous solid. i. low-frequency range', *The Journal of the Acoustical Society of America* **28**, 168–178.

Biot, M. (1956*b*), 'Theory of propagation of elastic waves in a fluid-saturated porous solid. ii. high-frequency range', *The Journal of the Acoustical Society of America* **28**, 179–191.

Blenkinsopp, C., Turner, I., Masselink, G. and Russell, P. (2011), 'Swash zone sediment fluxes: Field observations', *Coastal Engineering* **58**, 28–44.

Brutsaert, W. (1964), 'The propagation of elastic waves in unconsolidated unsaturated granular mediums', *Journal of Geophysical Research* **69**, 243–257.

Bruun, P. (1956), Coast erosion and the development of beach profiles, Technical Memo 44, Beach Erosion Board, USACE.

Bullock, G., Obhrai, C., Peregrine, D. and Bredmose, H. (2007), 'Violent breaking wave impacts. Part 1: Results from large-scale regular wave tests on vertical and sloping walls', *Coastal Engineering* **54**, 602–617.

Buscombe, D. and Masselink, G. (2006), 'Concepts in gravel beach dynamics', *Earth-Science Reviews* **79**, 33–52.

Butt, T., Evans, D., Russell, P., Masselink, G., Miles, J. and Ganderton, P. (2002), An integrative approach to investigate the role of swash in shoreline change., *in* 'Proceedings of the Twenty-eighth International Conference on Coastal Engineering, Cardiff, UK'.

Butt, T. and Russell, P. (2000), 'Hydrodynamics and cross-shore sediment transport in the swash-zone of natural beaches: A review.', *Journal of Coastal Research* **16**, 255–268.

Butt, T., Russell, P., Puleo, J., Miles, J. and Masselink, G. (2004), 'The influence of bore turbulence on sediment transport in the swash and inner surf zones', *Continental Shelf Research* **24**, 757–771.

Butt, T., Russell, P. and Turner, I. (2001), 'The influence of swash infiltrationŰexfiltration on beach face sediment transport: onshore or offshore?', *Coastal Engineering* **42**, 35–52.

Chang, K. and Liu, P. L.-F. (1997), Measurement of breaking waves using particle image

velocimetry, *in* 'Proceedings of the Twenty-fifth International Conference on Coastal Engineering, Orlando, Florida'.

Chanson, H. and Jaw-Fang, L. (1997), 'Plunging jet characteristics of plunging breakers', *Coastal Engineering* **31**, 125–141.

Cheng, N.-S. and Chiew, Y.-M. (1998), 'Turbulent open-channel flow with upward seepage', *Journal of Hydraulic Research* **36**, 415–431.

Chotiros, N. (1995), 'Biot model of sound propagation in water-saturated sand', *Journal of the Acoustical Society of America* **97**, 199–214.

Clukey, E., Kulhawy, F., Liu, P. L.-F. and Tate, G. (1985), 'The impact of wave loads and pore-water pressure generation on initiation of sediment transport', *Geo Marine Letters* **5**, 177–183.

Combes, J.-M., Grossmann, A. and Tchamitchian, P., eds (1989), *Wavelets. Time-Frequency Methods and Phase Space.*

Conley, D. C. and Inman, D. (1994), 'Ventilated oscillatory boundary layers', *Journal of Fluid Mechanics* **273**, 261–284.

Conley, D. and Griffin, J. (2004), 'Direct measurements of bed shear stress under swash in the field', *Journal of Geophysical Research* **109**, C03050.

Cox, D., Hobensack, W. and Sukumaran, A. (2000), Bottom stress in the inner surf and swash zone, *in* 'Proceedings of the 27th International Conference on Coastal Engineering, Sydney, Australia'.

Cox, D., Kobayashi, N. and Mase, H. (1991), Effects of fluid accelerations on sediment transport in surf zone, *in* 'Proceedings of a Specialty Conference on Quantitative Approaches to Coastal Sediment (Coastal Sediments 91), USA'.

Cox, S. and Cooker, M. (1999), 'The motion of a rigid body impelled by a sea-wave impact', *Applied Ocean Research* **21**, 113–125.

Dean, R. (1991), 'Equilibrium beach profiles: characteristics and applications', *Journal of Coastal Research* **7**, 53–84.

Dodd, N., Stoker, A., Calvete, D. and Sriariyawat, A. (2008), 'On beach cusp formation', *Journal of Fluid Mechanics* **597**, 145–169.

Elfrink, B. and Baldock, T. (2002), 'Hydrodynamics and sediment transport in the swash zone: a review of prospectives', *Coastal Engineering* **45**, 149–167.

Elgar, S., Gallacgher, E. and Guza, R. (2001), 'Nearshore sandbar migration', *Journal of Geophysical Research C* **106**, 11623–11627.

Emery, K. and Gale, J. (1951), 'Swash and swash mark', *Transactions of the American Geophysical Union* **32**, 31–36.

Farge, M. (1992), 'Wavelet transforms and their applications to turbulence', *Annual Review of Fluid Mechanics* **24**, 395–457.

Faybishenko, B. (1995), 'Hydraulic behaviour of quasi-saturated soils in the presence of entrapped air: laboratory experiments', *Water Resources Research* **31**, 2421–2435.

Flick, R. and George, R. (1990), Turbulence scales in the surf and swash, *in* 'Proceedings of the 22nd International Conference on Coastal Engineering'.

Foster, D., Bowen, A., Holman, R. and Natoo, P. (2006), 'Field evidence of pressure gradient induced incipient motion', *Journal of Geophysical Research* **111**, C05004.

Fredsøe, J. and Deigaard, R. (1992), *Mechanics of Coastal Sediment transport*, World Scientific Publishing.

Friigard, P. and Brorsen, M. (1995), 'A time-domain method for separating incident and reflected irregular waves', *Coastal Engineering* **24**, 205–215.

Goda, Y. (1975), 'Irregular wave deformation in the surf zone', *Coastal Engineering in Japan* **18**, 13–26.

Gurley, K. and Kareem, A. (1999), 'Applications of wavelet transforms in earthquake, wind and ocean engineering', *Engineering Structures* **21**, 149–167.

Hegge, B. and Masselink, G. (1991), 'Groundwater-table responses to wave run-up: an experimental study from western australia', *Journal of Coastal Research* **7**, 623–634.

Hibberd, S. and Peregrine, D. (1979), 'Surf and run-up on a beach: a uniform bore', *Journal of Fluid Mechanics* **95**, 323–345.

Hicks, B. (2010), Cross-shore transport on gravel beaches, PhD thesis, University of Delaware.

Hoagland, P., Jin, D. and Kite-Powell, H. (2012), 'The costs of beach replenishment along the u.s. atlantic coast', *Journal of Coastal Research* **28**, 199–204.

Holland, K. and Puleo, J. (2001), 'Variable swash motions associated with foreshore profile change', *Journal of Geophysical Research C* **106**, 1623–1643.

Horn, D. P. (2002), 'Beach groundwater dynamics', *Geomorphology* **48**, 121–146.

Horn, D. P. (2006), 'Measurements and modelling of beach groundwater flow in the swash-zone: a review', *Continental Shelf Research* **26**, 622–662.

Horn, D. P. and Li, L. (2006), 'Measurement and Modelling of Gravel Beach Groundwater Response to Wave Run-up: Effects on Beach Profile Changes', *Journal of Coastal Research* **22**, 1241–1249.

Horn, D. P. and Mason, T. (1994), 'Swash zone sediment transport modes', *Marine Geology* **120**, 309–325.

Hsu, T.-J. (2002), A two-phase flow approach for sediment transport, PhD thesis, Cornell University.

Hsu, T.-J. and Hanes, D. M. (2004), 'Effects of wave shape on sheet flow sediment transport', *Journal of Geophysical Research* **109**, C05025.

Hsu, T.-J., Jenkins, J. and Liu, P.-F. (2004), On two-phase sediment transport: sheet flow of massive particles, *in* 'Proceedings of the Royal Society of London (A)'.

Hsu, T.-J. and Raubenheimer, B. (2006), 'A numerical and field study on inner-surf and swash sediment transport', *Continental Shelf Research* **26**, 589–598.

Hughes, M. (1992), 'Application of a nonlinear shallow water theory to swash following bore collapse on a sandy beach', *Journal of Coastal Research* **8**, 562–578.

Hughes, M. and Baldock, T. (2004), 'Eulerian flow velocities in the swash zone: Field data and model predictions', *Journal of Geophysical Research C* **109**, C08009.

Hughes, M., Masselink, G. and Brander, R. (1997), 'Flow velocity and sediment transport in the swash zone of a steep beach', *Marine Geology* **138**, 91–103.

Hughes, S. (1983), 'Movable-bed modeling law for coastal dune erosion', *Journal of Waterway, Port, Coastal, and Ocean Engineering* **109**, 164–179.

Instituto Nicaragüense de Estudios Territoriales (2012), 'Bulletin of the global volcanism network (november 2011)'.
**URL:** *http://www.volcano.si.edu/reports/bulletin/contents.cfm?issue=3611display=complete*

Jamal, M. (2011), Modelling Coarse-Grained Beach Profile Evolution, PhD thesis, University of Plymouth.

Jamal, M., Simmonds, D., Magar, V. and Pan, S. (2010), Modelling infiltration on gravel beaches with an xbeach variant, *in* 'Proceedings of the 32nd International Conference on Coastal Engineering'.

Jayaratne, R. and Shibayama, T. (2011), A simple numerical simulation model for beach profile evolution, *in* '7th International Symposium on Coastal Engineering and Science of Coastal Sediment Processes (Coastal Sediments '11)'.

Jenkins, J. and Hanes, D. (1998), 'Collisional sheet flows of sediment driven by a turbulent fluid', *Journal of Fluid Mechanics* **370**, 29–52.

Jennings, R. and Shulmeister, J. (2002), 'A field based classification scheme for gravel beaches', *Marine Geology* **186**, 211–228.

Jensen, S., Aagaard, T. and Baldock, T. (2010), Swash zone bed level changes and sediment entrainment at the surf-swash boundary, *in* 'Proceedings of the 32nd International Conference on Coastal Engineering'.

Karunarathna, H. and Chadwick, A. (2007), 'On low-frequency waves in the surf and swash', *Ocean Engineering* **34**, 2115–2123.

Kobayashi, N., Hicks, B. and Figlus, J. (2011), 'Evolution of gravel beach profiles', *Journal of Waterway, Port Coastal and Ocean Engineering* **137**, 258–262.

Le Méhauté, B. and Koh, R. (1967), 'On the breaking of waves arriving at an angle to the shore', *Journal of Hydraulic Research* **5**, 67–88.

Li, L., Barry, D., Pattiaratchi, C. and Masselink, G. (2002), 'Beachwin: Modelling groundwater effects on swash sediment transport and beach profile changes', *Environmental Modelling and Software* **17**, 313–320.

López de San Román Blanco, B. (2003), Dynamics of gravel and mixed, sand and gravel, beaches, PhD thesis, Imperial College.

López de San Román-Blanco, B., Coates, T. T., Holmes, P., Chadwick, A. J., Bradbury, A., Baldock, T. E., Pedrozo-Acuña, A., Lawrence, J. and Grüne, J. (2006), 'Large scale experiments on gravel and mixed beaches: Experimental procedure, data documentation and initial results', *Coastal Engineering* **53**, 349–362.

López de San Román-Blanco, B., Whitehouse, R., Holmes, P. and Clarke, S. (2003), Mixed beaches (sand/gravel): Process understanding and implications for management, *in* 'Proceedings, 38th Defra Flood and Coastal Management Conference'.

Madsen, P., Sørensen, O. and Schäffer, H. (1997), 'Surf zone dynamics simulated by a Boussinesq type model. Part I. Model description and cross-shore motion of regular waves', *Coastal Engineering* **32**, 255–287.

Manoonvoravong, P. (2009), Sediment transport and beach morphodynamics induced by long waves, PhD thesis, University of Queensland.

Mase, H. (1988), 'Spectral characteristics of random wave run-up', *Coastal engineering* **12**, 175–189.

Mason, T. and Coates, T. (2001), 'Sediment transport processes on mixed beaches: a review for shoreline management.', *Journal of Coastal Research* **17**, 645–657.

Massel, S. R., Przyborska, A. and Przyborski, M. (2004), 'Attenuation of wave-induced groundwater pressure in shallow water Part 1', *Oceanologia* **46**, 383–404.

Massel, S. R., Przyborska, A. and Przyborski, M. (2005), 'Attenuation of wave-induced groundwater pressure in shallow water Part 2 Theory', *Oceanologia* **47**, 291–323.

Masselink, G. and Buscombe, D. (2008), 'Shifting gravel: a case study of slapton sands', *Geographical Review* **22**, 27–31.

Masselink, G., Evans, D., Hughes, M. and Russell, P. (2005), 'Suspended sediment transport in the swash zone of a dissipative beach', *Marine Geology* **216**, 169–189.

Masselink, G. and Hughes, M. (1998), 'Field investigation of sediment transport in the swash zone', *Continental Shelf Research* **18**, 1179–1199.

Masselink, G. and Li, L. (2001), 'The role of swash infiltration in determining the beach face gradient: a numerical study', *Marine Geology* **176**, 139–156.

Masselink, G. and Puleo, J. (2006), 'Swash-zone morphodynamics', *Continental Shelf Research* **26**, 661–680.

Masselink, G. and Russell, P. (2006), 'Flow velocities, sediment transport and morphological change in the swash zone of two contrasting beaches', *Marine Geology* **227**, 227–240.

Masselink, G. and Turner, I. (2012), 'Large scale laboratory investigation into the effect

of varying back barrier lagoon water levels on gravel beach morphology and swash zone sediment transport', *Coastal Engineering* **63**, 23–38.

MathWorks (2012), 'Continuous wavelet transform'.
**URL:** *http://www.lcs.syr.edu/faculty/lewalle/wavelets/cwt$_g$eneral.pdf*

McCowan, J. (1894), 'On the highest wave of permanent type', *Philosophical Magazine* **38**, 351–358.

Mendoza-Baldwin, E., Silva-Casarín, R., Sánchez-Dirzo, R. and Chávez-Cárdenas, X. (2010), Wave energy conversion using a blow-jet system, *in* 'Proceedings of the 32nd International Conference on Coastal Engineering'.

Meneses Fernández, A. (2009), Effectos del nivel freático en playas, Master's thesis, Univesidad Nacional Autónoma de México.

Miche, R. (1951), 'Le pouvoir reťfleťchissant des ouvrages maritimes exposeťs a' lŠaction de la houle', *Ann. Ponts Chaussees* **121**, 285–319.

Miles, J., Butt, T. and Russell, P. (2006), 'Swash zone sediment dynamics: a comparison of a dissipative and an intermediate beach', *Marine Geology* **231**, 181–200.

Mizuguchi, M. (1986), Experimental study on kinematics and dynamics of wave breaking, *in* 'Proceedings of the Twentieth Coastal Engineering Conference, Taipei'.

Moses, C. and Williams, R. (2008), 'Artificial beach recharge: the south east england experience', *Zeitschrift fur Geomorphologie N.E.* **52**, 107–124.

Nielsen, P. (1992), *Coastal Bottom Boundary Layers and Sediment Transport Advanced Series on Ocean Engineering*, World Scientific.

Nielsen, P. (1997), Coastal groundwater dynamics, *in* 'Proceedings of the 3rd Coastal Dynamics Conference, Plymouth, UK'.

Nielsen, P. (2002), 'Shear stress and sediment transport calculations for swash zone modelling', *Coastal Engineering* **45**, 53–60.

Nielsen, P., Aseervatham, R., Fenton, J. and Perrochet, P. (1997), 'Groundwater waves in aquifers of intermediate depth', *Advances in Water Resources* **20**, 37–43.

Oelze, M., O'Brien, W. and Darmody, R. (2002), 'Measurements of attenuation and speed of sound in soils', *Soil Science Society of America Journal* **66**, 788–796.

Oumeraci, H. and Partenscky, H. (1990), Wave-induced pore pressure in rubble mound breakwaters, *in* 'Proceedings of the International Conference on Coastal Engineering'.

Pedrozo-Acuña, A. (2005), Concerning Swash on Steep Beaches, PhD thesis, University of Plymouth.

Pedrozo-Acuña, A., Ruiz de Alegría-Arzaburu, A., Torres-Freyermuth, A., Mendoza, E. and Silva, R. (2011), 'Laboratory investigation of pressure gradients induced by plunging breakers', *Coastal Engineering* **58**, 722–738.

Pedrozo-Acuña, A., Simmonds, D. J., Chadwick, A. J. and Silva, R. (2007), 'A numerical-empirical approach for evaluating morphodynamic processes on gravel and mixed sand-gravel beaches', *Marine Geology* **241**, 1–18.

Pedrozo-Acuña, A., Simmonds, D. J., Otta, A. and Chadwick, A. J. (2006), 'On the cross-shore profile change of gravel beaches', *Coastal Engineering* **53**, 335–347.

Pedrozo-Acuña, A., Simmonds, D. J. and Reeve, D. E. (2008), 'Wave-impact characteristics of plunging breakers acting on gravel beaches', *Marine Geology* **253**, 26–35.

Pedrozo-Acuña, A., Torres-Freyermuth, A., Zou, Q., Hsu, T.-J. and Reeve, D. E. (2010), 'Diagnostic investigation of impulsive pressures induced by plunging breakers impinging on gravel beaches', *Coastal Engineering* **57**, 252–266.

Peregrine, D. (1983), 'Breaking waves on beaches', *Annual review of fluid mechanics* **15**, 149–178.

Plona, T. (1980), 'Observation of a second bulk compressional wave in a porous medium at ultrasonic frequencies', *Applied Physics Letters* **36**, 259–261.

Pride, S., Gangi, A. and Morgan, F. (1992), 'Deriving the equations of motion for porous isotropic media', *Journal of the Acoustical Society of America* **92**, 3278–3290.

Pritchard, D. and Hogg, A. (2005), 'On the transport of suspended sediment by a swash event on a plane beach', *Coastal Engineering* **52**, 1–23.

Przyborska, A. (2010), Attenuation of groundwater pressure due to surface waves, *in* 'EGU General Assembly Conference Abstracts', Vol. 12 of *EGU General Assembly Conference Abstracts*, p. 2971.

Puleo, J., Beach, R., Holman, R. and Allen, J. (2000), 'Swash zone sediment suspension and transport and the importance of the bore generated turbulence', *Journal of Geophysical Research C* **105**, 17021–17044.

Puleo, J., Farhadzadeh, A. and Kobayashi, N. (2007), 'Numerical simulation of swash zone fluid accelerations', *Journal of Geophysical Research C* **112**, C07007.

Puleo, J., Holland, K., Plant, N., Slinn, D. and Hanes, D. (2003), 'Fluid acceleration effects on suspended sediment transport in the swash zone', *Journal of Geophysical Research C* **108**, 3350.

Puleo, J. and Holland, T. (2001), 'Estimating swash zone friction coefficients on a sandy beach', *Coastal Engineering* **52**, 1–23.

Puleo, J., Lanckriet, T. and Wang, P. (2012), 'Near bed cross-shore velocity profiles, bed shear stress and friction on the foreshore of a microtidal beach', *Coastal Engineering* **68**, 6–16.

Pyrak-Nolte, L. and Nolte, D. (1995), 'Wavelet analysis of velocity dispersion of elastic interface waves propagating along a fracture', *Geophysical research letters* **22**, 1329–1332.

Rafiee, J., Tse, P., Harifi, A. and Sadeghi, M. (2009), 'A novel technique for selecting mother wavelet function using an intelligent fault diagnosis system', *Expert Systems with Applications* **36**, 4862–4875.

Rao, A. and Sitaram, N. (1999), 'Stability and mobility of sand bed channels effected by seepage', *Journal of Irrigation and Drainage* **125**, 370–379.

Raubenheimer, B., Elgar, S. and Guza, R. (2004), 'Observations of swash zone velocities: A note on friction coefficient', *Journal of Geophysical Research C* **109**, C01027.

Reeve, D., Chadwick, A. and Flemming, C. (2004), *Coastal engineering processes, theory and design practice*, Spon Press, London, UK.

Roelvink, J. and Brøker, I. (1993), 'Cross-shore profile models', *Coastal Engineering* **21**, 163–191.

Shields, A. (1936), 'Anwendung der ahnlichkeitsmechanik und der turbulentzforschung auf die geschiebebewegung', *Mitteilunger der Preussischen Versuchsanstalt für Wasserbau und Schiffbau* **26**, 5–24.

Shuto, N. (1974), 'Nonlinear Long Waves in a Channel of Varied Section', *Coastal Engineering in Japan* **17**, 1–12.

Simm, J., Brampton, A., Beech, N. and Brooke, J. (1996), Beach management manual, Technical report.

Soulsby, R. (1997), *Dynamics of Marine Sands: a manual for practical applications*, Thomas Telford Publications, London.

Soulsby, R. and Damgaard, J. (2005), 'Bedload sediment transport in coastal waters', *Coastal Engineering* **52**, 673–689.

Soulsby, R. and Whitehouse, R. (1997), Threshold of sediment motion in coastal environments, *in* 'Proceedings of Pacific Coasts and Ports '97'.

Stern, M., Bradford, A. and Millwater, H. (1985), 'Wave reflection from a sediment layer with depth dependent properties', *Journal of the Acoustical Society of America* **77**, 1781–1788.

Stive, M. (1980), Velocity and pressure field of spilling breakers, *in* 'Proceedings of the Seventeenth Coastal Engineering Conference, Sydney, Australia, March 23-28, 1980'.

Stoll, R. and Kan, T. (1981), 'Reflections of an acoustic waves at a water-sediment interface', *Journal of the Acoustical Society of America* **70**, 149–156.

Svendsen, I. and Hansen, J. (1976), Deformation up to breaking of periodic waves on a beach, *in* 'Proceedings of the Fifteenth International Conference on Coastal Engineering'.

Terrile, E., Strive, A., Tromp, M. and Jan Verhagen, H. (2006), 'Incipient motion of coarse particles under regular shoaling waves', *Coastal Engineering* **53**, 81–92.

*BARDEX - editorial* (2012), 'Bardex: A large-scale laboratory study of gravel barrier dynamics', *Coastal Engineering* **63**, 1–2.

Thornton, E. and Guza, R. (1983), 'Transformation of wave height distribution', *Journal of Geophysical Research* **88**, 5925–5938.

Ting, F. and Kirby, J. (1994), 'Observation of undertow and turbulence in a laboratory surf zone', *Coastal Engineering* **24**, 51–80.

Ting, F. and Kirby, J. (1995), 'Dynamics of surf-zone turbulence in a strong plunging breaker', *Coastal Engineering* **24**, 177–204.

Ting, F. and Kirby, J. (1996), 'Dynamics of surf-zone turbulence in a spilling breaker', *Coastal Engineering* **27**, 131–160.

Torrence, C. and Compo, G. (1998), 'A practical guide to wavelet analysis', *Bulletin of the American Meteorological Society* **79**, 61–78.

Tsai, C.-P., Chen, H.-B., Hwung, H.-H. and Huang, M.-J. (2005), 'Examination of empirical formulas for wave shoaling and breaking on steep slopes', *Ocean Engineering* **32**, 469–483.

Turner, I. (1993), 'Water table outcropping on macro-tidal beaches: a simulation model', *Marine Geology* **115**, 227–238.

Turner, I. and Masselink, G. (1998), 'Swash infiltration-exfiltration and sediment transport', *Journal of Geophysical Research* **103**, 30813–30824.

Turner, I. and Masselink, G. (2012), 'Coastal gravel barrier hydrology Ů observations from a prototype-scale laboratory experiment (bardex)', *Coastal Engineering* **63**, 13–22.

US Army Corps of Engineers (2012), 'Appendix a glossary of coastal terminology'.
**URL:** *http://publications.usace.army.mil/publications/eng-manuals/EM*$_1$110 − 2 − 1100$_v$*ol/AppA/a* − *a.pdf*

Van Dorn, W. (1978), 'Breaking invariants in shoaling waves', *Journal of Geophysical Research* **83**, 2981–2988.

Vanneste, D. and Troch, P. (2012), 'An improved calculation model for the wave-induced pore pressure distribution in a rubble-mound breakwater core', *Coastal Engineering* **66**, 8–23.

Velea, D., Shields, F. and Sabatier, J. (2000), 'Elastic wave velocities in partially saturated ottawa sand: Experimental results and modeling', *Soil Science Society of America Journal* **4**, 1226–1234.

Waddell, E. (1973), Dynamics of swash and implications to beach response, Technical Report 139, Coastal studies Institute, Louisiana State University.

Wang, H. (2000), *Theory of Linear Poroelasticity to Geomechanics and Hydrogeology*, Princeton University Press.

Weggel, J. (1972), 'Maximum breaker height', *Journal of Waterways, Harbors, Coastal Engineering Division, ASCE* **98**, 529–548.

White, J. (1975), 'Computed seismic speeds and attenuation in rocks with partial gas saturation', *Geophysics* **40**, 224–232.

Williams, J., Buscombe, D., Masselink, G., Turner, I. and Swinkels, C. (2012a), 'Barrier dynamics experiment (bardex): Aims, design and procedures', *Coastal Engineering* **63**, 3–12.

Williams, J., Ruiz de Alegría-Arzaburu, A., McCall, R. and Van Dongeren, A. (2012b), 'Modelling gravel barrier profile response to combined waves and tides using xbeach: Laboratory and field results', *Coastal Engineering* **63**, 62–80.

Yaghmaei-Sabegh, S. (2010), 'Detection of pulse-like ground motions based on continues (*sic*) wavelet transform', *Journal of Seismology* **14**, 715–726.

Yamamoto, T. (1983), 'Acoustic propagation in the ocean with a poro-elastic bottom', *Journal of the Acoustical Society of America* **73**, 1587–1596.

Yamamoto, T., Koning, H. L., Sellmeijer, H. and Van Hijum, E. (1978), 'On the response of a poro-elastic bed to water waves', *Journal of Fluid Mechanics* **87**, 193–206.

Yeh, H., Ghazali, A. and Marton, I. (1989), 'Experimental study of bore run-up', *Journal of Fluid MEchanics* **206**, 563–578.

Zanuttigh, B. and van der Meer, J. (2008), 'Wave reflection from coastal structures in design conditions', *Coastal Engineering* **55**, 771–779.

Zyserman, J. and Fredsøe, J. (1994), 'Data analysis of bed concentration of suspended sediment', *Journal of Hydraulic Engineering* **120**, 1021–1042.